

**Cation- π and Polarizability Effects in Biomimetic Catalysis and the
Design of a Photoactive Donor-Cyclophane-Acceptor Triad**

Thesis by
Alison McCurdy

In Partial Fulfillment of the Requirements
for the Degree of
Doctor of Philosophy

California Institute of Technology
Pasadena, California

1995

(Submitted August 4, 1994)

Acknowledgments

I would not have stayed to complete my doctorate if it weren't for my advisor Dennis Dougherty. I greatly admire him as a scientist and as a person. His knowledge of and interest in a staggering range of topics combined with his commitment to a life outside of science has always impressed me. During times of crisis he provided encouragement and advice. For better or worse, he gave me a great deal of freedom in the pursuit of my projects. The advantages and pitfalls of that experience taught me much....

I have benefited from the wisdom of many coworkers during my stay in the Dougherty group. David Stauffer, Leslie Jimenez, and David Shultz have had particular influence on me and my work. Discussions about life and lab work with David Kaisaki, Rich Barrans, Pat Kearney, Laura Mizoue, Kraig Andersen, Sandro Mecozzi, Mick Murray, Jon Forman, Jeff Clites, Scott Silverman, Anthony West, Jesse Lin, Wenge Zhong, Bruce Hietbrink, Seth Miller, Jennifer Ma, and Sarah Ngola were an integral part of my being here. Thanks to Sarah for carrying on the catalysis torch!

The friendships I enjoyed while being here have been invaluable. I only hope I can repay them in kind. I owe Tim Herzog, Nancy Shreve, Wayne Larson, Missy Richmond, Dom McGrath, Jennifer Herek, Kevin Condroski, Earl Potter, Mike Abrams, Jeff Clites, the Noyes drinking crew, Lynn Russell, and Sarah Ngola BIG.

Thanks go again to Jeff Clites, Sarah Ngola, Tim Herzog, and Jennifer Herek for helping me with this thesis.

Finally, I dedicate this thesis to my Mom and Dad, who have never stopped cheering me up or cheering me on.

Abstract

The role of the cation- π effect and polarizability in ground-state and transition-state stabilization by a cyclophane host **P** was explored. The family of guests that bind well to this host was expanded to include sulfonium salts and sulfoxides. The catalysis of the demethylation of aryl dimethylsulfonium salts with thiocyanate by host **P** and the related host **C** was observed. This reaction is a model for the demethylation of S-adenosylmethionine (SAM), a cofactor of methyltransferase enzymes. The effect of aryl substituents on reaction rates was presented in linear Hammett plots for the uncatalyzed reaction in aqueous buffer, the host-catalyzed reaction, and the uncatalyzed reaction in acetonitrile. The data revealed that the cation- π effect alone cannot be responsible for the biomimetic catalysis. Simple polarity effects were ruled out. To explain the catalysis data, the polarizability of the cyclophanes' cavities was invoked as the additional stabilizing factor. Sulfonium-aromatic interactions appear to be present in some methyltransferases, and the cation- π effect and polarizability of the SAM binding site are possibly catalytic mechanisms found in Nature.

Additional work involved the synthesis and study of other cyclophane macrocycles to further explore the cation- π effect. A host **PHOS** which uses phosphate groups as water-solubilizing groups was designed. This host should have superior solubility properties to host **P**. It also may be used to quantitatively assess the effect on cation binding affinities of negative charges on the macrocycle. The last synthetic step was unsuccessful. Small organic soluble cyclophanes **O** and **S** were synthesized to bind alkali metal cations. Although potassium-aromatic interactions have been invoked to explain selectivity in voltage-gated potassium channels, this kind of interaction was not detected in these cyclophanes.

Finally, progress toward the synthesis of a photoactive donor-cyclophane-acceptor triad has been made. This triad is a model for a macrocycle-crosslinked conducting

polymer-based sensor. A guest analyte would act as a conductivity switch by facilitating interchain hopping of charge carriers. A photoinduced electron donor ruthenium complex moiety and an acceptor quinone moiety will be linked to the host, fixed away from the binding cavity. The acceptor portion was successfully synthesized. However, while monodentate, bidentate, and tetradentate ligands for ruthenium have been synthesized, the formation of a stable ruthenium metal complex has been unsuccessful. Further work will be required to synthesize this triad.

Table of Contents

Acknowledgments	ii
Abstract	iii
List of Figures	vii
List of Tables	ix
Chapter 1: Biomimetic Catalysis	1
I. Introduction	2
A. Enzymatic Catalysis	2
B. Biomimetic Catalysis	5
C. Dougherty Model System	8
II. Results and Discussion	15
III. Conclusions and Future Directions	33
IV. Summary	38
Experimental Section	40
References	48
Chapter 2: New Macrocyclic Hosts to Explore the Cation-π Effect	51
I. Introduction	52
A. Cyclophane Solubilized by Phosphate Groups	53
1. Introduction	53
2. Results and Discussion	56
3. Future Work Toward Host PHOS	62
B. Cyclophane Receptors for Alkali Metal Cations	63
1. Introduction	63
2. Results and Discussion	66
3. Future Work for Alkali Cation Binders	68
II. Conclusions	68
Experimental Section	70
References	78
Chapter 3: Design of a Sensor for Organic Molecule Guests in Aqueous Media: A Photoactive Donor-Cyclophane-Acceptor Triad	79

I. Introduction	80
A. Sensors	80
B. Design Constraints	84
II. Results and Discussion	88
A. Electron Acceptor Portion of the Cyclophane	88
B. Photoinduced Electron Donor Portion of the Cyclophane	91
1. Monodentate Ligands	92
2. Bidentate Ligands	97
3. Tetradentate Ligand	103
III. Future Work	104
Experimental Section	107
References	118

List of Figures

Figure 1.1. Split-site model of ground-state and transition-state stabilization	4
Figure 1.2. Free energy diagram for catalyzed and uncatalyzed reactions	12
Figure 1.3. Binding free energies of substrate, transition state, and product	13
Figure 1.4. Substrates, transition states, and products of the dealkylation reaction	15
Figure 1.5. Adamantyltrimethylsulfonium tetrafluoroborate with D-values	21
Figure 1.6. Michaelis-Menten scheme	24
Figure 1.7. Experimental kinetics data in the presence and absence of host P	25
Figure 1.8. Kinetics Simulator output	26
Figure 1.9. BEP diagram for the dealkylation of aryltrimethylsulfonium salts	29
Figure 1.10. Hammett plot of dealkylation reaction rates	32
Figure 1.11. Reactions with positively-charged transition states	35
Figure 1.12. Crystal structure of SAM and a methyltransferase-tryptophan	36
Figure 1.13. Electrostatic potential surfaces for trimethyl sulfonium and tetramethylammonium ion	37
Figure 2.1. Synthetic route to unmodified host P	56-7
Figure 2.2. Proposed synthetic route to host PHOS	60-1
Figure 2.3. Primary sequence of the pore region of the voltage-gated potassium channel	64
Figure 2.4. Optimized benzene-cation-benzene complexes	65
Figure 3.1. Conducting polymer crosslinked by a macrocycle; photoactive donor-host-acceptor triad	81
Figure 3.2. Synthesis of cyclophane host P	87
Figure 3.3. Synthesis of the acceptor portion of the triad	89
Figure 3.4. Synthesis of model acceptor quinone 12	89

Figure 3.5. Proposed host synthesis by stepwise macrocyclization	90
Figure 3.6. Synthesis of the cycloadduct 18	93
Figure 3.7. Synthesis of 23 <i>via</i> cycloaddition of 22 and anthracene 7	95
Figure 3.8. Synthesis of 23 <i>via</i> cycloaddition of methyl 3-bromopropiolate and anthracene 7	96
Figure 3.9. Attempted synthesis of 28 <i>via</i> a bromobenzyne cycloaddition with anthracene 7	97
Figure 3.10. Synthesis of N(α)- <i>t</i> -butoxycarbonyl,N(im)-tosylhistamine (35)	101
Figure 3.11. Attempted synthesis of tosyl-protected ligand 33	101
Figure 3.12. Synthesis of bis(pyridyl ester) model host 38	102
Figure 3.13. Synthesis of bis(bipyridyl ester) model host 43	103
Figure 3.14. Proposed synthesis of ligands 46 and 47	105

List of Tables

Table 1.1	Binding Free Energies of Guests for Host P and Host C	10
Table 1.2.	Binding Free Energies to Host P and D-values for New Guests	16
Table 1.3.	Rate Enhancements and Binding Free Energies of Substrate, Transition-State and Product	27
Table 1.4.	Sulfonium Salt Dealkylation Rate Constants	28

Chapter 1

Biomimetic Catalysis

I. INTRODUCTION

A. Enzymatic Catalysis

Much work in biochemistry and chemistry involves the study of enzymes. Of particular interest are their enormous selectivity and rate enhancements. Approaches to understanding these phenomena can be separated into those that involve enzymes (protein-based) and those that involve model systems (non protein-based). Each method has its own advantages and restrictions.

Protein-based approaches include site-directed mutagenesis and chemical modification of amino acid residues.¹ Recently, Schultz has developed a technique which allows the incorporation of non-natural amino acids into proteins.² In all these protein-based approaches, altering side chains removes or creates individual interactions such as hydrogen bonds, electrostatic interactions, or van der Waals contacts. These modified intermolecular or intramolecular interactions may affect binding and catalysis. Thus, the effects of a modification can provide insight into the nature of binding and catalysis in the original protein. A disadvantage of these kinds of techniques is that the modification may cause alterations in the mode of substrate binding or the larger structure of the enzyme. Therefore, a definitive study requires detailed structural information about the enzyme and its variants. However, this information is not always available or easily obtained.

Non-protein-based approaches, which are necessarily model studies, have the advantage of structural simplicity and are therefore more amenable to spectroscopy. Also, functional group limitations are removed, since there is no restriction to amino-acid-based building blocks. Research groups use model synthetic hosts to systematically explore intermolecular interactions and to take advantage of such interactions in attempting to create enzyme active site mimics. The physical organic chemist, for example, would vary steric or electronic effects to learn more about a catalytic system. A model system may in turn

give new insight to natural systems.

Studies of natural systems have revealed some fundamental principles of molecular recognition and catalysis which are incorporated to various degrees in synthetic systems. These principles are based on enzyme interactions with both the ground state and the transition state of a reaction. A ground-state effect which has tremendous impact on reaction rates is that of simply bringing together the substrate(s) and the enzyme's catalytic site. This proximity effect essentially turns an intermolecular reaction into an intramolecular one. The entropy cost is compensated by favorable binding interactions, resulting in an overall favorable binding energy. As a result, the proximity effect can be responsible for a factor of 10^8 M increase in rates at 1 M and 25 °C in the absence of strain and solvation effects.³ This entropy effect is often discussed in terms of effective molarity (EM), which is the ratio of the rate constant for the intramolecular reaction to the second-order rate constant for the corresponding intermolecular process. Many pairs of nonenzymatic reactions have been studied this way⁴ and effective molarities as high as 10^{13} M have been recorded. In some cases, the relief of ground-state strain energy is responsible for such large EM values.

Another fundamental concept relevant to enzyme catalysis involves intermolecular forces between the active site and the bound substrate or transition state. Although the idea of the transition state of a reaction had yet to be developed, in 1921 Michael Polanyi suggested that rate enhancement by adsorption to a catalyst depends on the stronger affinity of the catalyst for the products than for the reactants.⁵ Linus Pauling proposed in 1946 that the "entire and sole source of catalytic power is the stabilization of the transition state; reactant-state interactions are by nature inhibitory and only waste catalytic power."⁶ The mode of catalysis in which an enzyme binds the transition state, or transition-state stabilization, is widely accepted. The binding affinities of transition-state analog enzyme inhibitors which have enhanced binding over the substrates by factors of 10^3 and 10^4 demonstrate this well.⁷ The success of catalytic antibodies raised against transition-state

analog inhibitors provides further support for this mechanism.⁸ In general, it is found that binding interactions which stabilize the transition state more than the ground state will result in a rate enhancement.

The adoption of a split-site model for enzyme-substrate binding⁹ allows a slightly different perspective on transition-state stabilization. This model (Figure 1.1) describes the energetics of substrate binding as the sum of interactions with the enzyme at distinct binding and reactive sites. Ground-state binding site interactions (of energy $\Delta(\text{ES}_\text{B})$) are preserved in the transition state, while reactive site interactions (of energy $\Delta(\text{ES}_\text{R})$) change upon moving from the ground state to the transition state.

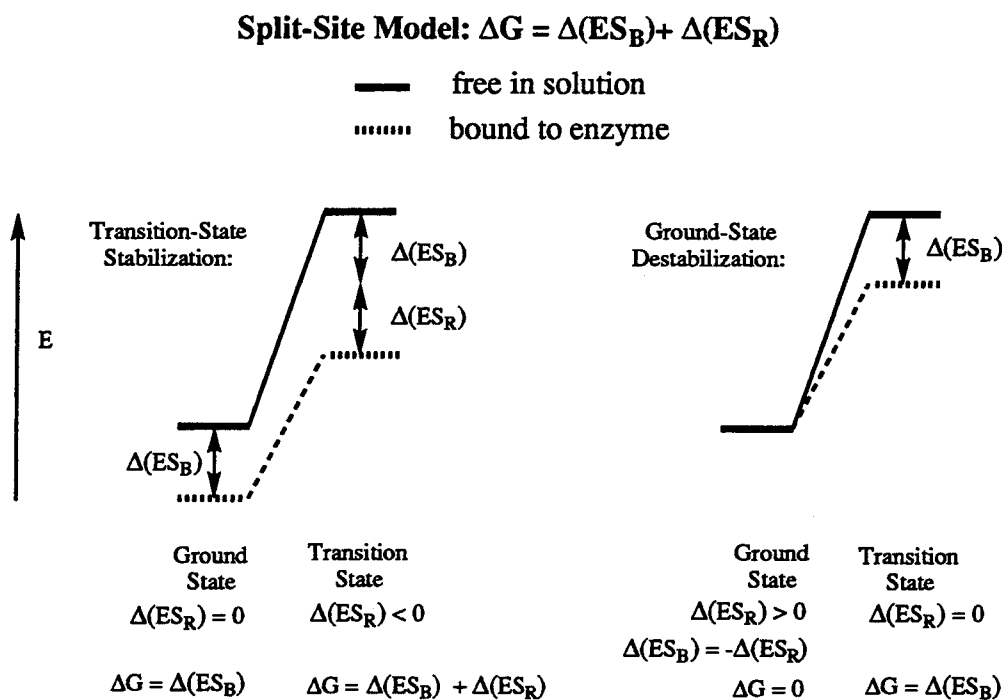


Figure 1.1. Split-site model describing the substrate's ground-state and transition-state binding in the case of transition-state stabilization and in the case of ground-state stabilization. For transition-state stabilization, pictured on the left, the substrate gains favorable interactions of energy $\Delta(\text{ES}_\text{R})$, while for ground-state destabilization, pictured on the right, the substrate loses unfavorable interactions of energy $\Delta(\text{ES}_\text{R})$.

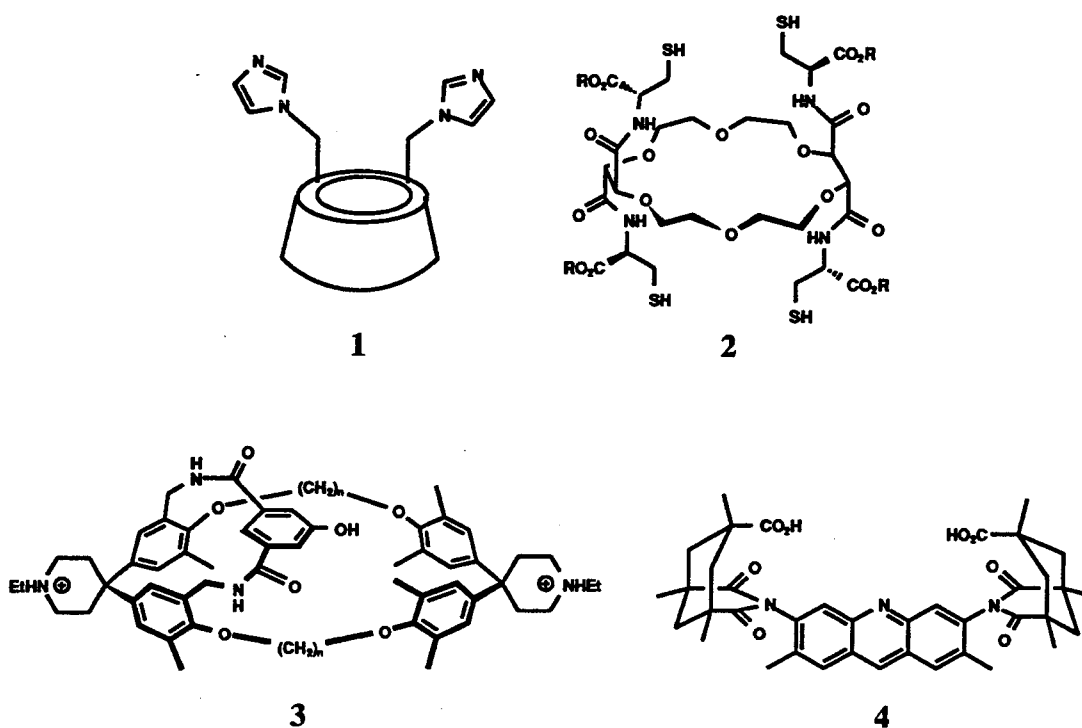
This model readily shows that not only transition-state stabilization, but also

substrate destabilization can be a mechanism for enzymatic rate enhancement. For transition-state stabilization, the reactive site develops stabilizing interactions as the reaction proceeds, while for ground-state destabilization the reactive site loses destabilizing interactions. Although both these mechanisms lead to net transition-state stabilization and rate-enhancements, one can envision different sorts of intermolecular interactions for each mechanism.

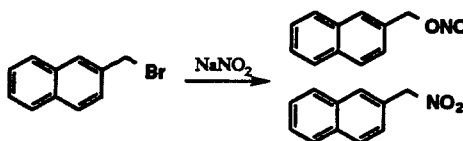
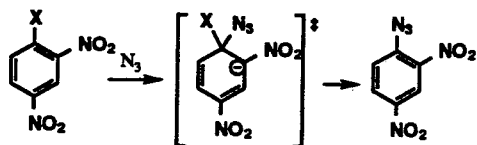
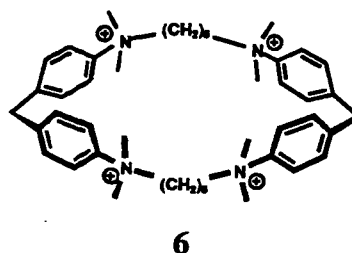
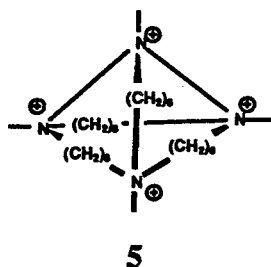
Although the proximity effect and net transition-state stabilization are understood to be the two main mechanisms of enzymatic catalysis, they are manifestations of specific molecular interactions. It is these interactions that are examined by biochemists and chemists. On a molecular level, the proximity effect and the ground-state and transition-state stabilization are due to one or more favorable interactions such as hydrophobic effects, complementary electrostatics, and hydrogen bonding. These effects have been thoroughly examined using organic host-guest complexes.¹⁰ Some unfavorable interactions involved in ground-state destabilization include desolvation of a reactive center, steric distortion, or loss of entropy.

B. Biomimetic Catalysis

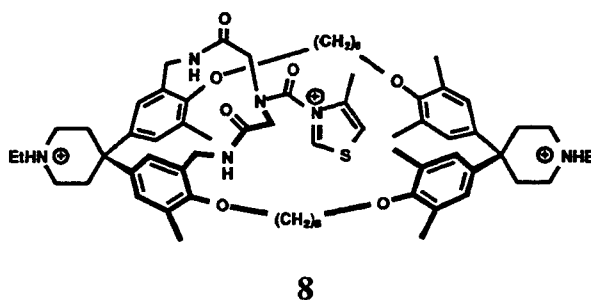
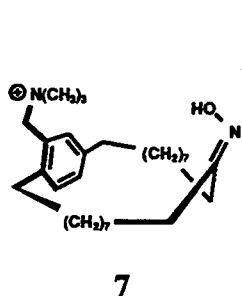
Many synthetic model systems have been designed to examine one or more of the rate-enhancing mechanisms thought to be found in enzymes. Alternatively, synthetic systems may explore molecular mechanisms which have yet to be discovered in natural systems. Various substrate binding sites have been constructed out of functionalized cyclodextrins, macrocyclic polyethers, and cyclophanes. Many workers have used the proximity effect to enhance rates by attaching accessible catalytic groups to the substrate binding site. Examples of each type are pictured below. These representative systems are models for ribonuclease (1), esterases (2, 3), and lysozyme (4).



A second approach in model systems is to use the microenvironment of the binding site to first bind the substrate and then to accelerate the reaction by affording net transition-state stabilization. These reactions may or may not be based on an actual enzymatic transformation. One example, pictured below, is a polymacrocyclic charged host (5) which catalyzes a nucleophilic aromatic substitution reaction by desolvating the nucleophile and stabilizing the extended delocalized negative charge in the transition state.¹¹ The reaction in question is drawn below the host. A system where the host cavity not only accelerates a reaction but also changes the reaction mechanism was developed by Schneider. In this system, drawn below, a positively charged cyclophane (6) suppresses the positively charged S_N1 transition state in favor of the negatively charged S_N2 transition state, as revealed by product ratios using the ambident nucleophile NO_2^- with the electrophile bromomethylnaphthalene.¹² Again, the reaction is presented below the cyclophane.



Catalytic systems which combine reactant proximity with a specific binding microenvironment to effect catalysis have also been devised. For example, pictured below is a paracyclophaneoxime (7) which uses a pendant positively charged group to stabilize the anionic transition state of an acyl transfer to its hydroxyl group.¹³ Another example is Diederich's thiamine pyrophosphate-based cyclophane (8), which catalyzes a benzoin condensation. The cavity desolvates and therefore activates the thiazolium group, providing a demonstration of ground-state destabilization.

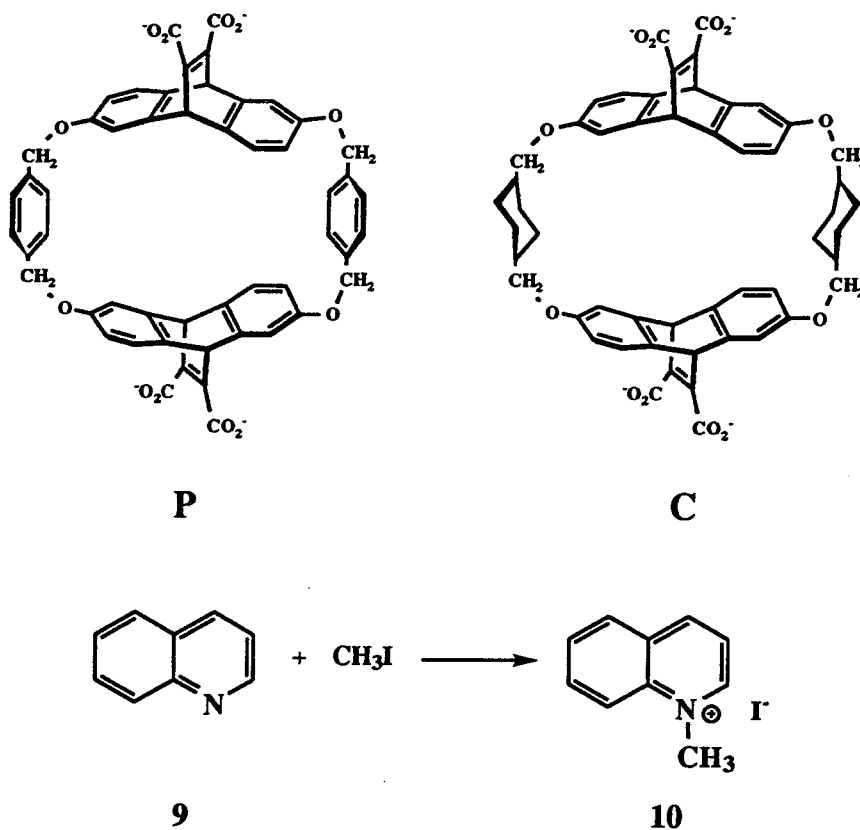


The two mechanisms of enzymatic catalysis, alone or together, have been successfully incorporated into simple model systems. The work that will be discussed in this thesis involves a model system that does not use the proximity effect to achieve

catalytic ability. Instead, the unique microenvironment of a cyclophane host has been explored and used as a catalytic medium.

C. Dougherty Model System

In the Dougherty group, the nature of the binding environment of host **P**, pictured below, has been exploited to catalyze a reaction which develops positive charge in the transition state.¹⁴ Although host **P** was not designed to mimic any known enzymatic catalytic mechanism, the principles involved may be relevant to enzymatic systems as well. The catalyzed reaction in question, an S_N2 Menshutkin reaction, is also shown below. Quinoline (**9**) is methylated to produce N-methylquinolinium iodide (**10**).



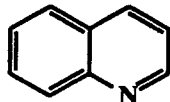
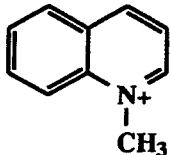
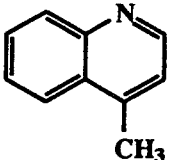
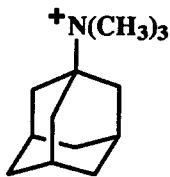
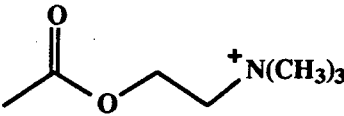
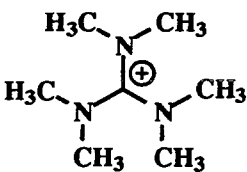
A review of the binding properties of the chiral (D_2) host sheds some light on this novel catalytic mechanism.¹⁵ The binding cavity of host **P** is hydrophobic and aromatic,

and has a surprisingly high affinity for charged compounds. Therefore, a transition state which develops positive charge is expected to be stabilized by the host. This behavior is not attributed to electrostatic stabilization by the carboxylates since they are fixed away from the binding cavity. Strikingly, the placement of a carboxylate group at the xylyl linker of the binding region does not substantially increase binding affinities of cationic guests.¹⁶ Instead, the π -electrons are thought to stabilize the cation by a combination of charge-dipole, charge-quadrupole, charge-induced dipole, and London dispersion interactions. These interactions are collectively called the cation- π interaction. The mechanism of catalysis is attributed to transition-state stabilization without the benefit of the proximity effect.

To further understand the nature of such transition-state stabilization, first the cation- π interaction must be examined. The stability of the cation- π interaction is demonstrated by substantial experimental and theoretical support.¹⁷ For example, evidence of aromatic compounds acting as hydrogen-bond acceptors has been well documented. Zewail et al. studied the dissociation of the tyrosine-benzene complex by picosecond photofragment spectroscopy and estimated the energy of the hydrogen bond to be 4 kcal/mole at room temperature *in vacuo*.¹⁸ Optical and microwave spectra of the benzene-ammonia dimer in the gas phase show a 2.4 kcal/mole hydrogen bond.¹⁹ Also, Burley and Petsko searched protein crystal structures and found a statistically significant occurrence of amino-aromatic interactions.²⁰ A high-resolution crystal structure of pancreatic trypsin inhibitor shows two hydrogen bonds with tyrosine, less than van der Waals distance, with upfield shifts of the hydrogen-bonded proton.²¹ Benzene and water form a hydrogen-bonding interaction as well.²² The T-shaped benzene-benzene interaction also reflects this property, since the edge of a benzene ring is positively charged and the face is negatively charged. In barnase, where tryptophan 94 faces the edge of histidine 18, workers determined a stabilization energy of 1.4 kcal/mole for the interaction with protonated histidine.²³

A quantitative evaluation of binding affinities of a representative sample of guest compounds for the Dougherty hosts is shown below in Table 1.1. As a preorganized cavity of aromatic rings, host **P** has binding properties consistent with that of a hydrophobic anionic site.

Table 1.1 Binding Free Energies (-kcal/mole) of Representative Guests for Host **P** and Host **C**

Guest	P	C
 (9)	5.3	5.9
 (10)	8.4	6.6
 (11)	5.9	6.0
 (12)	6.7	5.4
 (13)	6.2	--
 (14)	4.6	--

The guests can be roughly classified into two groups: flat aromatic compounds and tetraalkylammonium compounds. These differently shaped classes reflect the existence of two distinct binding conformations -- rhomboid and toroid -- of host **P**. These conformations are supported by CD measurements, NMR shift data, and computational studies. Considering the class of flat aromatic guests, one should compare lepidine (**11**) and N-methyl quinolinium (**10**) to see a 2.5 kcal/mole binding enhancement for the charged guest. This value is expected to be a good estimate of the magnitude of the cation- π effect, since the two structures are nearly identical in size, shape, and hydrophobic surface area. The binding of tetraalkylammonium compounds reveals high affinities as well. These data suggested that biological systems which involve ammonium compounds such as acetylcholine (**13**), which is bound by host **P** with an energy of 6.2 kcal/mole, might use aromatic rings as recognition elements in binding sites.²⁴ This prediction has been born out in the case of acetylcholine esterase, which is found to be rich in aromatic residues near the binding site.²⁵ This observation contradicts the previously proposed electrostatic stabilization by a carboxylate moiety.

A useful comparison molecule to study with host **P** is host **C**, which uses *trans*-1,4-dimethylenecyclohexyl groups instead of *p*-xylyl groups to link the two ethenoanthracene units. This comparison should help discern the contribution of hydrophobic versus aromatic effects to guest binding. Host **C** binds neutral molecules well, since cyclohexane is slightly more hydrophobic than benzene.²⁶ Host **P**, having two more aromatic rings than host **C**, binds positively charged compounds better, which is consistent with the extra stability provided by "onium"-aromatic interaction. It is this interaction which helps stabilize a partial positive charge in the transition-state.

However, the cation- π effect does not provide a complete explanation of the transition-state stabilization offered by host **P**. A better understanding of the catalysis is obtained by studying the energetics of the irreversible host-catalyzed and uncatalyzed reaction of quinoline and methyl iodide, described below. If the cation- π effect were the

sole stabilizing force, the fully charged product would be stabilized more than the partially charged transition state. Using the energy diagram below, in Figure 1.2, the transition-state stabilization energy can be derived from experimentally determined quantities. Binding affinities for substrates and products were determined by ^1H NMR titration experiments, and rate constants were determined by ^1H NMR integration versus an internal standard. Suitable non-macrocyclic controls and competitive inhibition studies were performed to demonstrate that binding in the aromatic cavity is a requirement for catalysis.

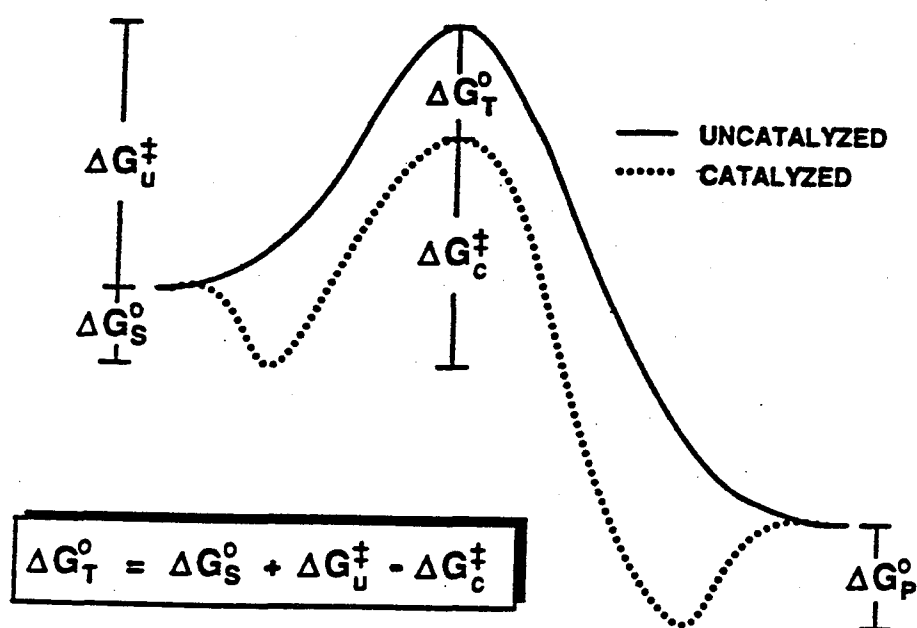


Figure 1.2. Schematic free energy diagram for catalyzed and uncatalyzed reactions.

Results for hosts P and C, shown below in Figure 1.3, demonstrate clearly that the charged product is bound more tightly than the neutral substrate due to the cation- π effect; however, it is the transition state that is bound most tightly. This phenomenon led to the proposal that the cation- π effect stabilizing the growing positive charge is augmented by the host's polarizable π electrons that stabilize the long, weak dipolar bonds of the transition state. In contrast, water cannot effectively solvate a short-lived dipole, since it is not very polarizable and water must reorient to change its dipole direction. Therefore, the π

electrons of the host may better respond to the fleeting transition-state dipoles than water does. Comparing host **C** with host **P** shows that host **C** is a less effective catalyst. Therefore, the aromatic character of host **P** is implicated as part of the catalytic mechanism. Note that none of the catalysis is due to the proximity effect, since the macrocycle does not bring the reactants together. The relatively small rate enhancement of 80 reflects the absence of this entropic effect.

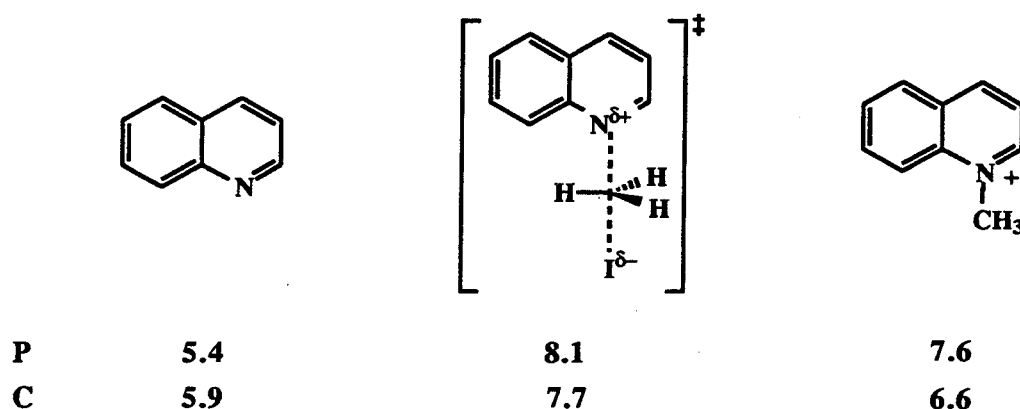
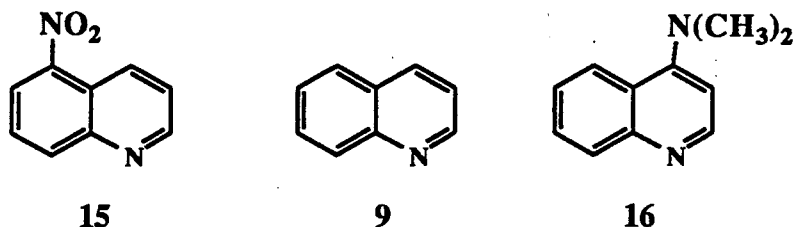


Figure 1.3. Binding free energies of substrate, transition state, and product for hosts **P** and **C** (kcal/mole).

A systematic study of reactant substituent effects should provide more information about the nature of the catalytic ability of the host. Concurrent with this thesis work, quinoline substituent effects on alkylation rates were studied by Dr. Leslie Jimenez.²⁷ The results for the three compounds drawn below reveal that host catalysis decreases from the substrates **16** > **9** > **15**. Therefore, early transition states with less positive charge are better stabilized by host **P** than later transition states with more positive charge. This preference further confirms the requirement for a stabilizing interaction beyond the cation- π effect to fully describe the nature of catalysis by host **P**. Not only are partially charged transition states better stabilized than fully charged products, but those alkylation transition states with least charge are stabilized the most. Here the relative polarizability of the

transition-states is more important than the relative amount of positive charge. The substrate with the substituent that disperses positive charge is best catalyzed by host **P**. This is the substrate that has a more polarizable transition state. These observations indicate that in alkylation reactions catalyzed by host **P**, the polarizability effect of the host predominates over the cation- π effect.



The data from Figure 1.3 above suggest that host **P** can also catalyze a dealkylation reaction, but since the Menshutkin reaction is irreversible under practical conditions, a more reactive substrate for an analogous dealkylation must be chosen. A new class of guest compounds, dialkyl aryl sulfonium salts,²⁸ was chosen to provide good candidates for these studies. These compounds are reactive, and variously substituting the aryl group provides a series of structurally similar compounds with different substituents amenable to Hammett analysis. The dealkylation reaction that was studied in detail in this thesis is shown below in Figure 1.4, where X represents the various substituents. The chirality of an appropriately substituted sulfur center provides another reason to study these compounds as substrates. These chiral compounds eventually can be used to study the enantioselectivity of binding and catalysis by host **P** and related hosts. In addition to providing mechanistic information for the cyclophane system at hand, the study of sulfonium salt substrates is biologically relevant. S-adenosylmethionine (SAM, **17**), drawn below, is a ubiquitous cofactor in biological methylations,²⁹ and insights from these model studies may be applicable to natural systems.

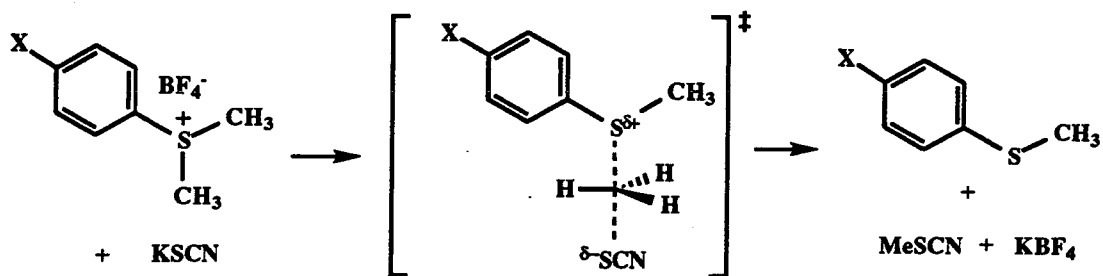
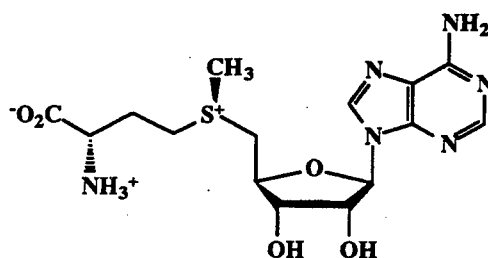


Figure 1.4. Scheme of substrates, transition states, and products of the dealkylation of dimethylaryl sulfonium salts.



17

II. RESULTS AND DISCUSSION

Since sulfonium salts were chosen as analogs to the quinolinium compounds used in alkylation reactions, and because they also represent a new class of guest molecules for host **P**, they were fully characterized in terms of their binding affinities and orientations. The choice of sulfonium salts studied was governed, in part, by their chemical and configurational stability. Solvolysis in the pH 9 borate buffer used to dissolve the hosts was a potential problem. However, water solvates the sulfonium salt better than the less polar transition state or product, so this hydrolysis is not favored for the less reactive sulfonium salts. For example, the rates of solvolysis of *t*-butyldimethylsulfonium salts in water are on the order of 10^{-4} s^{-1} .³⁰ The choice of a non-nucleophilic counterion such as tetrafluoroborate should minimize anion-assisted displacement reactions. Also, the barrier

to inversion for a sulfonium salt is not high enough to prevent eventual racemization via inversion at sulfur. The groups attached to sulfur profoundly affect the rate of racemization of sulfonium salts in known ways. Large, bulky groups speed racemization, while aryl groups and electron-withdrawing groups raise the inversion barrier. Dialkylaryl sulfonium salts represent the most stable salts, with a rate of racemization of $7.4 \times 10^{-7} \text{ s}^{-1}$ in methanol at 25°C .³¹ The class of sulfonium salts which most resemble N-methyl quinolinium compounds, the S-methyl benzothiophenes, are quite reactive alkylating agents but were eventually abandoned for use in catalysis studies. They will be discussed further below. Sulfoxide compounds are also chiral, but are much more stable to inversion. Because they exhibit some zwitterionic character, sulfoxides were selected as stable chiral candidates for studying the cation- π effect.

A group of sulfonium salts and sulfoxides were synthesized and aqueous NMR titration binding studies were performed with the (S,S,S,S) isomer of host **P**. The data are shown below in Table 1.2.

Table 1.2. Binding Free Energies to Host **P** and D-values for New Classes of Guests

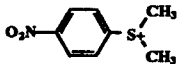

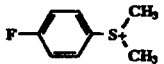
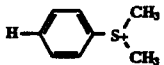
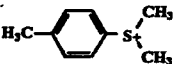
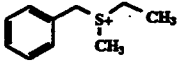
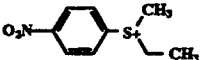
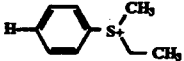
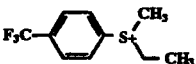
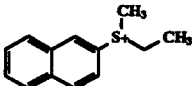
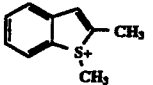
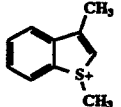
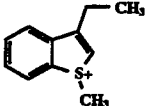
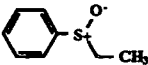
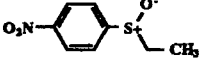
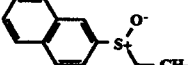
Guest ($-\text{BF}_4$ salts)		$-\Delta G$ (kcal/mole)	D-value $\alpha\text{-CH}_3$ (Hz)	D-value distal- CH_3 (Hz)	D-value aromatic-H (Hz)
	18	5.7 4.5(C) ^a	870, 680 160, 200	N/A N/A	1170, 970 --
	19	6.2	800, 680	N/A	1020, 616
	20	5.5	980, 840	N/A	1160, 580
	21	5.3	970, 800	N/A	960, 540
	22	5.9	890, 780	215	1160, 670

Table 1.2 (continued)

Guest ($\cdot\text{BF}_4$ salts)		$-\Delta G$ (kcal/mole)	D-value $\alpha\text{-CH}_3$ (Hz)	D-value distal- CH_3 (Hz)	D-value aromatic-H (Hz)
	23	5.7	880	540	>600
	24	6.4	850	280	>1000
	25	5.7	1100	670	>800
	26	6.3 6.6 ^b (^{19}F)	1120 N/A	560 N/A	>800 N/A
	27	6.6	630	390	>1200
	28	6.2	780	560	--
	29	5.8 6.0 ^c (TBP)	360 820	320 270	-- --
	30	6.3	720	260	--
	31	< 3.3	N/A	N/A	N/A
	32	6.0	370	120	690, 690
	33	5.9	310	60	>800

a) using host C

b) as determined by ^{19}F NMR chemical shifts

c) using host TBP in 10% acetonitrile pD = 9 buffer

A benefit of using NMR is that the chemical shift changes on binding reveal the shielding or deshielding environment experienced by the host and guest and therefore yield some information about the binding orientation(s) as well as the binding constants.

Analysis of an NMR titration experiment involves solving for two unknowns: the binding affinity (K_a) and the maximum upfield shift (D) of each proton in the bound state. The D -value is the difference between the chemical shift of a proton of an unbound guest and that of the same proton of the bound guest. D -values can be taken as a measure of how close a proton is to the shielding face of the aromatic rings deep inside the aromatic host. The relevant equations are defined mathematically as follows in terms of concentrations and NMR chemical shifts. Here, H is host, G is guest, $[X]_0$ represents total initial concentration, δ_{obs} is the observed NMR shift of a guest proton, δ_{free} is the NMR shift of the proton in an uncomplexed molecule, and δ_{bound} is the NMR shift of the proton in a completely bound molecule. Considerations and limitations of NMR titrations for the determination of binding constants have been reviewed elsewhere³² and will not be discussed here.

$$(1) \quad K_a = \frac{[HG]}{[H][G]}$$

$$(2) \quad \begin{aligned} [H]_0 &= [H] + [HG] \\ [G]_0 &= [G] + [HG] \end{aligned}$$

$$(3) \quad D = \delta_{\text{free}} - \delta_{\text{bound}}$$

$$(4) \quad \delta_{\text{obs}} = \delta_{\text{free}} \frac{[G]}{[G]_0} + \delta_{\text{bound}} \frac{[HG]}{[G]_0}$$

Substituting (2) into (1) and rearranging to get (5):

$$[HG] = \frac{1}{2} \left\{ [H]_0 + [G]_0 + \frac{1}{K} - \sqrt{\left([H]_0 + [G]_0 + \frac{1}{K} \right)^2 - 4[H]_0[G]_0} \right\}$$

Using (2) and (3) to put (4) in terms of D and [HG]:

$$(6) \quad \delta_{\text{obs}} = \delta_{\text{free}} - D \frac{[\text{HG}]}{[\text{G}]_0}$$

Substituting (5) into (6) to yield (7) in terms of the desired parameters K_a and D:

$$\delta_{\text{obs}} = \delta_{\text{free}} - D \left\{ \frac{[\text{H}]_0 + [\text{G}]_0 + \frac{1}{K} - \sqrt{\left([\text{H}]_0 + [\text{G}]_0 + \frac{1}{K}\right)^2 - 4[\text{H}]_0[\text{G}]_0}}{2[\text{G}]_0} \right\}$$

The data needed to analyze a binding titration consists of the chemical shifts of the unbound guest (in the absence of host) and the observed chemical shifts during the titration. Because the exchange rate between the free and bound states is fast on the NMR timescale, these observed resonances are weighted averages of the free and bound shifts. A nonlinear least-squares fit of all the observed resonances (equation 7) simultaneously will give a single K_a for the molecule and D-values for all protons examined. The fitting procedure is performed with a program developed in the Dougherty group called Multifit, and the error bars and statistical significance are determined with programs called Lucius and Portia.³³ All studies were performed at a concentration below the critical aggregation concentration of the host (CAC) to avoid nonspecific hydrophobic interactions.

Caution must be used in interpreting the titration data reported for chiral guest compounds (23-33). With racemic mixtures of guests, the NMR spectra showed resonance doubling of all protons. This diastereomeric interaction poses a problem for accurate data analysis. Since each enantiomer will have different D-values and binding constants in the chiral environment of the host, there are too many unknowns to allow a

solution. Therefore, the average of the shifts of the two enantiomers was used in data analysis for each titration point. This approach provides only a rough estimate of the magnitude of the binding affinities for these compounds.

The data suggest that the sulfonium salts and sulfoxides are bound well by host **P**, through well-known mechanisms. For example, more hydrophobic substituents on sulfur increase the binding constant, as do electron-deficient groups. This is consistent with the host cavity being hydrophobic and electron-rich. The higher binding affinities of the sulfoxides are probably due to their hydrophobicity. A comparison of sulfonium salt guests with quinolinium or tetraalkylammonium guests (Table 1.1) reveals that sulfonium salts have uniformly smaller binding affinities. This is possibly due to the pyramidal nature of the sulfonium center, since it is not sterically complementary to the binding cavity. In contrast, the quinolinium compounds are flat, and well accommodated by the rectangular rhomboid host **P** conformation.

The use of fluorine NMR to determine binding constants has been explored to a limited extent by following the trifluoromethyl fluorine resonance of sulfonium salt **26**. It was hoped that since fluorine has such a wide range of chemical shifts (greater than 150 ppm), the D-value would be large. This technique would then be a sensitive one for use in binding studies. Unfortunately, a maximum upfield shift of only 100 Hz was observed for the guest studied, which is less than that obtained by proton NMR. A binding study that used both proton and fluorine spectra at each concentration shows that the shifts of the two nuclei give approximately the same binding energy of 6.4 to within ± 0.2 kcal/mole.

A pattern of D-values is evident with all of the dialkyl aryl sulfonium salts, indicating that both the aryl group and the sulfonium center are inside the binding cavity. The shifts of the aromatic guest protons are often obscured by the host aromatic protons, so an accurate D-value could not be determined by Multifit analysis. A good estimate based on visual inspection of spectra (when greater than 90% of the guest is bound) reveals that the D-values of the aromatic protons are usually greater than 800 Hz. In general, the alpha

protons are shielded more than the beta protons. This can indicate that the aryl group, alpha methyl group, and the sulfur are buried in the hydrophobic pocket of the host. The electron-deficient guests bind to maximize π - π interaction and to include the sulfonium center and nitro group, if present.

Only two purely aliphatic sulfonium salts have been studied in the Dougherty group. One compound, trimethylsulfonium iodide, was studied prior to this work and has a weak binding constant of 170 M^{-1} .³⁴ The second compound, adamantyldimethylsulfonium tetrafluoroborate (**34**), has been examined in the course of this thesis research. It is pictured below in Figure 1.5 with D-values in Hz for all of its protons. The binding constant ($-\Delta G = 5.7 \text{ kcal/mole}$) is much higher than trimethylsulfonium because the hydrophobic effect of the adamantyl group augments the cation- π affinity. The pattern of D-values indicates that the sulfonium end of the molecule lies deepest within the host binding site. This parallels the findings for the analogous guest adamantyltrimethylammonium iodide (**12**), indicating that for both molecules the cation- π effect is stronger than the hydrophobic effect.

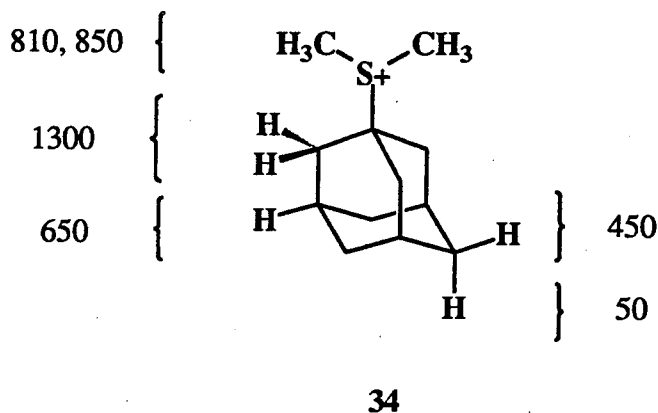
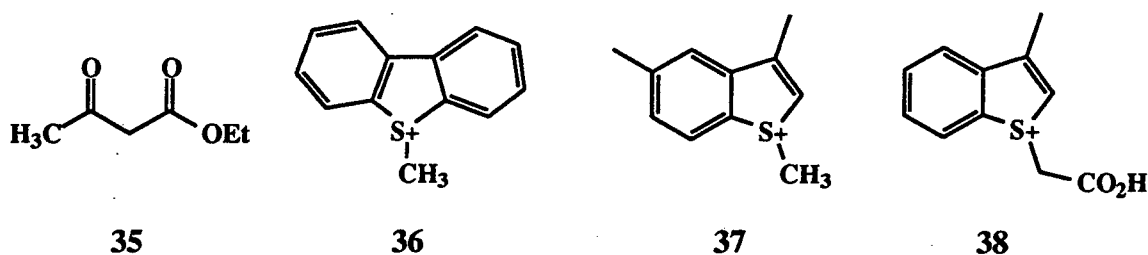


Figure 1.5. Adamantyldimethylsulfonium tetrafluoroborate with D-values in Hertz for each proton.

To study the kinetics of sulfonium salt dealkylation, an appropriate water-soluble

nucleophile and a suitable method for following the progress of the reaction had to be developed. Initially, the carbon nucleophile ethyl acetoacetate (**35**) drawn below was chosen for two reasons. First, the catalysis of carbon-carbon bond formation is a biologically and synthetically important objective.³⁵ Second, the enantioselectivity of the host-catalyzed reaction could be probed since the nucleophilic carbanion is prochiral. However, the use of HPLC to monitor the appearance of alkylated products was hampered by low product extinction coefficients. Additionally, the weak nucleophile required the use of the active alkylating agent S-methyl dibenzothiophenium (**36**), also pictured below. The carboxylates of the host are alkylated under these conditions, so this nucleophile and substrate had to be abandoned. The two nucleophiles *p*-nitrophenolate and phenolate were tested because of the ease of monitoring the disappearance of nitrophenolate or the appearance of anisole by ultraviolet spectroscopy. These too were less reactive than the host carboxylates toward alkylation.



Restricting the nucleophile to one which is water-soluble, fairly reactive, and non-basic, such as thiocyanate, the reactive S-methyl benzothiophene compounds were then assayed as potential substrates for dealkylation studies. Using NMR to follow the substrate disappearance in these relatively fast reactions, it was determined that 3-methyl,S-methyl benzothiophene (**29**) reacts more slowly in the presence of host. Assuming that this rate decrease was due to a binding conformation which placed the S-methyl group in a location that was sterically inaccessible to the nucleophile, differently substituted sulfonium salts (**28**, **30**, **37**, **38**), shown in Table 1.2 and above, were synthesized to correct this

problem. Although it was hoped that the substituents would favor a binding conformation in which the methyl group points out into solution, the 3-ethyl, S-methyl benzothiophene (30), the 3-methyl,5-methyl, S-methyl benzothiophene (37), and the 3-methyl,S-carboxymethyl benzothiophene (38) reacted more slowly in the presence of host. The 2-methyl,S-methyl benzothiophene (28) showed no change in rate in the presence of host.

The relatively unreactive dialkylaryl sulfonium salts were chosen next for study as candidates for host-catalyzed dealkylation by thiocyanate. The advantage of these compounds is that their probable binding conformations, as determined by NMR D-values and CPK models, always result in one alkyl group being exposed to solvent and therefore to the nucleophile. The use of ultraviolet spectroscopy and gas chromatography to monitor the appearance of sulfide product was attempted, but failed due to the very low solubility of product in the aqueous buffer. NMR was used to monitor alkylation reactions and the dealkylation reactions with more reactive substrates. However, alpha methyl protons of the guests undergo base-catalyzed deuterium exchange in D₂O at 35° C with a rate constant³⁶ of $5.0 \times 10^{-5} \text{ M}^{-1}\text{s}^{-1}$ which precludes their use for dealkylation studies. The best means of following the reaction over time was found to be the detection of sulfonium salt substrate disappearance by HPLC. This was accomplished by injecting aliquots of the reaction mixture and integrating relative peak areas of the sulfonium salt against an internal standard of potassium hydrogen phthalate over the course of the experiment. Standard curves were created to obtain a response factor for each sulfonium salt in the relevant concentration range.

The kinetics of dialkylarylsulfonium salt dealkylation by thiocyanate in the presence of host follows the kinetic scheme described below in Figure 1.6. In the scheme, X represents the nucleophile thiocyanate. This is a simple Michaelis-Menten scheme where the Michaelis constant K_M that describes enzymes is here exactly equal to $K_d = 1/K_S$, and the Michaelis k_{cat} is here defined to be the same as for enzymes. Note that this simple case is not commonly observed for enzymes because of multiple intermediates or slow

dissociation of product. Because of these complications, the Michaelis-Menten k_{cat} is often interpreted as a lower limit for the reaction rate constant, and K_M is interpreted as an apparent dissociation constant.³⁷ The uncatalyzed reaction is an irreversible S_N2 reaction with bimolecular rate constant k_{un} . The catalyzed reaction is an irreversible S_N2 reaction between the nucleophile and the host-substrate complex HS with bimolecular rate constant k_{cat} . The binding constants K_S and K_P are determined by NMR titration experiments as outlined above. The uncatalyzed rate constant is determined graphically under pseudo-first-order conditions.

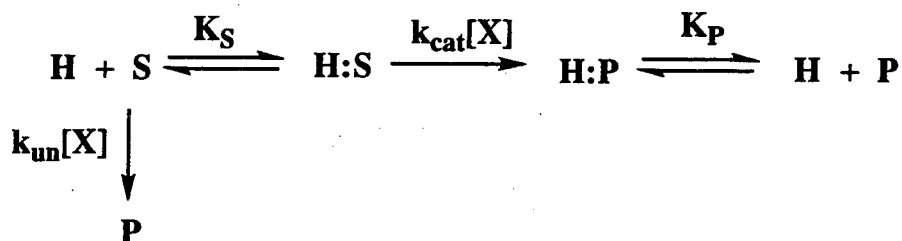


Figure 1.6. Michaelis-Menten scheme describing the kinetics of reactions in the presence of a host catalyst. (H = host, S = substrate, P = product, X = nucleophile.)

The determination of k_{cat} is more involved. Using the kinetic scheme in Figure 1.6 with experimentally determined binding constants, the rate constant without host (k_{un}), and the observed substrate concentration over time, one can produce a numerical simulation of the data that provides k_{cat} . The following rate equations describe the reaction rate outside (8) and inside (9, 11) the host cavity:

$$(8) \quad -\frac{d[S]}{dt} = k_{un}[S][SCN^-]$$

$$(9) \quad -\frac{d[\text{HS}]}{dt} = k_{\text{cat}}[\text{HS}][\text{SCN}^-]$$

$$(10) \quad [\text{HS}] = K_s[\text{H}][\text{S}]$$

$$(11) \quad -\frac{d[\text{HS}]}{dt} = k_{\text{cat}}K_s[\text{H}][\text{S}][\text{SCN}^-]$$

In the presence of host, both catalyzed and uncatalyzed reactions are occurring simultaneously, giving the following rate equation:

$$(12) \quad -\left(\frac{d[\text{S}]}{dt} + \frac{d[\text{HS}]}{dt}\right) = (k_{\text{un}} + k_{\text{cat}}K_s[\text{H}])([\text{S}][\text{SCN}^-])$$

Both [S] and [HS] change throughout the study, and the product formed can compete with the substrate for the host binding site. This system of equations must be solved numerically and was accomplished using the kinetics simulation software which was written by Dr. Richard Barrans.³⁸ Unlike quinoline alkylation, the sulfonium salt dealkylation does not suffer from product inhibition since the product is bound less tightly than the substrate.

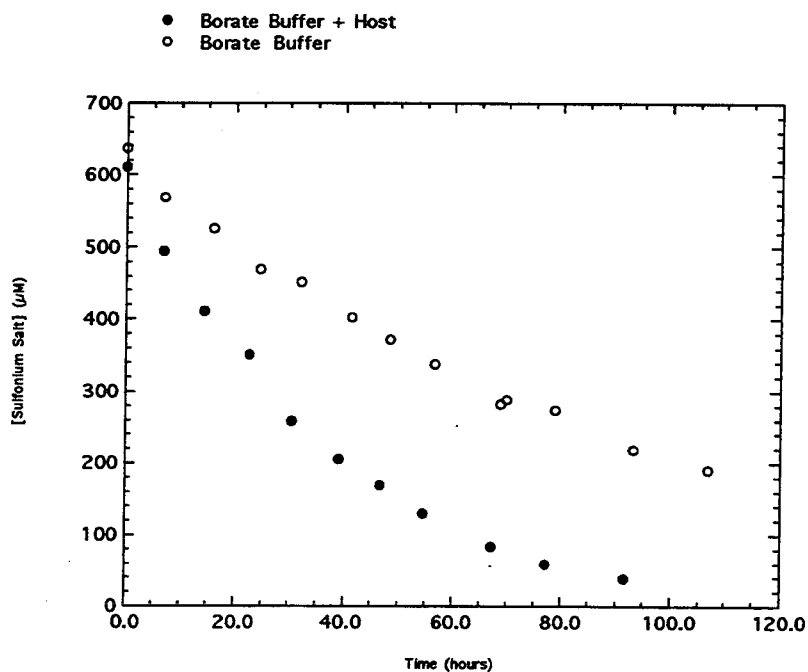


Figure 1.7. Experimental kinetics data showing the decrease in sulfonium salt concentration over time in the presence and absence of host P.

A sample of experimental data for uncatalyzed and host-catalyzed dealkylation of dimethyl-(*p*-nitrophenyl)sulfonium tetrafluoroborate is given above in Figure 1.7.

Concentrations of reagents used in the reaction mixture were as follows: $[H]_0 = 554 \mu\text{M}$, $[G]_0 = 610 \mu\text{M}$, $[\text{KSCN}]_0 = 25.56 \text{ mM}$. The graph in Figure 1.8 is the output of the Kinetics Simulator, demonstrating the goodness of fit between the experimental data points of Figure 1.7 and the course of a simulated reaction if $k_{\text{cat}} = 3.99 \times 10^{-4} \text{ M}^{-1}\text{s}^{-1}$. Host P does in fact catalyze dealkylation of all sulfonium salts studied, as predicted by earlier work and detailed in the introduction.

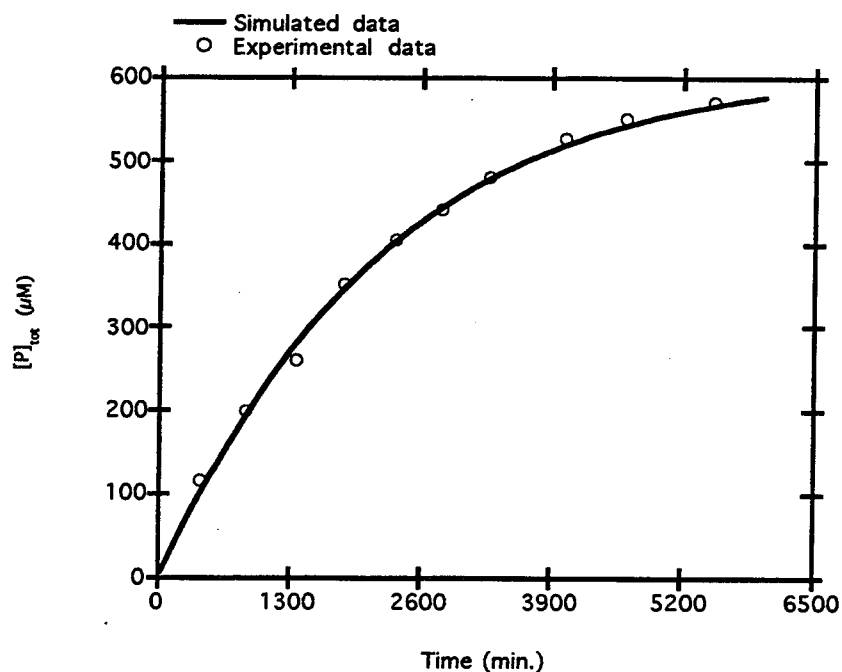


Figure 1.8. Kinetics Simulator output showing observed and simulated data for a dealkylation reaction in the presence of host P.

Various control experiments support this kinetic scheme. The kinetics are first-order in thiocyanate, in both the presence and absence of host. That the catalyzed reaction is first order in $[\text{HS}]$ is supported by the goodness of fit between experimental and

simulated data using this model as shown in Figure 1.8. Another important control was the addition of a competitive inhibitor, 5-nitroquinoline (15). A competitive inhibitor binds to the host, displacing the substrate and therefore lowering the observed rate constant (k_{obs}) for a catalyzed reaction. The simulation program includes a parameter to account for the presence of an inhibitor of known binding constant K_I , and describes the observed suppression of k_{obs} with good accuracy. The dealkylation was monitored on three separate occasions for the compound ethylmethyl(*p*-nitrophenyl)sulfonium tetrafluoroborate, yielding the same value for k_{cat} with good reproducibility.

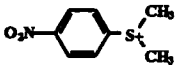
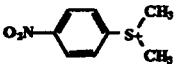
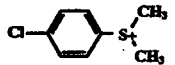
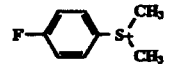
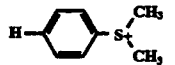

The free energy diagram for these reactions given in Figure 1.2 in the introduction shows that ΔG_T can be simply calculated using the experimentally obtained parameters, where ΔG_T is the free energy difference between the transition state energy in aqueous buffer and its energy in the host binding site. Thus ΔG_T is exactly a measure of transition-state stabilization. The relevant data from the studies are listed in Table 1.3 below. The rate constants for each reaction are listed in Table 1.4.

Table 1.3. Rate Enhancements and Binding Free Energies of Substrate, Transition-State and Product (-kcal/mole)

Substrate	Host	$k_{\text{cat}}/k_{\text{un}}$	$-\Delta G_s$ (kcal/mole)	$-\Delta G_t$ (kcal/mole)	$-\Delta G_p^a$ (kcal/mole)
	P	3.3	5.7	6.5	4.4
	C	9.4	4.5	5.9	4.4
	P	2.6	6.2	6.8	4.4
	P	2.3	5.5	6.0	3.9
	P	2.0	5.3	5.7	3.9
	P	1.9	5.9	6.3	4.4

a) estimated, due to poor solubility in buffer

Table 1.4. Sulfonium Salt Dealkylation Rate Constants

Substrate	Host	k_{un} ($M^{-1} s^{-1}$)	k_{cat} ($M^{-1} s^{-1}$)
	P	1.20×10^{-4}	3.99×10^{-4}
	C	1.20×10^{-4}	1.13×10^{-3}
	P	8.18×10^{-6}	2.16×10^{-5}
	P	5.46×10^{-6}	1.25×10^{-5}
	P	4.32×10^{-6}	8.56×10^{-6}
	P	2.22×10^{-6}	4.18×10^{-6}

In all cases studied, the transition state is bound more tightly than the substrate or the product. The resulting rate enhancements, described by k_{cat}/k_{un} , are generally smaller than for alkylation reactions. This was anticipated to be true, considering the hypothetical reverse of the quinoline alkylation reaction, described in the introduction in Figure 1.3, that would have been catalyzed by $7.2 - 7.8 = -0.6$ kcal/mole at room temperature. This agreement is coincidental, since two different reactions are being studied. Again, this catalytic system does not take advantage of any proximity effects to increase rates. A noteworthy observation is that host C is a more effective dealkylation catalyst than host P. Clearly, this information, coupled with the observation that the partially charged transition state is better stabilized by the host than the fully charged substrate, demonstrates that the cation- π effect is not the sole stabilizing force in this catalytic system.

A description of the charge of the transition states in the buffer and in the host microenvironment would reveal the nature of the transition state that is best stabilized by the host. Hammett plots are often used to obtain α , which some workers interpret as a quantitative estimate of the effective charge of the transition-state.³⁹ However, there is

some dispute as to whether the linear free energy relationships that yield α can provide this type of information.⁴⁰

Although a quantitative assessment of transition-state structure is impossible, a qualitative approach can still provide some information to help elucidate the nature of the observed catalysis. One qualitative way to examine how substituent effects change transition-state structure is through the application of the Bell-Evans-Polanyi (BEP) principle.⁴¹ This analysis can be applied to single-step reactions where bonds are simultaneously formed and broken. The diagram in Figure 1.9 below illustrates the analysis for the sulfonium salt dealkylation reaction.

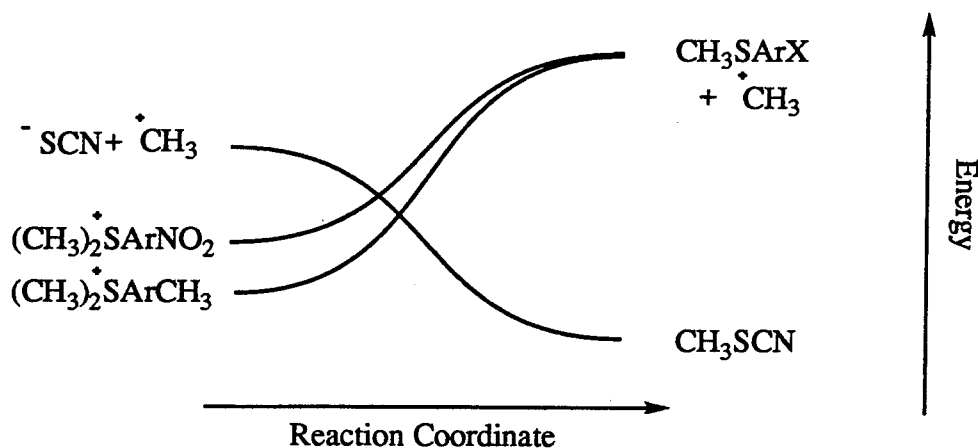


Figure 1.9. BEP diagram for the dealkylation of variously substituted aryldimethylsulfonium salts by thiocyanate.

The reaction, as analyzed by the BEP diagram above, is divided into bond-making and bond-breaking steps. First, the bond-breaking curve showing the change in energy as a function of reaction coordinate is plotted. In this case, the bond broken is the sulfur-methyl bond to yield methyl cation and methyl aryl sulfide. There are two curves, demonstrating that the electron-donating substituent ($-\text{CH}_3$) stabilizes the ground state more effectively than the electron-withdrawing substituent ($-\text{NO}_2$) does. Next, a bond-making

curve is generated from these fragments. In this case, it is the methyl cation plus thiocyanate, making methylthiocyanate. The points where the curves cross are transition states. If a series of reactions is described adequately by this model, two conclusions can be drawn from this type of figure. The first is that for a closely related series of reactions, there is a linear relation between activation energy and the enthalpy of reaction. This result rationalizes the success of linear free-energy relationships. Second, more exothermic reactions have earlier transition states. This idea is better known as the Hammond postulate.

The BEP diagram shows that electron-withdrawing substituents on the leaving group lead to an earlier (reactant-like) transition state with a lower activation energy. Here, this corresponds to a transition state with more positive charge on the sulfur and on the methyl reaction center. Additionally, it suggests a long, polarizable bond between thiocyanate and the methyl reaction center. The lower activation barrier is a result of the ability of the nitro group to disperse accumulating electron density in the transition state. Substrates with more charge-dispersing substituents are more polarizable. Experimentally, electron-withdrawing substituents that can disperse negative charge on the leaving group (methyl aryl sulfide) are found to increase rates both inside and outside the host, as expected for a reaction where the leaving group gains electron density. The response of $k_{\text{cat}}/k_{\text{un}}$ to substituents is in the same direction, indicating that the host preferentially stabilizes earlier, more cationic, and more polarizable transition states. This suggests the cation- π effect is in fact playing some part in the transition-state stabilization. Unlike the alkylation transition states best stabilized by the host, the dealkylation transition states best stabilized by the host are both more cationic and more polarizable.

Although Hammett plots cannot reliably predict absolute transition-state structure, they may be used to analyze the effect of medium changes on reaction rates. This will provide more information about the host's microenvironment. The Hammett equation is:

$$\log \frac{K_x}{K_0} = \rho \sigma_x$$

In this type of analysis, the effect of substituents on the rate or equilibrium constant of the reaction to be studied is compared to their effect on the rate or equilibrium constant of a model reaction. Here, the model reaction is the acid dissociation of substituted benzoic acids. Hammett defined a σ for each substituent such that a plot of $\log[K_x/K_0]$ versus σ will give a slope (ρ) of unity, where K_0 is the equilibrium constant for unsubstituted benzoic acid, and K_x is that for the substituted benzoic acid. These substituent constants (σ_{para} , σ_{meta}) can be used to examine substituent effects for other types of reactions. The success of applying the Hammett relationship to other reaction types depends on the relative importance of inductive and resonance stabilization by the substituent being the same for both the model reaction and the reaction being studied. This ratio of effects turns out to be constant for a surprisingly large number of reaction types. A linear Hammett plot indicates that the transition-state charge does not change significantly with different substituents. This is because σ is defined by a substituent's interaction with the unchanging negative charge of the deprotonated substituted benzoic acids. The substituent effect ρ is a measure of the change in an electrostatic interaction between the reaction center and the substituent. A positive ρ indicates a reaction in which electron density increases at the reaction center adjacent to the aryl group.

The Hammett plot produced from the series of sulfonium salts provides additional insight about the nature of the catalytic mechanisms. Based on NMR D-values, all members of the series have similar binding orientation in the host cavity, so their reactivities may be meaningfully compared. The plot is shown in Figure 1.10 below. The σ_{para} values were used for this analysis since they have been found by others to give excellent correlation for sulfonium salt demethylation in water and acetonitrile.⁴² The linear least-squares fit to each set of data points yields a correlation coefficient greater than 0.99, indicating an excellent fit. The slope for each reaction medium is as follows: $\rho_{\text{buffer}} =$

1.82, $\rho_{\text{host}} = 2.09$, and $\rho_{\text{acetonitrile}} = 1.71$. The $\rho_{\text{acetonitrile}}$ determined in this study is identical to the literature value obtained when hydroxide was used as the nucleophile. The substituent effects are greater in the host medium than in the buffer or in acetonitrile, suggesting either that the host medium best enhances the interaction between the substituent and reaction center somehow, or that the developing charge of the transition state (growing more negative relative to the ground state) is greatest in the host microenvironment.

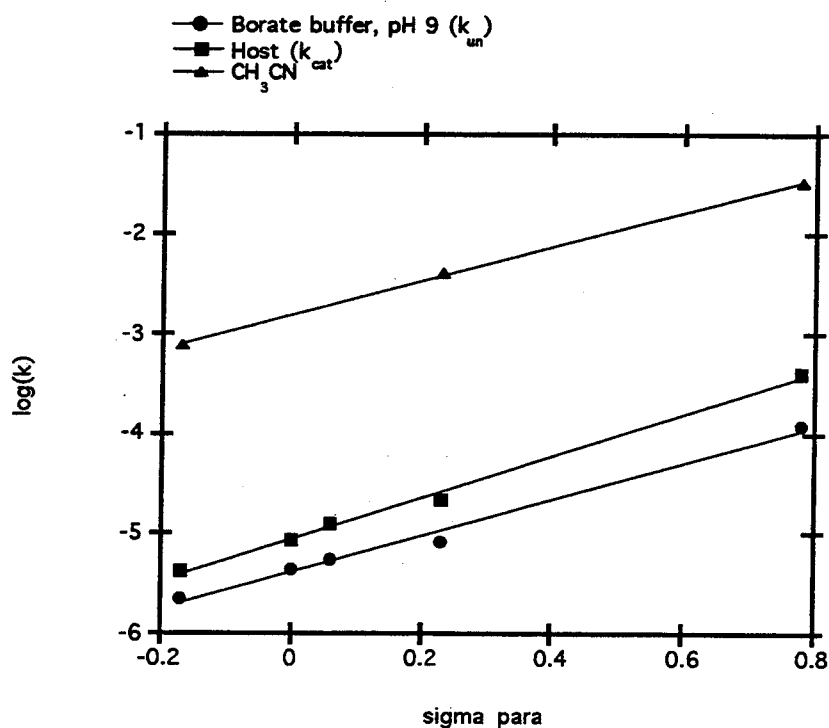


Figure 1.10. Hammett plot of dealkylation reaction rates in borate buffer, acetonitrile, and host P.

The superior ability of host C to catalyze these dealkylation reactions also indicates that the cation- π effect is augmented by some other factor in catalysis. The replacement of two phenyl groups with cyclohexyl groups obviously reduces any cation- π interactions. However, cyclohexane is more polarizable than benzene.²⁶ Host C is therefore a more polarizable microenvironment than host P, and can better stabilize polarizable transition

states.

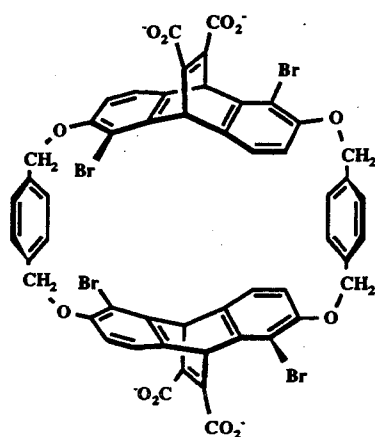
One possible alternative explanation for the enhanced dealkylation rates by hosts **P** and **C** is that the hosts are simply nonpolar media that preferentially stabilize the transition state which has less charge than the ground state. Examination of the ρ of the Hammett plots provides evidence that host **P** is not acting merely as a hydrophobic medium. Relative to rates in buffer, acetonitrile (smaller ρ) decreases substituent's effects while the host (larger ρ) increases them. This qualitative difference indicates the host does not provide a microenvironment entirely similar to a less polar solvent. Additional insight is obtained from thorough studies of reaction rate acceleration by solvent polarity effects.⁴³ Those results show that for reactions with a charged nucleophile, the desolvation of the nucleophile upon going from a protic to a nonprotic solvent is the largest contributor to the rate enhancements. This desolvation effect could be manifested as ground-state destabilization by the host. However, the nucleophile has not been detected to be complexed by the host, and therefore it should not be desolvated by the host. Surprisingly, within a series of dipolar aprotic solvents, the reaction of bromide ion and trimethylsulfonium goes faster in more polar solvents when the desolvation of the nucleophile is factored out. The available information indicates that the rate enhancement is not simply a polarity effect.

III. CONCLUSIONS AND FUTURE DIRECTIONS

The cation- π effect which stabilizes positively charged compounds in the host binding cavity does not fully explain the observed catalysis by host **P**. The additional stabilizing force invoked by the Dougherty group in both catalyzed alkylation and dealkylation reactions is based on the polarizability of the host cavity. Transition states are polarizable and these hosts are also polarizable, in contrast to water. The hosts should better "solvate" a fleeting dipolar polarizable transition state than can water. This

polarizability effect is the best resolution of the data that cannot be explained by the cation- π effect alone. These data include the host's preference for partially charged transition states over fully charged ground states and its preference for earlier alkylation transition states (less charge) than later ones, as well as the superior ability of host **C** over host **P** to catalyze dealkylation reactions. In both alkylation and dealkylation reactions, substrates with substituents that disperse charge and therefore have increased polarizability in the transition state are better stabilized by host **P**.

The next step in confirming the role of polarizability is to test the prediction that a host with polarizable substituents will be a more effective catalyst. This study is being undertaken by Sarah Ngola, using a tetrabrominated host (**TBP**) shown below. Other ways of introducing polarizability to the aromatic system of the host microenvironment may also be fruitful. The catalysis of other reactions with polarizable, cationic transition states is another possible avenue of study. Sample reactions, pictured below in Figure 1.11, include hydride transfer, acid-catalyzed decarboxylation, or acyl transfer. The hydride transfer has been catalyzed previously by a chiral synthetic host through the proximity effect,⁴⁴ but the catalysis by these hosts would be through transition-state (and product) stabilization.



TBP

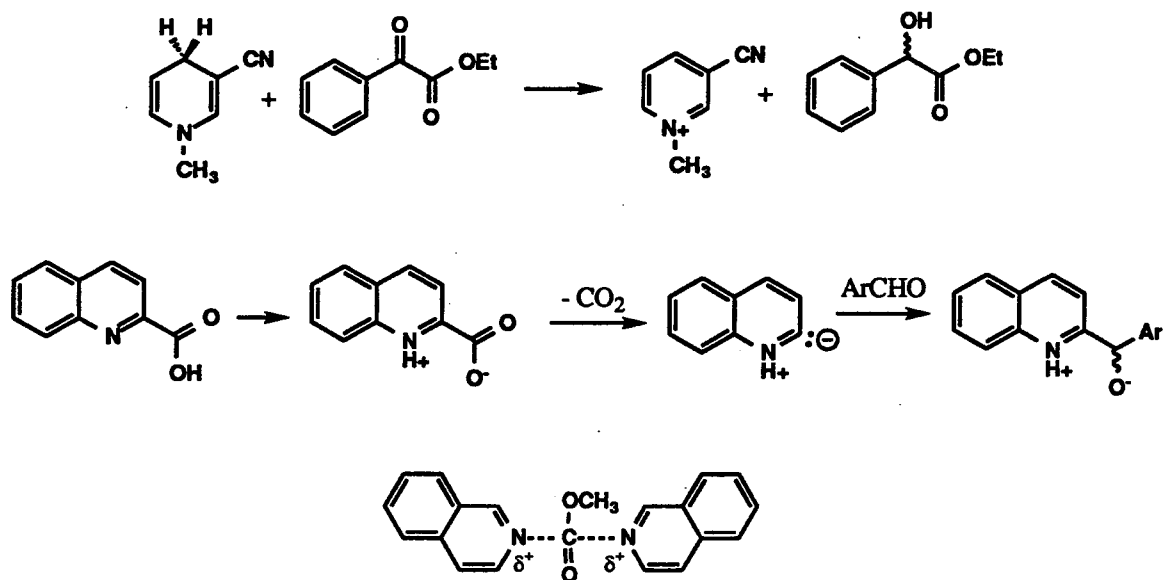


Figure 1.11. Reactions with positive transition states which may be catalyzed by host P.

Another area which warrants further exploration is the enantioselectivity of host P or host TBP. Enantiomeric resolution of sulfoxides or sulfonium salts, or asymmetric oxidation of sulfides to sulfoxides, and subsequent binding studies could be performed to explore ground-state enantioselectivity. Dealkylation of a racemic mixture of sulfonium salts could demonstrate kinetic resolution by the host. Reactions which create stereocenters can also be used to assess the degree of chiral induction by the host environment. For example, the first two reactions drawn above in Figure 1.11 produce stereocenters and so would be suitable probes. However, unlike dealkylation of chiral sulfonium salts, the stereocenter is not cationic and thus may not be close enough to the chiral host environment to have significant asymmetric induction.

The cation- π effect and the polarizable nature of aromatic rings may be viable transition-state stabilizing factors in natural systems. Biological methylations using S-adenosylmethionine (**17**) as a methyl donor are good candidates for such mechanisms. These methylations are ubiquitous, and substrates include proteins, phospholipids, DNA,

RNA, and catecholamines.⁴⁵ The use of aromatic residues as molecular recognition elements for the sulfonium center of SAM and for its transmethylation transition state may be feasible in nonpolar reactive sites. An aromatic residue would preferentially stabilize the transition state, whereas an anionic residue presumably would preferentially stabilize the full positive charge of the ground state of SAM. Kagan and Clarke determined that an amino acid sequence which is unusually rich in aromatic residues is a motif common to several methyltransferases.⁴⁶ The authors suggest that this motif is part of the SAM binding region.

The crystal structures of two methyltransferases are known;⁴⁷ one shows the sulfonium center to be in van der Waals contact with the aromatic ring of a tryptophan residue.^{47a} The picture below (Figure 1.12), taken from Brookhaven Protein Data Bank coordinates of the SAM complex with Hha1 cytosine-DNA methyltransferase, shows this interaction. The sulfur is colored yellow, and the aromatic tryptophan residue is located below it, with the π -system orthogonal to the page.

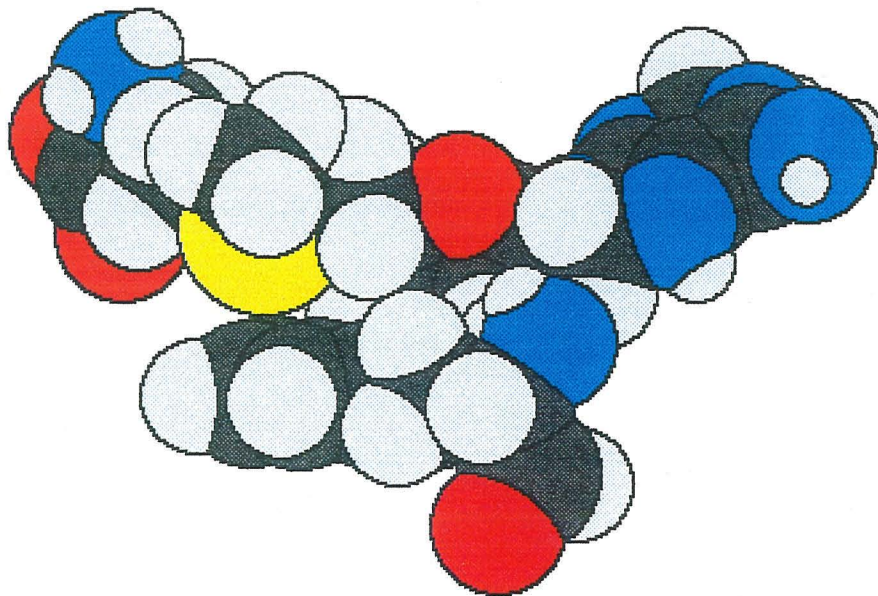


Figure 1.12. The crystal structure showing van der Waals contact between the sulfur of SAM and the aromatic ring of a tryptophan in Hha1 DNA-methyltransferase.

One aspect of sulfonium-aromatic interactions that has been neglected in this discussion is the asymmetry of the interaction. The electron density of the pyramidal sulfonium salts is non-uniform, with the least density around the lone-pair region. This is shown below in Figure 1.13 using a calculated (AM1) electrostatic potential surface for the trimethylsulfonium ion and the tetramethylammonium ion. Using the program Spartan, the electrostatic potentials were calculated and mapped onto the surfaces of total molecular electron density. The same color scale was used for both molecules. Blue indicates lowest electron density, and red indicates highest.

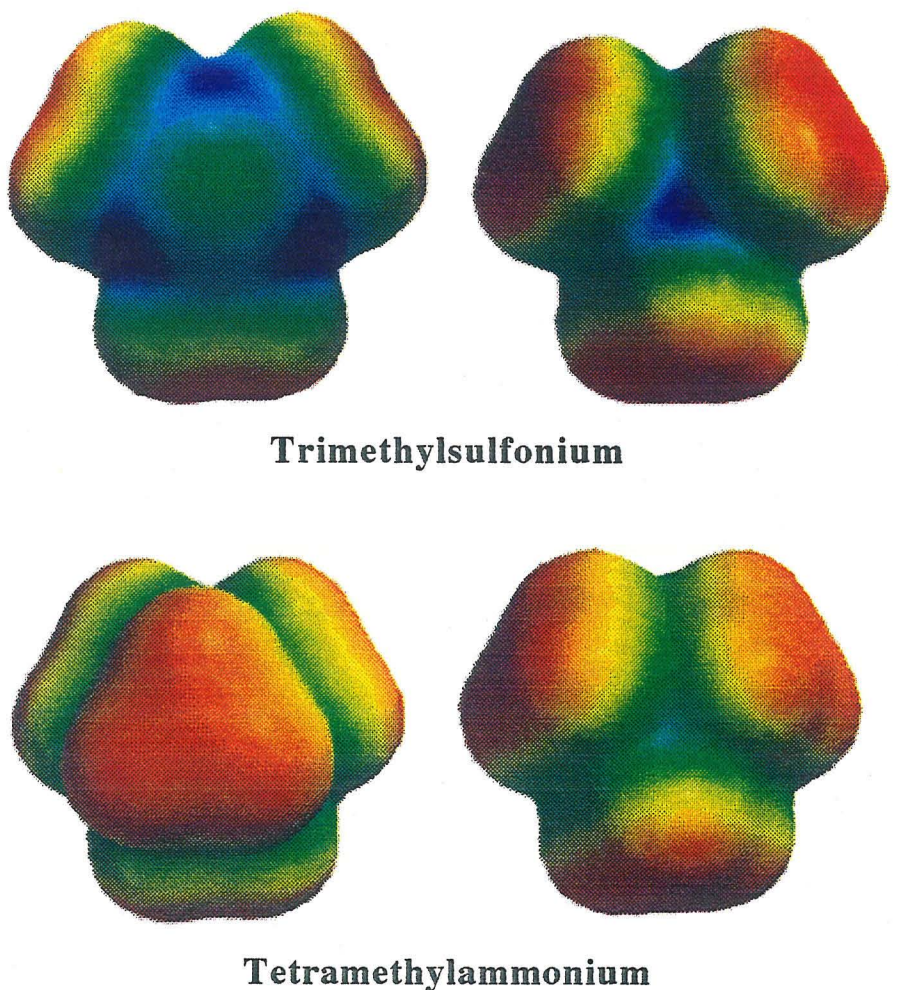


Figure 1.13. Electrostatic potential surfaces for trimethylsulfonium ion (above) and tetramethylammonium ion (below). Blue (electrostatic potential 150) represents the least electron density; red (electrostatic potential 101) represents the most electron density.

One would anticipate from this electrostatic surface that a cation- π effect would be stronger on one side of the sulfonium molecule than on the other. For SAM, both the requirement of a methyl group accessible to the substrate nucleophile and the requirement of a strong cation- π effect dictate that a sulfonium-aromatic interaction be on the same side of the salt, away from the methyl group. The residues pictured in Figure 1.12 display this optimal configuration.

Perhaps this motif of complementary polarizability and cation- π stabilization can be extended to any natural system which stabilizes polarizable transition states, especially those with developing positive charges. For example, one intriguing reaction requiring the SAM cofactor is the methylation of unactivated double bonds in marine sterol side chains. This difficult reaction apparently involves a reactive carbocationic intermediate.⁴⁸ Although negatively charged carboxylates and phosphates are commonly invoked to stabilize cationic transition states, there may be circumstances in which aromatic rings can be as or more effective as a stabilizing microenvironment.

IV. SUMMARY

The further exploration of biomimetic catalysis in the Dougherty group has not only expanded knowledge of the cyclophane model system, but also suggested that both the cation- π effect and the role of polarizability are relevant to natural systems. A new class of water-soluble guests for host **P** was examined and found to have similar binding properties to the organic charged guests previously studied in the Dougherty group. A new reaction type, dealkylation, was discovered to be catalyzed by the host cavity. These data have lead to the idea that the polarizability of the host binding microenvironment can be an important factor in stabilizing polarizable transition states. The model cyclophane system described in this chapter was used to determine the role of cation- π interactions and polarizability in

biomimetic catalysis. These findings are perhaps also relevant to natural catalytic mechanisms, especially those involving the ubiquitous S-adenosylmethionine.

Experimental Section

Uncorrected melting points were recorded on a Thomas-Hoover melting point apparatus. ^1H spectra were recorded on JEOL JNM GX-400 spectrometer. Routine spectra were referenced to the residual proton and carbon signals of the solvents and are reported (ppm) downfield of 0.0 as δ values, except where noted. Spectra from aqueous binding studies were referenced to an internal standard of 3,3-dimethylglutarate (DMG, δ 1.09). The following packing material was used in column chromatography: E. Merck silica gel 60, 0.04-0.063 mm. HPLC was performed on a Waters dual 510 pump liquid chromatograph system equipped with a Waters 490E variable wavelength UV detector and a Phase Separations Spherisorb ODS1 column (25 cm x 4.6 mm). Solvents used for HPLC were spectrophotometric grade acetonitrile (Burdick and Jackson) and doubly distilled water passed through a Milli-Q filtration system.

Tetrahydrofuran (THF) was dried over sodium under a nitrogen atmosphere. 5-nitroquinoline, trifluoroacetic acid (TFA, spectrophotometric grade), potassium thiocyanate (KSCN), thioanisole, dibenzothiophene, 1,8-diazabicyclo[5.4.0]undec-7-ene (DBU), 3,3-dimethylglutarate (DMG), and potassium hydrogen phthalate (KHP) were commercially available.

Hosts. Host P and C were prepared as reported in the literature.⁴⁹

Alkyl aryl sulfides. Except where noted, the sulfides were all prepared from aryl thiol, alkyl halide, and DBU in benzene or petroleum ether as described in the literature.⁵⁰ The reaction mixture was filtered and the filtrate was purified by column chromatography after the solvent was removed *in vacuo*.

Ethyl 2-naphthyl sulfide.⁵¹ ^1H NMR (CDCl_3) δ 7.76 (m, 3H), 7.39 (m, 4H), 3.05 (q, J = 10.5 Hz, 2H), 1.38 (t, J = 10.5 Hz, 3H).

Ethyl *p*-nitrophenyl sulfide.⁵² Mp = 41-44°C; ¹H NMR (CDCl₃) δ 8.10 (d, *J* = 8.8 Hz, 2H), 7.30 (d, *J* = 8.8 Hz, 2H), 3.04 (q, *J* = 7.3 Hz, 2H), 1.38 (t, *J* = 7.3 Hz, 3H).

Methyl *p*-nitrophenyl sulfide.⁵³ Mp = 68-71°C; ¹H NMR (CDCl₃) δ 8.12 (d, *J* = 9.0 Hz, 2H), 7.27 (d, *J* = 9.0 Hz, 2H), 2.53 (s, 3H).

Methyl *p*-chlorophenyl sulfide.⁵³ ¹H NMR (CDCl₃) δ 7.21 (d, *J* = 8.6 Hz, 2H), 7.14 (d, *J* = 8.6 Hz, 2H), 2.42 (s, 3H).

Methyl *p*-fluorophenyl sulfide.⁵³ ¹H NMR (CDCl₃) δ 7.23 (m, 2H), 6.97 (m, 2H), 2.45 (s, 3H).

Methyl *p*-tolyl sulfide.⁵³ ¹H NMR (CDCl₃) δ 7.18 (d, *J* = 8.1 Hz, 2H), 7.09 (d, *J* = 8.3 Hz, 2H), 2.45 (s, 3H), 2.30 (s, 3H).

(4-Trifluoromethylphenyl) ethyl sulfide. The aryl thiol⁵⁴ was formed by the slow addition of a solution of 4-bromobenzotrifluoride in diethyl ether to a flask containing magnesium and diethyl ether under a nitrogen atmosphere. After the addition was complete, the reaction flask was heated for 30 min. Sulfur was added to the Grignard reagent and left stirring for 1 hour. The solution was acidified with 3N HCl and extracted with ether. Extraction of this organic layer with 10% aqueous NaOH was followed by the acidification of the aqueous layer. This layer was then extracted with ether and the product thiol was distilled. The thiol was used as described above to generate the alkyl aryl sulfide. ¹H NMR (CDCl₃) δ 7.38 (d, *J* = 8.2 Hz, 2H), 7.22 (d, *J* = 8.2 Hz, 2H), 2.87 (q, *J* = 7.3 Hz, 2H), 1.23 (t, *J* = 7.3 Hz, 3H).

Ethyl benzyl sulfide.⁵⁵ ¹H NMR (CDCl₃) δ 7.15 (m, 5H), 3.60 (s, 2H), 2.32 (q, *J* = 9.0 Hz, 2H), 1.11 (t, *J* = 9.0 Hz, 3H).

2-Methylbenzo[b]thiophene.⁵⁶ The sulfide was obtained by adding *n*-butyllithium to a flask equipped with a reflux condenser of benzo[b]thiophene and tetrahydrofuran under an atmosphere of nitrogen. This solution was heated to reflux for 45 min, after which it was cooled and methyl *p*-toluenesulfonate was added with further

cooling. The reaction was quenched with methanol and placed in a separatory funnel with diethyl ether and water. The product was distilled at aspirator pressure. ^1H NMR (CDCl_3) δ 7.72 (d, $J = 8.3$ Hz, 1H), 7.62 (d, $J = 8.3$ Hz, 1H), 7.25 (m, 2H), 6.95 (s, 1H), 2.57 (s, 3H).

3-Methylbenzo[b]thiophene.⁵⁷ (Phenylthio)acetone was formed by adding chloroacetone dropwise over 30 min to a solution of thiophenol in 30% aqueous NaOH under an atmosphere of nitrogen, maintained at 0 °C. The reaction was left to stir overnight, and then was partitioned between diethyl ether and water. The organic solvent was removed *in vacuo*, and the product and phosphorus pentoxide were placed in a flask and heated to 170 °C for 30 min. The benzothiophene was extracted from the mixture and purified by column chromatography. ^1H NMR (CD_3CN) δ 7.88 (d, $J = 8$ Hz, 1H), 7.76 (d, $J = 9$ Hz, 1H), 7.38 (m, 2H), 7.19 (s 1H), 2.42 (d, $J = 1$ Hz, 3H).

3-Ethylbenzo[b]thiophene. The procedure for 3-methylbenzo[b]thiophene was employed, using 1-bromo-2-butanone instead of chloroacetone. The product was purified by column chromatography in petroleum ether. ^1H NMR (CDCl_3) δ 7.85 (d, $J = 7.1$ Hz, 1H), 7.74 (d, $J = 7.1$ Hz, 1H), 7.35 (m, 2H), 7.07 (s 1H), 2.86 (q, $J = 7.6$ Hz, 2H), 1.37 (t, $J = 7.6$ Hz, 3H).

3,5-Dimethylbenzo[b]thiophene. The procedure for 3-methylbenzo[b]thiophene was employed, *p*-thiocresol instead of thiophenol. ^1H NMR (CDCl_3) δ 7.71 (d, $J = 8.1$ Hz, 1H), 7.49 (d, $J = .7$ Hz, 1H), 7.16 (d, $J = 8.1$ Hz, 1H), 7.02 (d, $J = 1.2$ Hz, 1H), 2.48 (s, 3H), 2.40 (d, $J = 1.2$ Hz, 3H).

Sulfoxides. These compounds were synthesized by stirring the alkyl aryl sulfide with *m*-chloroperoxybenzoic acid in methylene chloride at 0 °C overnight. The product was isolated by chromatography over silica gel.

Ethyl 2-naphthyl sulfoxide (33).⁵⁸ ^1H NMR (CDCl_3) δ 8.16 (s, 1H), 7.92 (m, 4H), 7.57 (m, 2H), 2.96 (m 1H), 2.84 (m, 1H) 1.18 (t, $J = 7.4$ Hz, 3H).

Ethyl *p*-nitrophenyl sulfoxide (32). ^1H NMR (500 MHz, CD_3CN) δ 8.32 (d, $J = 10$ Hz, 2H), 7.75 (d, $J = 10$ Hz, 2H), 2.98 (m, 1H), 2.74 (m, 1H), 1.17 (t, $J = 7.5$ Hz, 3H).

Sulfonium tetrafluoroborate salts. Except where noted, the sulfonium salts were all prepared⁵⁹ from stirred, refluxing mixtures of alkyl aryl sulfide and trimethyloxonium tetrafluoroborate in methylene chloride (which was distilled from CaH_2). The reaction continued overnight, after which the solvent was removed *in vacuo* and the residue was partitioned between acetonitrile and petroleum ether and washed two more times with petroleum ether. The solvent was removed *in vacuo*, and the solid was triturated twice from acetonitrile with diethyl ether.

Ethyl methyl *p*-nitrophenyl sulfonium tetrafluoroborate (24).⁶⁰ ^1H NMR (acetone- d_6) δ 8.59 (d, $J = 9.1$ Hz, 2H), 8.50 (d, $J = 9.1$ Hz, 2H), 4.05 (m, 1H), 3.98 (m, 1H), 2.81 (s, 3H), 1.47 (t, $J = 7.4$ Hz, 3H).

Ethylmethylphenylsulfonium tetrafluoroborate (25).⁶⁰ ^1H NMR (CD_3CN) δ 7.81 (m, 5H), 3.57 (m, 1H), 3.48 (m, 1H), 3.14 (s, 3H), 1.26 (t, $J = 6.5$ Hz, 3H).

Ethylmethyl(4-trifluoromethylphenyl)sulfonium tetrafluoroborate (26). ^1H NMR (CD_3CN) δ 8.04 (AB, $J = 9.5$ Hz, $\Delta\nu = 22$ Hz, 4H), 3.62 (m, 1H), 3.55 (m, 1H), 3.17 (s, 3H), 1.28 (t, $J = 9.5$ Hz, 3H); FAB-MS m/e 221(M^+); HRMS 221.0613, calc. for $\text{C}_{10}\text{H}_{12}\text{F}_3\text{S}$: 221.0612.

Benzylethylmethylsulfonium tetrafluoroborate (23).⁶⁰ ^1H NMR (CD_3CN) δ 7.50 (m, 5H), 4.52 (AB, $J = 13.7$ Hz, $\Delta\nu = 31$ Hz, 2H), 3.24 (m, 1H), 3.15 (m, 1H), 2.71 (s, 3H), 1.42 (t, $J = 9.5$ Hz, 3H); FAB-MS m/e 203 (M^+); HRMS 203.0897, calc. for $\text{C}_{13}\text{H}_{15}\text{S}$: 203.0894.

Ethylmethyl(2-naphthyl)sulfonium tetrafluoroborate (27). ^1H NMR (CD_3CN) δ 8.53 (d, $J = 5.3$ Hz, 1H), 8.24 (d, $J = 9.0$ Hz, 1H), 8.10 (dd, $J = 5.2, 9.1$

Hz, 1H), 7.79 (m, 4H), 3.59 (m, 2H), 3.20 (s, 3H), 1.27 (t, $J = 9.3$ Hz, 3H); FAB-MS m/e 203 (M^+); HRMS 203.0897, calc. for $C_{13}H_{15}S$: 203.0894.

Dimethyl*p*-nitrophenyl sulfonium tetrafluoroborate (18).⁴² $M_p = 116-120^\circ\text{C}$; ^1H NMR (CD_3CN) δ 8.45 (d, $J = 8.8$ Hz, 2H), 8.17 (d, $J = 9.1$ Hz, 2H), 3.23 (s, 6H); FAB-MS m/e 184 (M^+), 455 ($2M^+ + \text{BF}_4^-$); HRMS 184.0440.

Dimethyl*p*-chlorophenyl sulfonium tetrafluoroborate (19).⁴² $M_p = 112-118^\circ\text{C}$; ^1H NMR (CD_3CN) δ 7.89 (d, $J = 8.7$ Hz, 2H), 7.71 (d, $J = 8.8$ Hz, 2H), 3.13 (s, 6H); FAB-MS m/e 173 (M^+), 433 ($2M^+ + \text{BF}_4^-$); HRMS 173.0192.

Dimethyl*p*-fluorophenyl sulfonium tetrafluoroborate (20).⁴² $M_p = 165-170^\circ\text{C}$; ^1H NMR (CD_3CN) δ 7.97 (m, 2H), 7.46 (m, 2H), 3.11 (s, 6H); FAB-MS m/e 157 (M^+), 401 ($2M^+ + \text{BF}_4^-$); HRMS 157.0472.

Dimethylphenyl sulfonium tetrafluoroborate (21).⁴² $M_p = 128-132^\circ\text{C}$; ^1H NMR ($\text{acetone-}d_6$) δ 8.16 (m, 2H), 7.81 (m, 3H), 2.85 (s, 6H); FAB-MS m/e 139 (M^+), 365 ($2M^+ + \text{BF}_4^-$); HRMS 139.0572.

Dimethyl*p*-tolyl sulfonium tetrafluoroborate (22).⁴² $M_p = 100-104^\circ\text{C}$; ^1H NMR (CD_3CN): δ 7.78 (d, $J = 8.5$ Hz, 2H), 7.51 (d, $J = 8.3$ Hz, 2H), 3.09 (s, 6H), 2.44 (s, 3H); FAB-MS m/e 153 (M^+), 393 ($2M^+ + \text{BF}_4^-$); HRMS 153.0475.

S-methyl(2-methyl)benzo[b]thiophene tetrafluoroborate (28).⁶¹ ^1H NMR ($\text{acetone-}d_6$) δ 8.40 (d, $J = 8.0$ Hz, 1H), 7.94 (d, $J = 8.0$ Hz, 1H), 7.85 (m, 1H), 7.73 (m, 2H), 2.95 (s, 3H), 1.65 (s, 3H).

S-methyl(3-methyl)benzo[b]thiophene tetrafluoroborate (29).⁶¹ ^1H NMR (CD_3CN) δ 8.17 (d, $J = 8$ Hz, 1H), 7.89 (m, 2H), 7.77 (m, 1H), 6.99 (s 1H), 3.15 (s 3H), 2.47 (d, $J = 1$ Hz, 3H).

S-methyl(3-ethyl)benzo[b]thiophene tetrafluoroborate (30). ^1H NMR (CD_3CN) δ 8.17 (d, $J = 8.1$ Hz, 1H), 7.88 (m, 2H), 7.31 (m, 1H), 6.94 (s 1H), 3.15 (s, 3H), 2.87 (q, $J = 7.7$ Hz, 2H), 1.34 (t, $J = 7.3$ Hz, 3H).

Adamantyl dimethyl sulfonium tetrafluoroborate (34).⁶² 1-

Bromoadamantane was added to a solution of silver tetrafluoroborate. Dimethyl sulfide is added slowly while the flask was cooled. After stirring overnight, the solvent is removed *in vacuo* and the crystals were washed several times with diethyl ether. The solid was taken up in dry acetonitrile and filtered. The solid was purified as above. ¹H NMR (methanol-*d*₄) δ 2.79 (s, 6H), 2.31 (s, 3H), 2.01 (d, d, $J = 1$ Hz, 3H), 1.78 (AB, $J = 13.5$ Hz, $\Delta\nu = 18$ Hz 6H).

S-methyldibenzothiophenium tetrafluoroborate (36). ¹H NMR (CD₃CN) δ 8.27 (d, $J = 7.3$ Hz, 2H), 8.21 (d, $J = 7.8$ Hz, 2H), 7.92 (m, 2H), 7.76 (m, 2H), 3.15 (s, 3H).

S-methyl(3,5-dimethyl)benzo[b]thiophenim tetrafluoroborate (37). ¹H NMR (CD₃CN) δ 8.02 (d, $J = 8.3$ Hz, 1H), 7.74 (s, 1H), 7.57 (d, $J = 6.8$ Hz, 1H), 6.95 (d, $J = 1.5$ Hz, 1H), 3.11 (s, 3H), 2.52 (s, 3H), 3.11 (s, 3H) 2.44 (d, $J = 1.7$ Hz, 1H).

Buffers. Binding studies and kinetics studies were run in 10mM pD = 9 borate and HPLC 10mM pH = 9 borate buffers, respectively. The pD 9 borate buffer was prepared by dissolving 32mg of high purity boric oxide (B₂O₃) in 100g of D₂O (Aldrich, 99.8atom%D), adding enough CsOD in D₂O (e.g., 400 microliters of 1M CsOD) to attain pD = 9, and mixing thoroughly.⁴⁹ The HPLC pH = 9 borate buffer was made by using doubly distilled water passed through a Milli-Q filtration system instead of using the D₂O used to make the pD = 9 borate buffer.

Binding and Kinetics Studies. Stock solutions for host (~1.6 mM), guest (~2-7 mM), KSCN (0.426 M), DMG, and KHP (9.25 mM) for the ¹H NMR binding and the kinetics experiments were prepared from the buffers described above. All volumetric measurements of aqueous solutions were made using adjustable volumetric pipets. Concentrations were determined by NMR integrations versus the internal standard (DMG) of known concentration. All pulse delays for the integration experiments were at least 5

times the measured T_1 for the species involved. Binding constants were determined by performing a ^1H NMR titration of guest added to host using the chemical shifts referenced to internal DMG (1.09 ppm) at 8 to 10 different guest:host concentration ratios in an iterative least-squares fitting procedure.⁴⁹ Binding studies of product sulfides (17 - 21) were not possible due to low solubility in the buffer. All binding studies of compounds were performed at 400MHz. Binding constants are reported in Table 1.2. The second-order rate constant for reactions with no host present are determined under pseudo-first-order conditions, as described in detail below for each study. This rate constant (k_{un}) combined with binding constants of substrate and product and rate data with host present allow determination of k_{cat} using a simulation program based on Figure 1.6. Table 1.4 contains rate constants.

Kinetics of Sulfonium Salt Dealkylation. Stock solutions of host (1.49 mM) and KSCN (.426 M) were made in 10 mM deuterated cesium borate buffer at $\text{pD} = 9$. Stock solutions of the internal integration standard KHP (9.25 mM), 5-nitroquinoline (1.38 mM), and the sulfonium salts (3.8 -6.8 mM) for HPLC studies were made by weighing each solid and dissolving it in 10.0 mL of HPLC borate buffer in a 10-ml volumetric flask. The reaction rates were monitored by integration of substrate and internal standard peak areas from an HPLC trace using a Waters Baseline 810 software package. Each kinetics run using ethylmethyl(*p*-nitrophenyl)sulfonium salt as a substrate was performed twice. Sample reaction mixtures for each kind of experiment (without and with a competitive inhibitor) follow. For host-catalyzed dealkylation of the dimethyl*p*-nitrophenyl sulfonium salt, the reaction mixture consisted of 80 μL of sulfonium salt stock solution (3.80mM), 30 μL of KHP stock solution, 120 μL of host stock solution, 30 μL of KSCN stock solution, and 240 μL of buffer. The uncatalyzed reaction used 160 μL buffer instead of host stock solution. The reaction mixtures for the competitive inhibition study consisted of 70 μL of ethylmethyl(*p*-nitrophenyl)sulfonium stock solution, 30 μL of KSCN stock solution, 30 μL of KHP stock solution, 210 μL of 5-nitroquinoline stock solution, and 160 μL of host

stock solution. For the uncatalyzed reaction, 160 μL of buffer was added instead of host solution.

For each experiment, the buffered pH 9 solution of substrate, inhibitor (if any), internal standard, and host (for catalyzed reactions) was prepared without nucleophile in an Eppendorf tube and cooled to -5°C in a salt-ice water bath. The solution of nucleophile (chilled) is added and the tube is shaken vigorously just prior to the first injection of sample. The tube is then placed in an oil bath maintained at 46°C by a ThermoWatch. At each time point, the reaction mixture is cooled to -5°C , a 20 microliter aliquot is removed and neutralized with 20 microliters of pH 7 phosphate buffer. This 40 microliter sample is injected onto the column and the reaction mixture is returned to the oil bath. A gradient elution was used to separate the reaction mixture components. Solvent A was H_2O , .1% TFA by volume; solvent B was acetonitrile, .1% TFA by volume. Elution was performed at 1.8 ml/min. with 100% solvent A from 0 to 2 minutes, a linear gradient to 100% solvent B from 2 to 10 minutes, maintained at 100% B from 10 to 15 minutes, brought back to 100% solvent A from 15 to 20 minutes, and washed from 20 to 35 minutes with solvent A. Compounds were detected at 254nm and at 230nm. A calibration consisting of measuring relative peak areas of five samples of various sulfonium salt concentrations and fixed KHP concentration was used to convert peak areas to concentrations.

References

1. a) Winter, G.; Fersht, A. R.; Wilkinson, A. J.; Zoller, M.; Smith, M. *Nature (London)*, **1982**, 299, 756.
b) Zoller, M. J.; Smith, M. *Methods Enzymol.* **1983**, 100, 468.
2. a) Chung, H.-H.; Benson, D.R.; Schultz, P. G. *Science* **1993**, 259, 806-809.
b) Ellman, J.; Mendel, D.; Anthony-Cahill, S.; Noren, C. J.; Schultz, P. G. In *Methods in Enzymology* Academic Press: New York, 1991; Vol. 202, pp 301-337.
3. a) Page, M. I. *Chem. Soc. Rev.* **1973**, 2, 295.
b) Page, M. I.; Jencks, W. P. *Proc. Natl. Acad. Sci. USA* **1971**, 68, 1678.
4. Kirby, A. J. *Adv. Phys. Org. Chem.* **1980**, 17, 183.
5. Polanyi, M. Z. *Elektrochem.* **1921**, 27, 143.
6. Pauling, L. *Chem. Eng. News* **1946**, 24, 1375.
7. Kirby, A. J. *Phil Trans. R. Soc. Lond. A* **1993**, 345, 67-76.
8. Stewart, J. D.; Benkovic, S. J. *Chem. Soc. Rev.* **1993**, 213-219.
9. Menger, F. M. *Biochemistry* **1992**, 31, 5368-5373.
10. Schneider, H.-J. *Angew. Chem., Int. Ed. Engl.* **1991**, 30, 1417-1436.
11. a) Schmidtchen, F. P. *Angew. Chem., Int. Ed. Engl.* **1981**, 20, 466.
b) Schmidtchen, F. P. *Chem. Ber.* **1984**, 117, 725.
12. Schneider, H.-J.; Busch, R. *Angew. Chem., Int. Ed. Engl.* **1984**, 23, 912.
13. Murakami, Y. et al., *J. Chem. Soc. Perkin Trans. 2* **1977**, 24.
14. Stauffer, D. A.; Barrans, R. E., Jr.; Dougherty, D. A. *Angew. Chem., Int. Ed. Engl.* **1990**, 250, 1558-1560.
15. Kearney, P. C.; Mizoue, L. S.; Kumpf, R. A.; Forman, J. E.; McCurdy, A.; Dougherty, D. A. *J. Am. Chem. Soc.* **1993**, 115, 9907-9919.
16. Kearney, P. C.; Dougherty, D. A. submitted to *Angew. Chem., Int. Ed. Engl.*
17. Perutz, M. F. *Phil. Trans. R. Soc. Lond. A* **1993**, 345, 105-112.
18. Knee, J. L.; Khundkar, L. R.; Zewail, A. H., *J. Chem. Phys.* **1987** 87 115-127.
19. Rodham, D. A.; Suzuki, S.; Sueram, R. D.; Lovas, F. J.; Dasgupta, S.; Goddard, W. A., III; Blake, G. A. *Nature* **1993**, 362, 735-737.
20. Burley, S. K.; Petsko, G. A. *FEBS Lett.* **1986** 203, 138-143.
21. Tuschsen, E.; Woodward, C. *Biochemistry* **1987**, 26, 1918-1925.
22. Suzuki, S.; Green, P. G.; Bumgarner, R. E.; Dasgupta, S.; Goddard, W. A., III; Blake, G. A. *Science*, **1992**, 257, 942-945.
23. Loewenthal, K.; Sancho, J.; Fersolt, A. R. *J. Mol. Biol.* **1992**, 225, 759-770.

24. Dougherty, D. A.; Stauffer, D. A. *Science* **1990**, *250*, 1558-1560.
25. Sussman, J. L.; Harel, M.; Frolow, F.; Oeffner, C.; Goldman, A.; Toker, L.; Silman, I. *Science* **1991**, *253*, 872-879.
26. a) Franke, J.; Vögtle, F. *Top. Curr. Chem.* **1986**, *132*, 135-170.
b) Wolfenden, R. *Science (Washington, DC)* **1983**, *222*, 1087-1093.
c) Odashima, K.; Soga, T.; Koga, K. *Tetrahedron Lett.* **1981**, *22*, 5311-5314.
27. McCurdy, A.; Jimenez, L.; Stauffer, D. A.; Dougherty, D. A. *J. Am. Chem. Soc.* **1992**, *114*, 10314-10321.
28. a) *The Chemistry of the Sulphonium Group*; Stirling, C. J. M.; Patai, S., Eds.; John Wiley and Sons: New York, 1981.
b) Stirling, C. J. M. In *Organic Chemistry of Sulfur*, Oae, S., Ed.; Plenum Press: New York, 1977; Chapter 9.
29. *Biochemistry of S-Adenosylmethionine and Related Compounds*; Usdin, E.; Borchardt, R.; Creveling, C. R., Eds.; Macmillan: London, 1982.
30. Andersen, K.K.; Caret, R. L.; Ladd, D. L. *J. Org. Chem.* **1976**, *41*, 3096.
31. Darwish, D.; Scott, C. E. *Can. J. Chem.* **1973**, *51*, 3647.
32. a) Deranleau, D. A. *J. Am. Chem. Soc.* **1969**, *91*, 4044.
b) Person, W. B. *J. Am. Chem. Soc.* **1965**, *87*, 167-170.
c) Wilcox, C. S. In *Frontiers in Supramolecular Organic Chemistry and Photochemistry*, Schneider, H.-J.; Durr, H., Eds.; VCH: Weinheim, 1990.
33. Barrans, R. E., Jr. Ph.D. Thesis, California Institute of Technology, 1993.
34. Stauffer, D. A. Ph.D. Thesis, California Institute of Technology, 1989.
35. Winkler, J. D.; Finck-Estes, M. *Tetrahedron Lett.* **1989**, *30*, 7293-7296.
36. Barbarella, G.; Garbesi, A.; Fava, A. *Helv. Chim. Acta* **1971**, *54*, 2297.
37. Fersht, A. *Enzyme Structure and Mechanism*; W. H. Freeman and Company: New York, 1985.
38. Barrans, R. E., Jr. Ph.D. Thesis, California Institute of Technology, 1993.
39. Williams, A. *Acc. Chem. Res.* **1984**, *17*, 425-430.
40. Lewis, E. S. *J. Phys. Org. Chem.* **1990**, *3*, 1-8.
41. Dewar, M. J. S.; Dougherty, R. C. *The PMO Theory of Organic Chemistry*; Plenum: New York, 1975; Chapter 5.
42. Coward, J. K.; Sweet, W. D. *J. Org. Chem.* **1971**, *36*, 2337-2346.
43. Parker, A. J. *Chem. Rev.* **1969**, *69*, 1-32.
44. Kellogg, R. M. *Angew. Chem., Int. Ed. Engl.* **1984**, *23*, 782-794.
45. a) *Biochemistry of S-Adenosylmethionine and Related Compounds*; Usdin, E.; Borchardt, R.; Creveling, C. R., Eds.; Macmillan: London, 1982.

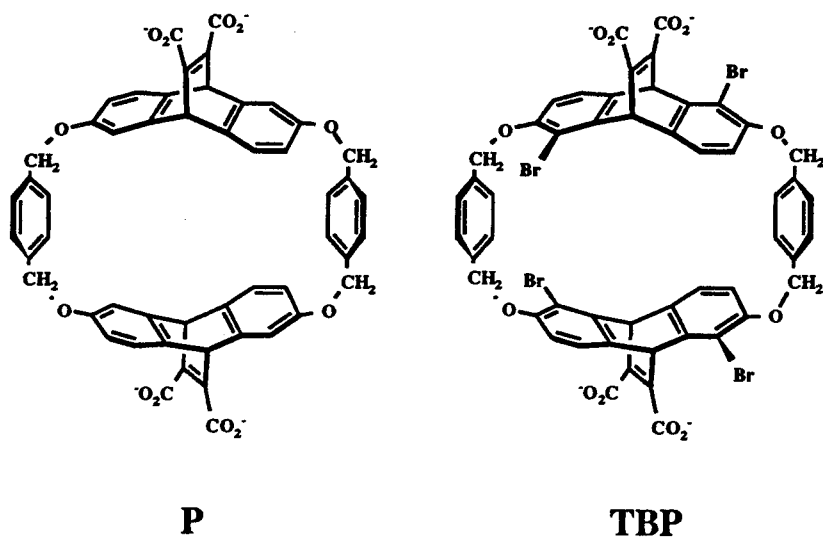
- b) Maw, G. A. In *The Chemistry of the Sulphonium Group*; Stirling, C. J. M.; Patai, S., Eds.; John Wiley and Sons: New York, 1981; Chapter 17.
46. Kagan, R. M.; Clarke, S. *Arch. Bioch. Biophys.* **1994**, *310*, 417-427.
 47. a) Cheng, X.; Kumar, K. S.; Posfai, J.; Pflugrath, J. W.; Roberts, R. J. *Cell* **1993**, *74*, 299-307.
 b) Klimasauskas, S.; Kumar, S.; Roberts, R. J.; Cheng, X. *Cell* **1994**, *76*, 357-369.
 48. Mercer, E. I. *Lipids* **1991**, *26*, 584-597.
 49. Petti, M. A.; Shepodd, T. J.; Barrans, R. E.; Dougherty, D. A. *J. Am. Chem. Soc.* **1988**, *110*, 6825-6840.
 50. Ono, N.; Miyake, H.; Saito, T.; Kaji, A. *Synthesis* **1980**, 952.
 51. Node, M.; Nishide, K.; Ohta, K.; Fuji, K.; Fujita, E.; Hori, H. Inayama, S. *Chem. Pharm. Bull* **1983**, *31*(2), 545-551.
 52. Evans, T. L.; Kinnard, R. D. *J. Org. Chem.* **1983**, *48*, 2496-2499.
 53. Jeminet, G.; Kergomard, A. *Bull. Soc. Chim. Fr.* **1967**, *9*, 3233-3243.
 54. Yachandra, V. K.; Hare, J.; Moura, I.; Spiro, T. G. *J. Am. Chem. Soc.* **1983**, *105*, 6455-6461.
 55. Takido, T.; Itabashi, K. *Synthesis* **1987**, 817-819.
 56. Shirley, D. A.; Cameron, M. D. *J. Am. Chem. Soc.* **1952**, *74*, 664-665.
 57. Werner, E. G. G. *Rec. Trav. Chim.* **1949**, *68*, 509-519.
 58. Kim, Y. H.; Lee, H. K. *Chem. Lett.* **1987**, 1499-1502.
 59. Corey, E. J.; Jautelat, M.; Oppolzer, W. *Tetrahedron Lett.* **1967**, 2325.
 60. Darwish, D.; Scott, C. E. *Can. J. Chem.* **1973**, *51*, 3647-3648.
 61. Acheson, R. M.; Harrison, D. R. *J. Chem. Soc.* **1970**, 1764-1784.
 62. Kevill, D. N.; Anderson, S. W. *J. Am. Chem. Soc.* **1986**, *108*, 1579-1585.

Chapter 2

New Macrocyclic Hosts to Explore the Cation- π Effect

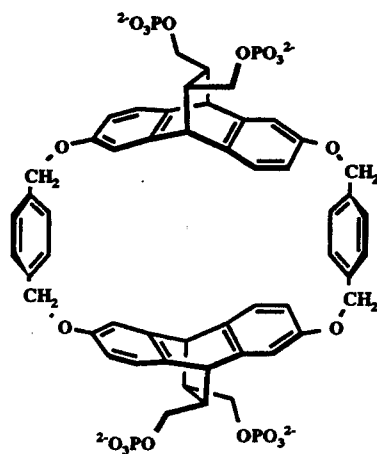
I. INTRODUCTION

The intermolecular interactions between the water-soluble cyclophane host **P** (pictured below) and small organic guest molecules have been thoroughly characterized through the measurement of binding constants. These ground-state interactions are detailed in the literature¹ and also in Chapter 1 of this thesis. These studies have revealed a stabilizing interaction between aromatic rings and organic cations that is distinct from hydrophobic effects. This cation- π interaction is manifested by larger binding affinities for cationic organic molecules than for neutral molecules with similar shapes.

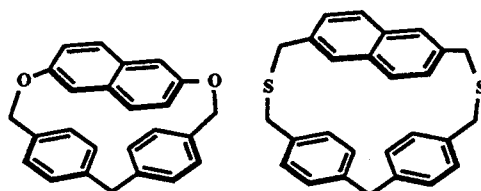


New host macrocycles have been designed to further explore the nature of the cation- π interaction of host **P**. The first macrocycle **PHOS** (pictured below) was designed to have superior solubility properties to those of host **P**. More importantly, this host may also be used to measure the contribution of Coulombic effects of the negative charges on the macrocycle to cation binding affinities in aqueous media. The next pair of macrocycles, **O** and **S**, were designed to demonstrate the cation- π effect for alkali cations in organic media. A measurable affinity of alkali cations for a cyclophane host would also provide

support for the hypothesis that aromatic residues play an active role in potassium channel conductance through cell membranes. The first section of this chapter will address the phosphate-containing macrocycle, and the second section will address the cyclophanes **O** and **S**.



PHOS



O

S

A. Cyclophane Solubilized by Phosphate Groups

1. Introduction

Work on binding and catalysis projects using hosts **P** and **TBP** (pictured above) has shown that the carboxylate groups used to solubilize the hosts are not an ideal

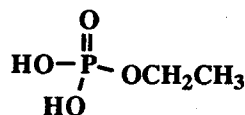
functional group choice. They place restrictions on experimental conditions, creating technical difficulties that prevent certain studies from being performed. Additionally, and more importantly, the question of what effect the charges of the carboxylates have on the binding and catalysis exhibited by the hosts must be explored. The interpretation of the binding studies of cationic guests relies on the assumption that the carboxylates do not provide much, if any, electrostatic stabilization to charged guests.

The main restrictions that the carboxylates place on experiments arise from limited solubility and the necessity of using a high pH medium. The carboxylate groups allow only modest solubility without nonspecific aggregation for host **P**, and even lower solubility for the more hydrophobic host **TBP**. Specifically, the critical aggregation concentration of host **P** is 250 μM and of **TBP** is 95 μM . Therefore, all studies with **TBP** must be performed in a mixed aqueous and organic solvent (10% acetonitrile in borate buffer). This limited solubility can restrict the kinds of studies that may be performed with these cyclophanes. For example, limitations in solubility can preclude the attainment of binding constants for strongly binding guests by NMR.²

The more significant restriction which the conjugated carboxylates place on the solution studies of these hosts is the high pH of the buffer needed to dissolve the host. The pK_a 's of host **P** should be slightly larger than those of maleic acid (1.83 and 6.07) due to the inductive effect of the alkyl substituents. Therefore, in order to assure complete deprotonation and maximum solubility, the hosts are studied in a pH 9 borate buffer. The ability to perform these studies at neutral pH would not only allow studies under physiological conditions which are relevant to biomimetic projects, but would also allow studies involving more reactive species. For example, the alkylating agents reactive enough to be used in catalysis studies also undergo significant solvolysis by the basic buffer. These properties of the carboxylates place strict constraints on experimental conditions, and therefore also limit the information that could be obtained from studies of a cyclophane with carboxylate solubilizing groups.

The use of positively charged organic groups to solubilize the host would eliminate pH effects, but the cation- π effect would cause the host to be a good receptor for itself. This would increase aggregation and interfere with the binding of other small guests or substrates. Negatively charged solubilizing groups are a better choice, in spite of pH restrictions.

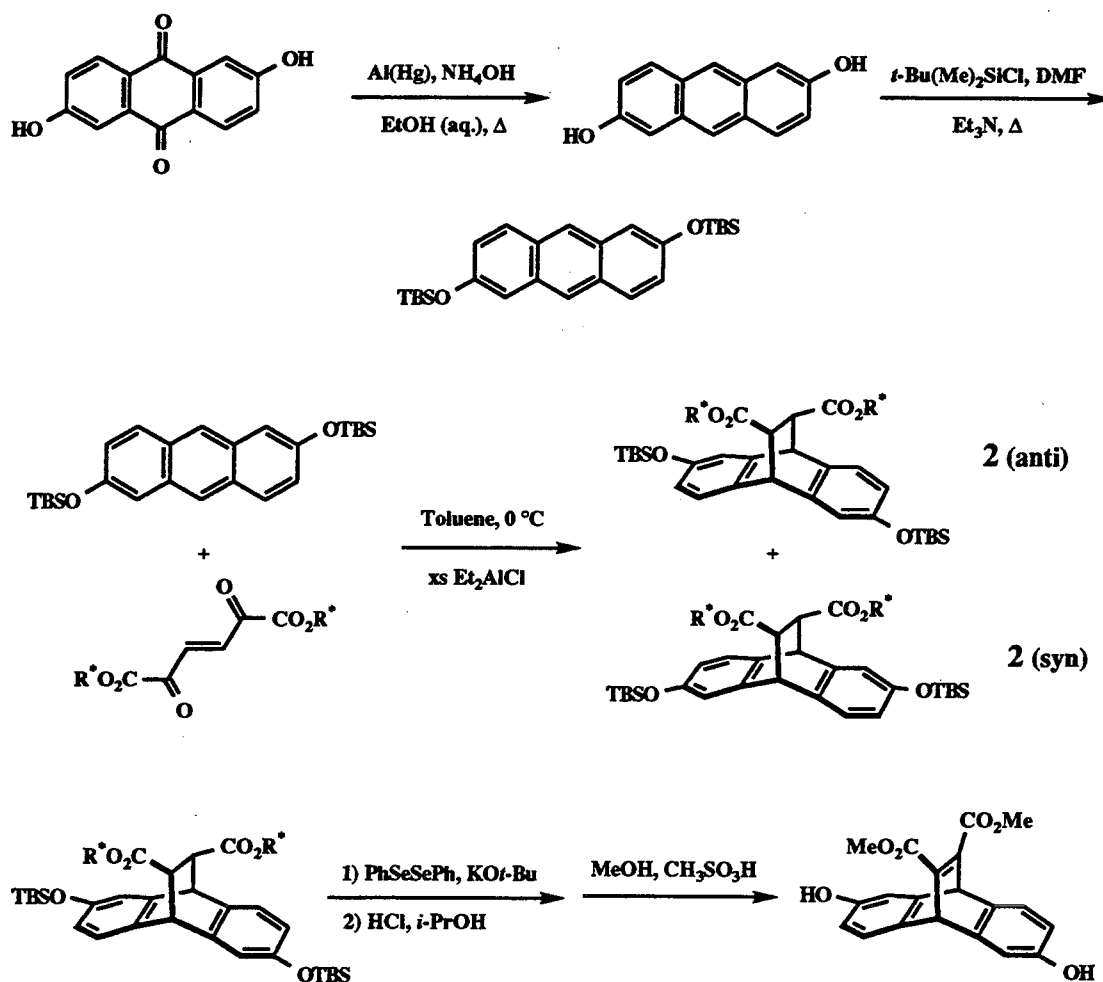
One approach to circumventing these problems is to use four phosphate groups instead of four carboxylate groups to solubilize these hosts. Based on the acid dissociation constants of ethyl phosphate (**1**) pictured below, the first pK_a should be 1.60, while the second pK_a should be 6.31.³ Clearly, at neutral pH each phosphate will be at least singly deprotonated. This should allow host **PHOS** to have the solubility properties at pH = 7 that host **P** has at pH = 9. Additionally, the phosphate groups are likely to be fully deprotonated at pH = 8.3. The presence of eight charges instead of four should increase host solubility in aqueous buffers.

**1**

Because the tetra-anion and octa-anion of host **PHOS** differ only in net charge, a quantitative analysis of host charge effects may be easily performed. This experiment may be accomplished by comparing binding constants obtained in buffers of different pH. These buffers would control the degree of deprotonation, and therefore the charge of the macrocycle. In this way, the assertion⁴ that the remote carboxylates of host **P** do not play a large role in cation binding may be affirmed. This modification to the host should circumvent some experimental difficulties, while also addressing the issue of host charge effects on binding constants.

2. Results and Discussion

The host **PHOS** retains the elements of host **P** that make it a successful cyclophane receptor. They include a relatively rigid, preorganized macrocycle having water-solubilizing groups fixed away from the binding cavity. Additionally, the synthesis already developed for host **P**, drawn in Figure 2.1, should be easily modified to produce **PHOS**. In this scheme for host **P** synthesis, R^* is (+)-menthyl. Like **P**, the macrocycle **PHOS** should have a synthetic route that allows easy modification either of the linkers or of the etheno- or ethanoanthracene unit.



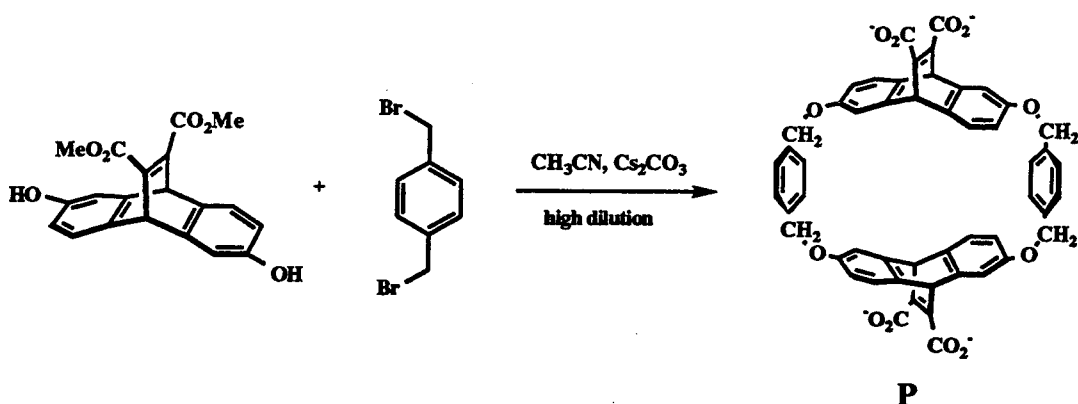
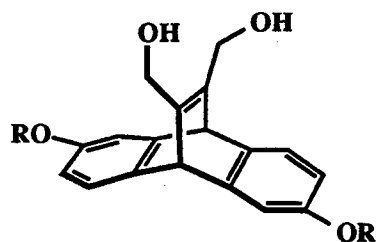
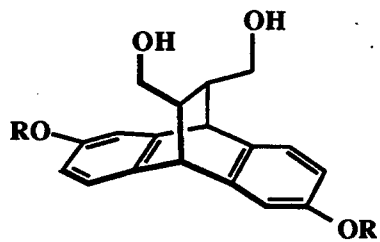


Figure 2.1. The synthetic route to unmodified host **P**. TBS is *t*-butyldimethylsilyl-, R* is (+)-menthyl.

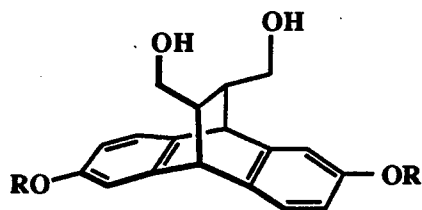
The first task was to develop a method of synthesizing the key intermediate diol compounds **3** and **4** below. The presence of alcohol groups will allow many kinds of functional groups to be added to the host structure. The simplest synthetic approach is to reduce the methyl or menthyl esters resulting from the Diels-Alder adduct. Reducing agents such as lithium aluminum hydride or triethoxysilane with cesium fluoride yielded no product with *t*-butyldimethylsilyl-protected or benzyl-protected phenols. The use of “super-hydride” (lithium triethylborohydride) worked very well for the reduction of both unsaturated methyl esters and saturated syn and anti menthyl esters. These reactions are drawn below, where R is (4-methyl)benzyl (Bn') or *t*-butyldimethylsilyl (TBS). This reduction occurred smoothly both with TBS-protected or with (4-methyl)benzyl-protected phenols. However, the use of superhydride with unsaturated methyl esters seemed to produce more side-products than with the saturated menthyl ester. The rest of the synthesis accordingly relied on the reduction of saturated menthyl esters.



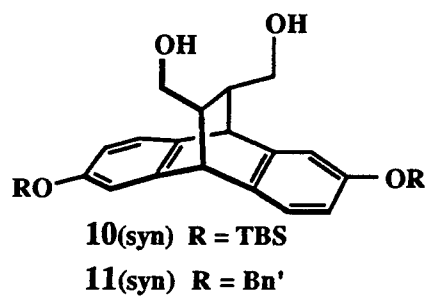
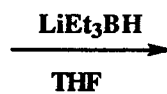
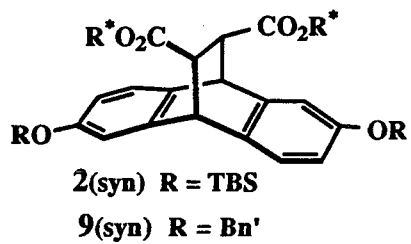
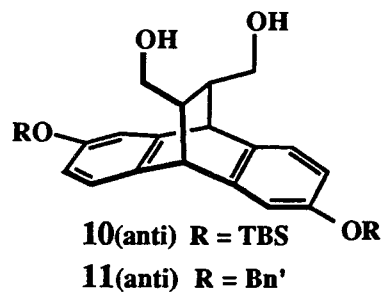
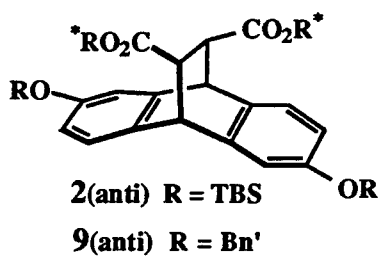
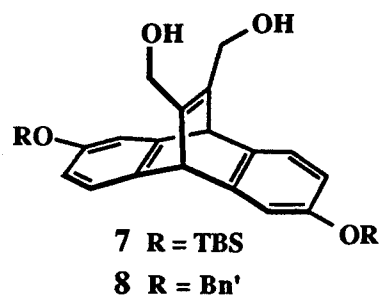
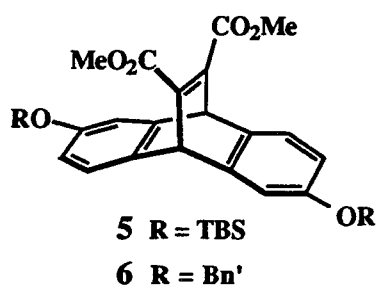
3



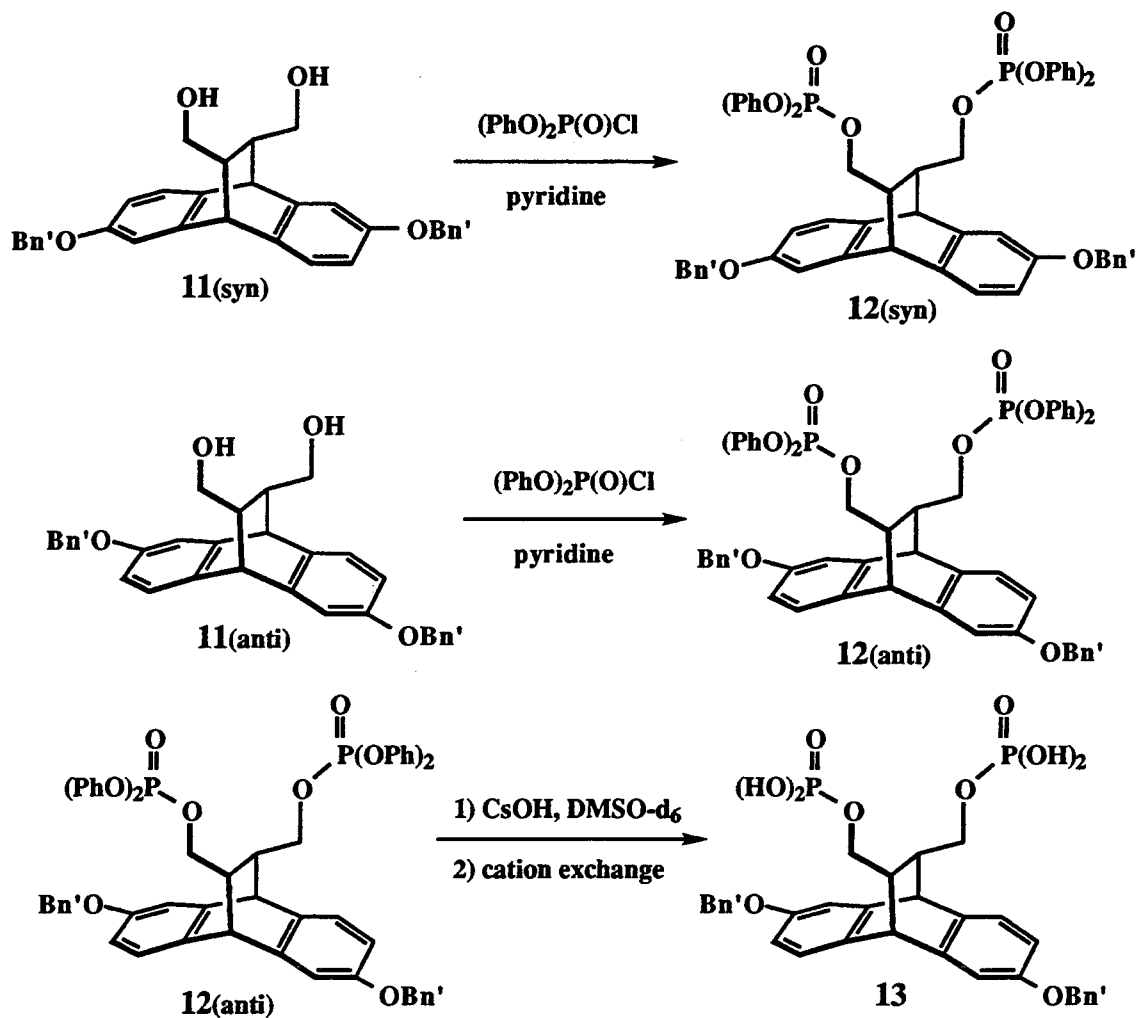
4 (anti)

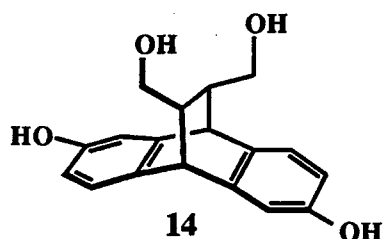


4 (syn)

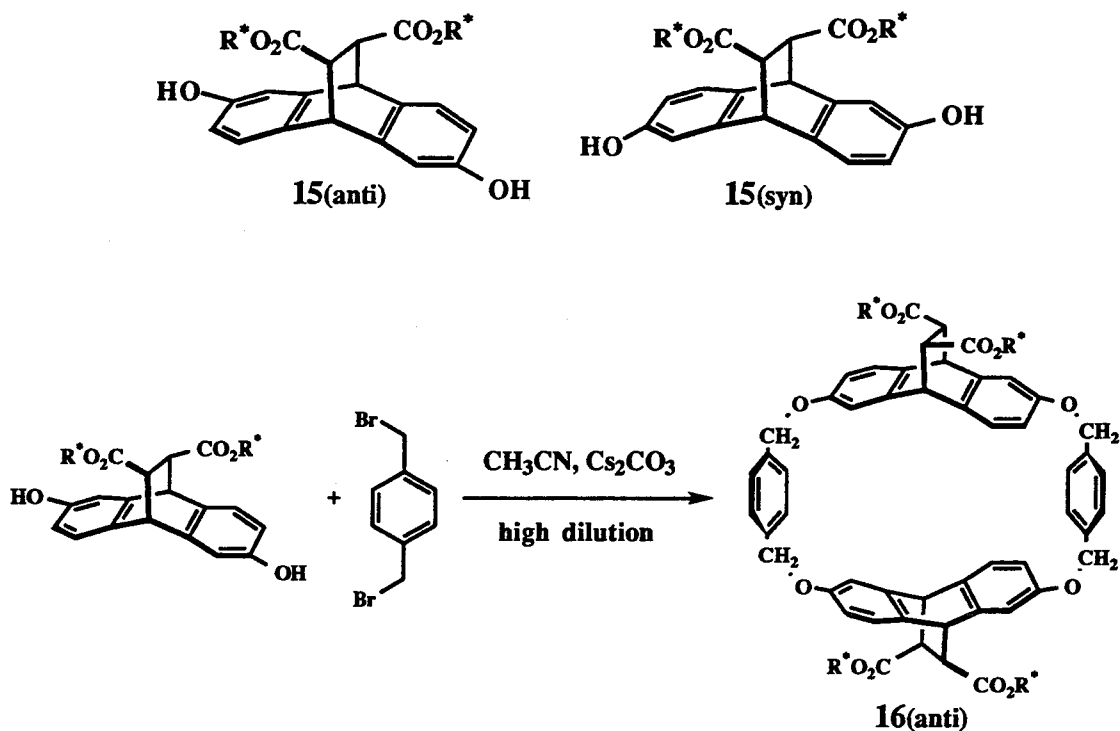


The esterification of the alcohols with diphenyl chlorophosphate in pyridine proceeded smoothly with both syn and anti diastereomers with (4-methyl)benzyl-protected phenols. These reaction conditions resulted in decomposition of the TBS protecting groups. Therefore, the esterification should be performed on the host macrocycle instead of the half-molecule **2**. Hydrolysis of these phosphate esters with cesium hydroxide and subsequent neutralization and cation exchange of the mixture was performed to produce the diphosphate model compound. It was then placed in a suitable deuterated buffer for NMR studies. The hydrolysis appeared to be successful for the model compound, so further work on the macrocycle was pursued.





Since the deprotected diol half-molecule (**14**) had poor solubility properties, the macrocyclization was carried out with the menthyl ester half-molecule (**15**) (pictured below). As shown in Figure 2.2, the resulting macrocycle was reduced, esterified, and hydrolyzed. At this stage, hydrolysis did not proceed smoothly. The phenyl phosphate esters should react thirty-fold faster than alkyl phosphate esters,⁵ but the conditions necessary to hydrolyze all eight phenyl esters in a reasonable time also hydrolyzed some alkyl linkages to the host molecule. By NMR, no symmetrical species was obtained during hydrolysis.



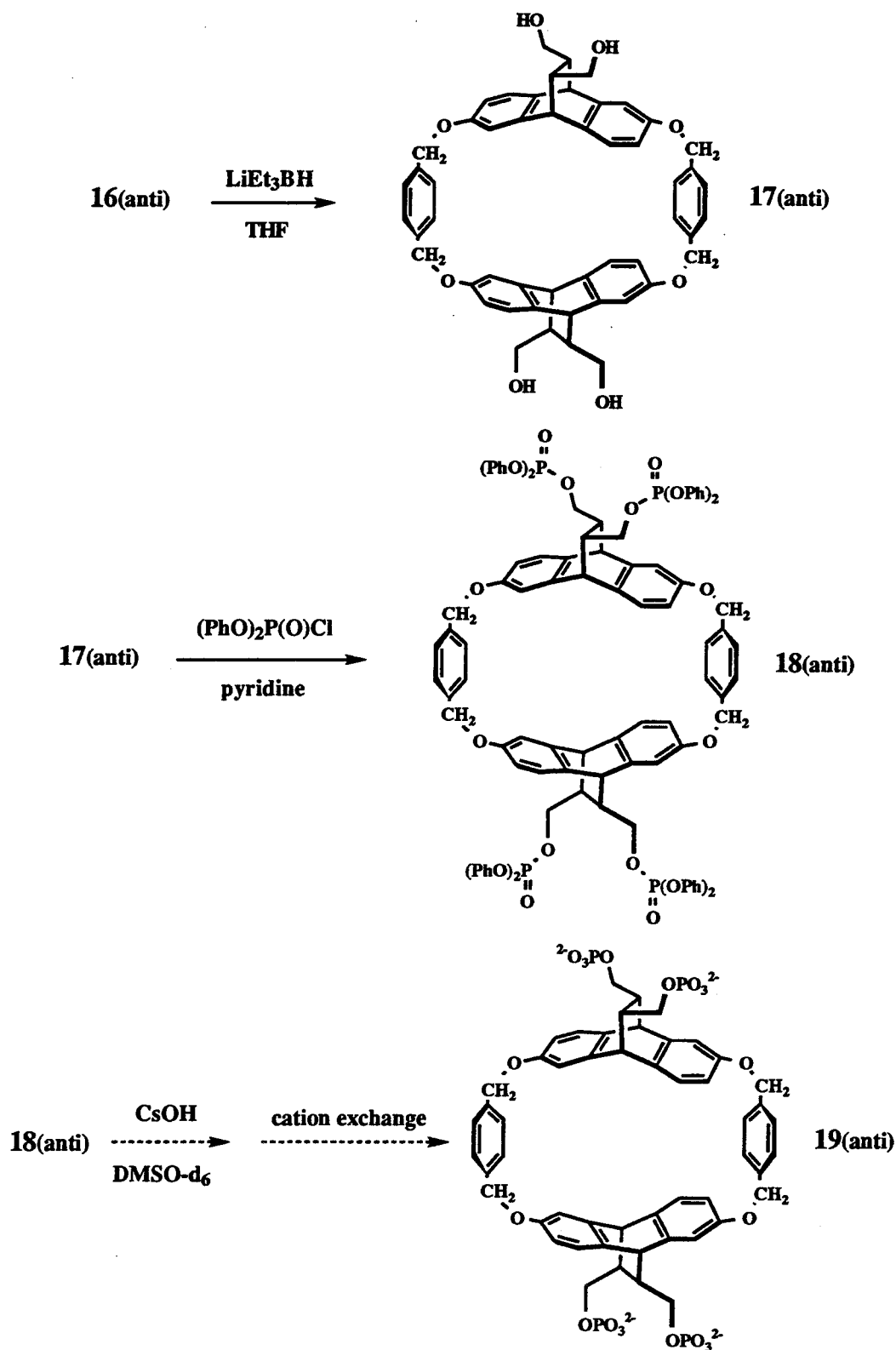
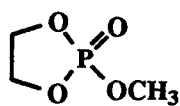
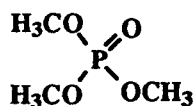
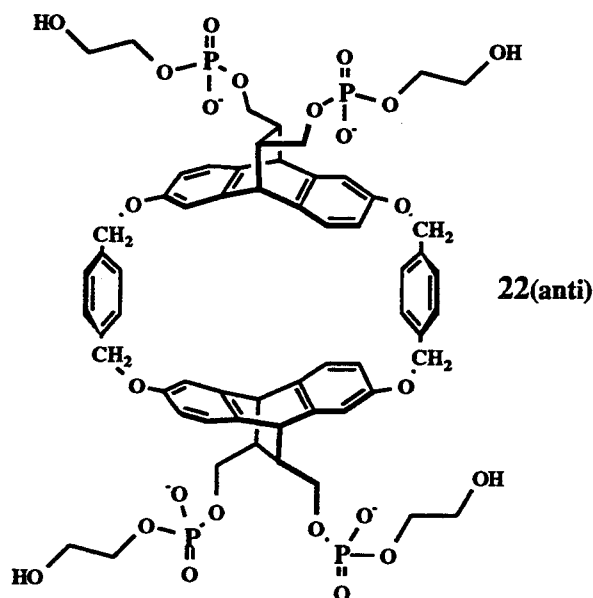


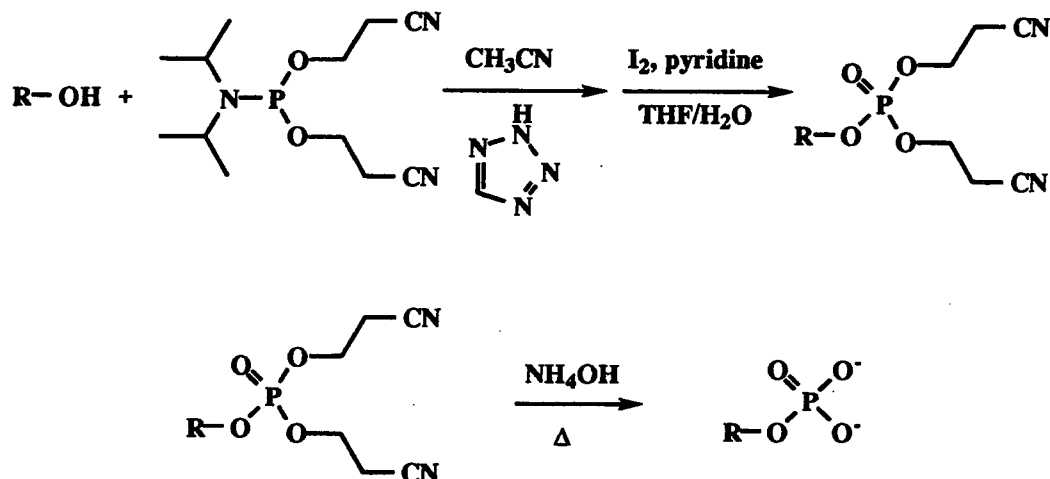
Figure 2.2. Proposed synthetic route to host **PHOS**. Dotted arrows indicate unsuccessful reactions.

3. Future Work Toward Host PHOS

A more reactive leaving group than phenol is desirable to promote specific ester cleavage. Strained cyclic phosphate esters such as **20** hydrolyze 10^6 - 10^8 times faster than dialkyl phosphate esters such as **21**.³ The resulting host would then have only four negative charges like host **P**. However, it would be completely deprotonated at pH = 7, unlike host **P** which requires pH = 9 for full deprotonation.

**20****21**

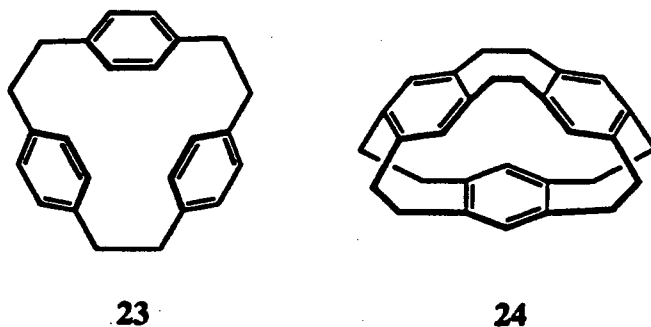
An alternative synthesis⁶ proposed below should lead to the desired host **PHOS**. However, each step proceeds in only moderate yield and must be performed four times on the host macrocycle. Further work will be required to complete the synthesis of host **PHOS**.



B. Cyclophane Receptors for Alkali Metal Cations

1. Introduction

The detection of alkali metal cation binding by cyclophane receptors in organic media would be a dramatic demonstration of cation- π stabilization. This is especially true since there would be no additional stabilization by the hydrophobic effect. Related efforts to use benzene rings as π -donors have been unsuccessful in attempts to complex silver (I) ions by " π -prismant" (23) and "deltaphane" (24) pictured below.⁷ However, " π -prismant" does form a complex with gallium (I) ions.⁸ Although η^6 benzene ligands are known for transition metal ions, as in bis(η^6 -benzene)chromium, this kind of complexation with alkali metal cations has not been observed in the solution phase. However, Kebarle has shown that potassium ion binds to benzene in the gas phase with a free energy of 11.6 kcal/mole.⁹ This energy is comparable to potassium's binding free energy to a water molecule, which is 11.5 kcal/mole. The cation- π effect provides approximately 2 kcal/mole of binding energy in aqueous media (see Chapter 1), so it is expected to be a measurable interaction in organic media.



Evidence for alkali metal stabilization by aromatic rings would also support the hypothesis that the cation- π effect plays a role in potassium conductance through the voltage-gated potassium ion channel. Two striking features of the potassium channel are that it is favorable for a well-solvated potassium ion to enter a relatively nonpolar membrane, and that the channel is selective for potassium over the smaller ion sodium. Other models of cation conductance through a membrane pore and of potassium selectivity rely on electrostatic effects between partially solvated potassium and negatively charged residues lining the channel. However, the pore region of the four subunits that make up the channel includes only two conserved negatively-charged residues per subunit. Interestingly, there are four conserved aromatic residues.¹⁰ Figure 2.3 below shows the pore-forming region of one subunit of the *Shaker* channel. This possible cation- π interaction was investigated computationally by the Dougherty group.¹¹

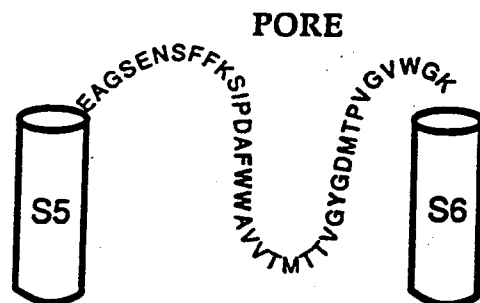


Figure 2.3. Drawing of the primary sequence of the pore region of one subunit of the *Shaker* voltage-gated potassium channel.

Computational studies performed in the Dougherty group have indicated that potassium-aromatic interactions can account for the selectivity observed in the voltage-gated potassium channel. The high-level *ab initio* calculations were performed to obtain binding energies in the gas phase of lithium, sodium, potassium, and rubidium to one benzene and to a pair of benzenes in a "sandwich" around the ion. In the gas phase without water molecules, the calculations indicate that the most stable complexes are those with lithium, followed in order by sodium, potassium, and rubidium. This order reflects pure electrostatic interactions that would favor interactions with smaller ions of higher charge density. However, when water is included in the calculations using MC/SPT, the sandwich complexes show that potassium is stabilized more than lithium, sodium, and rubidium. This can be rationalized by the desolvation of lithium and sodium by the benzene rings. The potassium is large enough to allow direct solvation by water molecules. Overall, there is a balance struck between favorable electrostatic interactions with the benzene ring and desolvation of the cation. This balance is most favorable for the potassium ion. These interactions are pictured below in Figure 2.4.

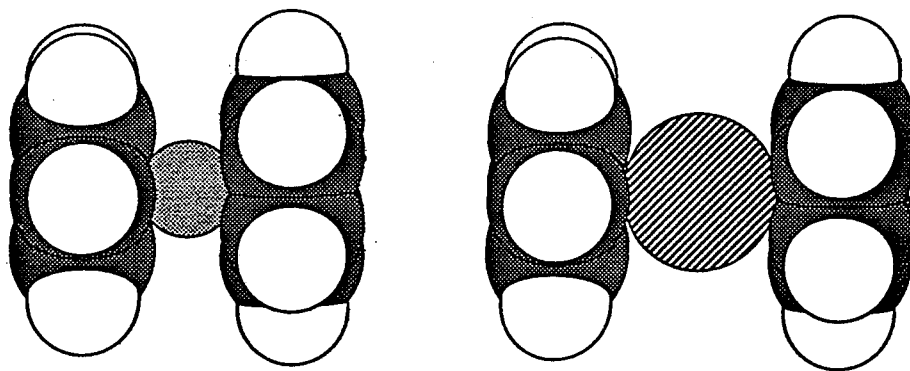
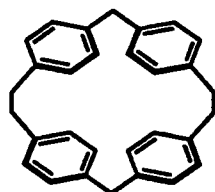
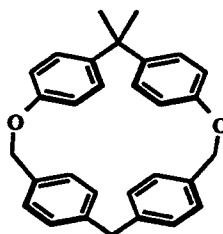


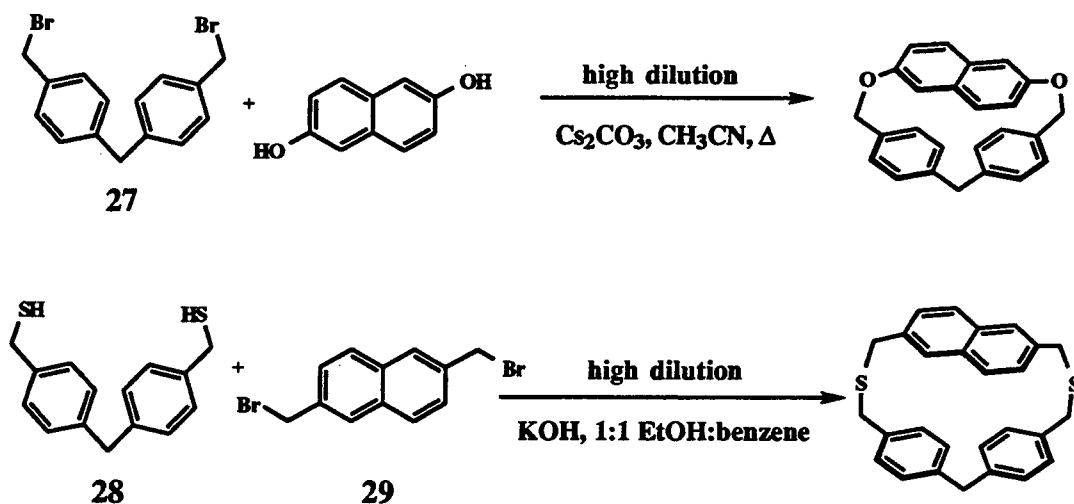
Figure 2.4. Optimized benzene-cation-benzene complexes. On the left, the cation is lithium; on the right the cation is potassium.

Other small cyclophane hosts **25** and **26** (pictured below) have been tested in the Dougherty group for binding of alkali cations. Dr. Rich Barrans tested them exhaustively, but they did not exhibit measurable binding affinities for the alkali cations.¹²

**25****26**

2. Results and Discussion

The O and S cyclophanes were synthesized readily by the following reactions. For host O, the 2,6 dihydroxynaphthalene was commercially available. The dibromide **27** was synthesized according to the literature. Room temperature macrocyclization conditions failed, presumably due to strain. (The construction of CPK models indicates that phenyl group rotation is hindered.) Slow addition over several days of a mixture of the bisphenol and the dibromide to a refluxing suspension of cesium carbonate in dry acetonitrile resulted in the desired product in 5% yield. For host S, the dithiol compound **28** must be added separately from the dibromide (**29**), because **28** is reactive even in the absence of base. The dithiol in degassed ethanol/benzene solution was added separately from, and simultaneously with, the dibromide dissolved in tetrahydrofuran to a stirred suspension of ethanol/benzene over potassium hydroxide over three days.



Several methods were employed to try to measure alkali metal binding constants, including NMR binding titrations that would monitor host proton shifts upon cation binding, liquid-liquid extraction, and solid-liquid extraction. The NMR binding studies were performed by adding solutions of the picrates of lithium, sodium, potassium, rubidium, and cesium to solutions containing either host O or host S. The solvents surveyed include acetonitrile-*d*₃, acetone-*d*₆, and tetrahydrofuran-*d*₈. The tetraphenylborate salts (30) of the alkali metals were studied in chloroform-*d*. No shifting of host protons or of counterion protons was observed.

Since the binding constants may be very small, and since UV is a more sensitive detector, both liquid-liquid extraction studies and solid-liquid extraction studies were performed and quantitated by UV absorbance. The procedure for both kinds of study was taken from the thesis of Dr. Rich Barrans.¹² Briefly, the liquid-liquid extraction studies were performed by adding water solutions of picrate salts to two sets of chloroform solutions in tubes. One set of chloroform solutions contained cyclophane S, while the other was pure chloroform. All these tubes were agitated by vortexing, and then centrifuged. The absorbance of the chloroform layer at 380nm (where picrate absorbs) was monitored. No enhancement of picrate solubility in the organic layer was observed in

samples containing host cyclophane. The solid-liquid extraction studies were performed with both host **O** and host **S**. Solid picrate salts of the alkali cations were placed in three sets of glass tubes. To one set of tubes was added pure chloroform, while to the other two were added solutions of cyclophane host **O** and host **S**. All these tubes were sonicated for 40 minutes and centrifuged for 45 minutes. Aliquots from each tube reveal that the same amount or even less picrate is present in the samples which contain cyclophane hosts **O** or **S**. Taken together, these results indicate that cyclophane **O** and cyclophane **S** are not viable alkali cation binders, even when solvation by water does not compete for the ion.

3. Future Work for Alkali Cation Binders

The inability to measure a cation- π effect for alkali cations in solution does not mean that it does not exist. For example, the cyclophane host **P** does not bind primary ammonium compounds well, even though they are positively charged. However, there are many instances in biological systems where protonated primary amines do interact with the face of aromatic residues.¹³

The next step would be to design different configurations of phenyl groups and different sizes of the binding cavity in an effort to achieve a perfect fit between alkali cations and cyclophane hosts.

II. CONCLUSIONS

The hosts **PHOS**, **O**, and **S** have been designed to explore more subtle aspects of the cation- π effect. Host **PHOS** is within synthetic reach, and should provide insight on macrocycle charge effects on cation binding as well as serve as a more soluble host in neutral aqueous solutions. The hosts **O** and **S** did not demonstrate the cation- π effect for alkali metal cation guests, but a different cyclophane may be designed and synthesized that

will. If this goal is achieved, the data would provide additional strong support for the hypothesis that aromatic residues play an active role in potassium ion conductance in voltage-gated ion channels.

Experimental Section

I. Synthesis

¹H spectra were recorded on a JEOL JNM GX-400 spectrometer. Routine spectra were referenced to the residual proton and carbon signals of the solvents and are reported (ppm) downfield of 0.0 as δ values. The following packing material was used in column chromatography: E. Merck silica gel 60, 0.04-0.063 mm.

A. Host PHOS and related compounds

The compounds 2,6-Dihydroxyanthracene,⁴ 2,6-Bis(*tert*-butyldimethylsiloxy)anthracene,⁴ (9*S*,10*S*,11*R*,12*R*)- and (9*R*,10*R*,11*R*,12*R*)-2,6-Bis(*tert*-butyldimethylsiloxy)-9,10-dihydro-11,12-dicarboxyethanoanthracene Bis[(+)-menthyl ester] (**2**),⁴ 2,6-Bis(*tert*-butyldimethylsiloxy)-9,10-dihydro-11,12-dicarbomethoxyethenoanthracene (**5**),⁴ 2,6-Dihydroxy-9,10-dihydro-11,12-dicarbomethoxyethenoanthracene,⁴ host **P**,⁴ 2,6-Bis[(4-methyl)benzyloxy]-9,10-dihydro-11,12-dicarbomethoxyethenoanthracene (**6**),¹⁴ 1,2'-methylenebis(4-bromomethylbenzene) (**27**),¹² 1,1-methylenebis(4-benzylmercaptan) (**28**),¹² and alkali tetraphenylborate salts (**30**)¹⁵ were made according to literature methods.

Deprotection of phenol groups. The TBS-protected **2** was added to a 25 mL flask with a stir bar. The solid was dissolved in 10 mL of methanol and 2 mL of methylene chloride. Then, 1 - 2 mL of saturated aqueous HCl was added. The progress of the reaction was followed by thin layer chromatography using a molybdate stain to visualize the spots on the plate. When the reaction was complete (one or two days) most of the solvent was removed by rotary evaporation and the residue was partitioned between water

and diethyl ether. The product was isolated by silica gel chromatography using 1:1 petroleum ether:diethyl ether as eluant.

(9S,10S,11R,12R)- and (9R,10R,11R,12R)-2,6-Dihydroxy-9,10-dihydro-11,12-dicarboxyethanoanthracene Bis[(+)-menthyl ester] (15)

syn ^1H NMR (CDCl_3): δ 7.14 (d, $J = 7.8$ Hz, 2H), 6.67 (d, $J = 2.4$ Hz, 2H), 6.51 (dd, $J = 2.7, 8.1$ Hz, 2H), 4.54 (td, 2H), 4.51 (s, 2H), 3.31 (s, 2H), 1.93 (d quintets, 2H), 1.78, 1.63, 1.37, (m's, 16H), .93 (d, $J = 7.6$ Hz, 6H), .83 (d, $J = 6.6$ Hz, 6H), .72 (d, $J = 6.8$ Hz, 6H). FAB-MS m/e 603 (MH $^+$) ; HRMS 603.3669, calc. for $\text{C}_{38}\text{H}_{50}\text{O}_6$. 603.3686.

anti ^1H NMR (CDCl_3): δ 6.99 (d, $J = 8.1$ Hz, 2H), 6.82 (d, $J = 2.4$ Hz, 2H), 6.47 (dd, $J = 2.4, 7.8$ Hz, 2H), 4.54 (td, 2H), 4.50 (s, 2H), 3.29 (s, 2H), 1.93 (d quintets, 2H), 1.79, 1.65, 1.38, (m's, 16H), .93 (d, $J = 7.1$ Hz, 6H), .82 (d, $J = 6.3$ Hz, 6H), .72 (d, $J = 6.8$ Hz, 6H). FAB-MS m/e 603 (MH $^+$) ; HRMS 603.3651, calc. for $\text{C}_{38}\text{H}_{50}\text{O}_6$ 603.3686.

Tetramenthyl ester macrocycle (16). Compound **15** (0.166 mmol) and α,α' -dibromo-*p*-xylene (0.166 mmol) were placed in an oven-dried 25 mL flask. Excess cesium carbonate and 125 mL of dry acetonitrile were added to an oven-dried 250 mL 3-necked flask equipped with a stir bar and a condenser. The diphenol and dibromide were dissolved in 10 mL of dry acetonitrile and taken up in a 30 mL gastight syringe. The 25 mL flask was rinsed twice with dry acetonitrile and the washings were taken up in the syringe. The large flask was heated to reflux, and the solution in the syringe was added over a period of two to three days by syringe pump. The reaction was refluxed for one additional day. The reaction, including some precipitated product, was cooled. The bulk of the solvent was removed by rotary evaporation and the residue was partitioned between chloroform and water. The water layer was extracted three times with chloroform. The

organic layer was dried with sodium sulfate. The solvent was removed by rotary evaporation. The product was isolated in 12% yield by silica gel chromatography in which the sample was dry-loaded and eluted in 25% diethyl ether in petroleum ether. (**16 anti**) ^1H NMR (CDCl_3): δ 6.88 (d, $J = 8.3$ Hz, 4H), 6.83 (d, $J = 2.2$ Hz, 4H), 6.45 (dd, $J = 2.4$, 8.1 Hz, 4H), 5.10 (AB $\Delta\nu = 31$, $J = 16$ Hz, 8H), 4.52 (td, 2H), 4.41 (s, 2H), 3.24 (s, 2H), 1.91 (d quintets, 2H), 1.80, 1.65, 1.36, (m's, 16H), .92 (d, $J = 7.1$ Hz, 6H), .82 (d, $J = 6.3$ Hz, 6H), .69 (d, $J = 6.8$ Hz, 6H). FAB-MS m/e 1432 (MNa^+).

Reduction of methyl and menthyl esters. The ester was added to an oven-dried flask with a stir bar. Dry tetrahydrofuran was added to create a .05 to .1 M solution. The lithium triethylborohydride (commercially available in 1M solution in tetrahydrofuran) was added dropwise, using 2.2 equivalents per ester to be reduced. After stirring overnight, at room temperature, ethyl acetate was added to quench excess reductant and the solvent was removed by rotary evaporation. The residue was partitioned between water and ethyl acetate. The organic layer was dried and concentrated. The product was purified by silica gel chromatography, generally using 40% petroleum ether in ethyl acetate as an eluant for **7**, **8**, **10**, and **11**. For **17**, ethyl acetate or 5% methanol in ethyl acetate was used instead.

2,6-Bis(tert-butyldimethylsiloxy)-9,10-dihydro-11,12-dimethylethanoanthracene Bis(-ol) (7). ^1H NMR (CDCl_3): δ 7.07 (d, $J = 7.8$ Hz, 2H), 6.79 (d, $J = 2.4$ Hz, 2H), 6.35 (dd, $J = 2.2$, 7.8 Hz, 2H), 4.98 (s, 2H), 4.27 (s, 4H). FAB-MS m/e 542 (MNH_4^+); HRMS 542.3157, calc. for $\text{C}_{30}\text{H}_{48}\text{NO}_4\text{Si}_2$. 542.3122.

2,6-Bis[(4-methyl)benzyloxy]-9,10-dihydro-11,12-dimethylethanoanthracene Bis(-ol) (8). ^1H NMR (CD_3CN): δ 7.26 (d, $J = 7.5$

Hz, 4H), 7.16 (d, $J = 7.6$ Hz, 4H), 7.12 (d, $J = 8.1$ Hz, 2H), 6.95 (d, $J = 2.5$ Hz, 2H), 6.39 (dd, $J = 2.5, 8.1$ Hz, 2H), 5.13 (s, 2H), 4.96, (s, 4H), 4.15 (s, 4H), 2.29 (s, 6H).

(9S,10S,11R,12R)- and (9R,10R,11R,12R)-2,6-Bis(tert-butyltrimethylsiloxy)-9,10-dihydro-11,12-dicarboxyethanoanthracene Bis(-ol) (10).

syn ^1H NMR (CDCl_3): δ 7.06 (d, $J = 9.4$ Hz, 2H), 6.72 (d, $J = 2.6$ Hz, 2H), 6.65 (dd, $J = 2.5, 9.4$ Hz, 4H), 4.04 (s, 2H), 3.43 (m, 2H), 3.04 (m, 2H), 1.67 (m, 2H), 0.95 (s, 18H), 0.12 (s, 12H).

anti ^1H NMR (CD_3CN): δ 7.08 (d, $J = 9.3$ Hz, 2H), 6.97 (d, $J = 3.1$ Hz, 2H), 6.56 (dd, $J = 2.8, 9.4$ Hz, 4H), 4.15 (s, 2H), 3.08 (m, 2H), 2.98 (m, 2H), 1.32 (m, 2H), 0.95 (s, 18H), 0.16 (s, 12H).

(9S,10S,11R,12R)- and (9R,10R,11R,12R)-2,6-Bis[(4-methyl)benzyloxy]-9,10-dihydro-11,12-dimethylethanoanthracene Bis(-ol) (11).

anti ^1H NMR (CDCl_3): δ 7.28 (d, $J = 7.4$ Hz, 2H), 7.16 (d, $J = 7.4$ Hz, 2H), 7.11 (d, $J = 8.2$ Hz, 2H), 6.92 (d, $J = 2.2$ Hz, 2H), 6.66 (dd, $J = 2.1, 8.3$ Hz, 4H), 4.93 (s, 4H), 4.08 (s, 2H), 3.45 (m, 2H), 3.10 (m, 2H), 2.32 (s, 6H), 1.67 (m, 2H).

syn FAB-MS m/e 529 (MNa^+), 507 (MH^+); HRMS 529.2368, calc. for $\text{C}_{34}\text{H}_{34}\text{O}_4$ 529.2355.

Tetra-ol macrocycle (17).

anti ^1H NMR (CD_3OD): δ 7.21 (s, 8H), 7.01 (d, $J = 8.3$ Hz, 4H), 6.76 (d, $J = 2.2$ Hz, 4H), 6.55 (dd, $J = 8.3, 2.7$ Hz, 4H), 5.05 (AB $\Delta\nu = 17.6$, $J = 14.4$ Hz, 8H), 4.07 (s, 4H), 3.24 (m, 4H), 2.97 (m, 4H), 1.32, (s (br.), 4H). FAB-MS m/e 801 (MH^+); HRMS 823.3246 (MNa^+), calc. for $\text{C}_{52}\text{H}_{48}\text{O}_8\text{Na}$ 823.3247.

Phosphate esters. The alcohol (0.257 mmol) was placed in a 25 mL flask with a stir bar and 10 mL of dry pyridine. The flask was chilled to 0 °C and the diphenylchlorophosphate (2.58 mmol) was added dropwise. The reaction was left to warm to room temperature and then heated overnight at 60°C. The reaction was cooled to room temperature, water was then poured into the reaction, and it was stirred for 30 minutes. The product was extracted with ethyl acetate. The aqueous layer was extracted several times. The organic layer was dried with sodium sulfate and the solvent was removed by rotary evaporation. The product was purified by silica gel chromatography using 1:1 petroleum ether:ethyl acetate as eluant.

Bis(Diphenyl) (9S,10S,11R,12R)- and (9R,10R,11R,12R)-2,6-Bis[(4-methyl)benzyloxy]-9,10-dihydro-11,12-dimethylethanoanthracene Bis(phosphate) (12)

syn FAB-MS *m/e* 971 (MH⁺) ; HRMS 971.3081, calc. for C₅₈H₅₃O₁₀P₂ 971.3114.

Tetraphosphate ester macrocycle (18).

anti ¹H NMR (CDCl₃): δ 7.24 (m, 40H), 7.20 (s, 8H), 6.86 (d, *J* = 8.3 Hz, 4H), 6.67 (d, *J* = 2.2 Hz, 4H), 6.47 (dd, *J* = 2.4, 8.1 Hz, 4H), 5.11 (AB Δ*v* = 17.6, *J* = 14.4 Hz, 8H), 3.96 (s, 4H), 3.89 (m, 4H), 1.61 (s br., 4H). FAB-MS *m/e* 1751 (M⁺); HRMS 1751.4425, calc. for C₁₀₀H₈₄O₂₀NaP₄ 1751.4404.

syn FAB-MS *m/e* 1752 (MNa⁺).

Phosphate ester hydrolysis. The phosphate ester was placed in a 10 ml flask with 20-fold excess of solid cesium hydroxide. Next, 0.5 mL of DMSO-d₆ was added and the mixture was sonicated for 5 minutes. The reaction stirred at room temperature

overnight. As a precipitate formed, D₂O was added to dissolve the partially hydrolyzed substrate. The reaction was monitored by ¹H NMR. For the macrocycle 18, the reaction was heated to 50 °C for one week. No single symmetric product was formed.

B. Alkali cation binders.

2,6-Bis(bromomethyl)naphthalene (29). 2,6-dimethylnaphthalene (1.62mmol) and 2.05 equivalents of N-bromosuccinimide (3.32mmol) were placed in an oven-dried 250mL round bottom flask equipped with a stir bar and condenser. Dry methylene chloride was introduced by cannula. The flask was exposed to a sunlamp for two hours. The reaction mixture was poured into aqueous bicarbonate and extracted with methylene chloride several times. The product was purified by silica gel chromatography by dry-loading the sample and eluting in 10% chloroform in petroleum ether. ¹H NMR (CDCl₃): δ 7.80 (d, *J* = 8.1 Hz, 2H), 7.78 (d, *J* = 1.3 Hz, 2H), 7.51 (dd, *J* = 1.4, 8.6 Hz, 2H), 4.64 (s, 4H).

Macrocycle O. Into an oven-dried 500 mL 3-necked flask equipped with a condenser and stir bar was placed 1 g of cesium carbonate and 200 mL of dry acetonitrile. This flask was heated to reflux. 2,6-Dihydroxynaphthalene (2.66 mmol) and 1,2'-methylenebis(4-bromomethylbenzene) (27) were dissolved in a solution of 10 mL dry acetonitrile and 15 mL of dry dimethylformamide and taken up in a gas-tight syringe. This solution was added over three days to the refluxing acetonitrile and base. Periodically, cesium carbonate was added to the reaction mixture, which was a blue or blue-green color. The reaction was cooled and most of the solvent was removed by rotary evaporation. The residue was partitioned between water and chloroform, and the aqueous layer was extracted several times with chloroform. The organic layer was dried with sodium sulfate and solvent was removed by rotary evaporation. The product was purified by silica gel

chromatography by dry-loading the sample and eluting in 1:1 chloroform:petroleum ether. ^1H NMR (CDCl_3): δ 7.08 (d, J = 8.6 Hz, 2H), 6.91 (dd, J = 2.4, 8.6 Hz, 2H), 6.80 (m, 8H), 6.67 (d, J = 2.4 Hz, 2H), 5.22 (AB $\Delta\nu$ = 17.9, J = 11.4 Hz, 4H), 3.50 (s, 2H). FAB-MS m/e 352 (M^+) ; HRMS 352.1475, calc. for $\text{C}_{25}\text{H}_{20}\text{O}_2$. 352.1463.

Macrocycle S. 500mL of a 1:1 mixture of punctilious ethanol:benzene was degassed. 100 mL of this solution and KOH (3.67 mmol) were added to a 500 mL 3-necked flask equipped with a stir bar and two pressure-equalizing addition funnels. The 1,1-methylenebis(4-benzylmercaptan) (**28**) (.85 mmol) was dissolved in 125 mL of the 1:1 solvent and placed in one of the addition funnels. The 2,6-bis(bromomethyl)naphthalene (**29**) (.85 mmol) was dissolved in 125 mL of dry tetrahydrofuran and placed in the other funnel. The simultaneous addition took place over three days. Most of the solvent was removed by rotary evaporation. The residue was partitioned between water and chloroform, and the aqueous layer was extracted several times with chloroform. The organic layer was dried with sodium sulfate and solvent was removed by rotary evaporation. The product was purified by silica gel chromatography by dry-loading the sample and eluting in 30% chloroform in petroleum ether. ^1H NMR (CD_3CN): δ 7.30 (s (br.), 2H), 7.21 (d, J = 8.5 Hz, 2H), 7.06 (dd, J = 2.1, 8.4 Hz, 2H), 6.97 (d, J = 9.0 Hz, 4H), 6.68 (d, J = 9.1 Hz, 4H), 3.93 (s, 4H), 3.83 (s, 4H), 3.50 (s, 2H). FAB-MS m/e 412 (M^+) ; HRMS 412.1307, calc. for $\text{C}_{27}\text{H}_{24}\text{S}_2$. 412.1319.

II. Binding Studies

NMR Studies. In acetonitrile- d_3 , the concentrations of species in the NMR tubes were 150 μM host **O** or **S** and 3.02 mM lithium picrate, 2.97 mM sodium picrate, 2.49 mM potassium picrate, 1.33 mM rubidium picrate, and 1.27 mM cesium picrate. In acetone- d_6 the concentrations of species in the NMR tubes were 310 μM host **O** or **S** and

2.88 mM picrate salt, except for cesium picrate (2.52mM). In tetrahydrofuran-*d*₈, only the cesium picrate (2.50 mM) was studied with host O (310 μ M). No shifting of host protons were observed.

Liquid-liquid extraction.¹² Solutions of picrates in Milli-Q purified water were made: lithium picrate (14.94 mM), sodium picrate (14.98 mM), potassium picrate (14.95 mM), rubidium picrate, (9.99 mM), and cesium picrate (9.98 mM). A solution in ethanol-free chloroform of host S (about 2.5 mM) was made. Using a Hamilton gastight syringe, 0.50 μ L of S stock solution was added to six 13 x 100 mm test tubes. The picrate salts were added, while the sixth tube had pure water added. A set of blank tubes were similarly made using 0.50 μ L of pure ethanol-free chloroform. Each tube was vortexed for 2 minutes and then centrifuged for 40 minutes. A 250 μ L gastight syringe was used to take 200 μ L of each sample's chloroform layer. These samples were diluted in 2 mL volumetric flasks with acetonitrile. Absorbance at 380nm was measured. The tubes which contained cyclophane had the same or slightly lower absorbance at 380 nm than the tubes containing pure chloroform.

Solid-liquid extraction. In six 13 x 100 mm tubes were placed 0.30 mL of host O stock solution in chloroform (3.1mM) plus 1 -3 mg of one of each picrate salt. These tubes were sealed with septa and parafilm and sonicated for 40 minutes. The tubes were then centrifuged for 45 minutes, and aliquots were removed and diluted up to 2.0 mL with acetonitrile in a volumetric flask. The absorbances of each sample at 380 nm were recorded. The same procedure for host S was followed. No enhanced absorbance at 380 nm was observed for samples containing either cyclophane.

References

1. Kearney, P. C.; Mizoue, L. S.; Kumpf, R. A.; Forman, J. E.; McCurdy, A.; Dougherty, D. A. *J. Am. Chem. Soc.* **1993**, *115*, 9907-9919.
2. a) Deranleau, D. A. *J. Am. Chem. Soc.* **1969**, *91*, 4044.
b) Person, W. B. *J. Am. Chem. Soc.* **1965**, *87*, 167-170.
c) Wilcox, C. S. In *Frontiers in Supramolecular Organic Chemistry and Photochemistry*, Schneider, H.-J.; Durr, H., Eds.; VCH: Weinheim, 1990.
3. Corbridge, D. E. C. *Phosphorus: An Outline of its Chemistry, Biochemistry, and Technology*; Elsevier: New York, 1990.
4. Petti, M. A.; Shepodd, T. J.; Barrans, R. E.; Dougherty, D. A. *J. Am. Chem. Soc.* **1988**, *110*, 6825-6840.
5. Corbridge, D. E. C. *Phosphorus: An Outline of its Chemistry, Biochemistry, and Technology*; Elsevier: New York, 1990.
6. a) Kearney, P. C. Ph. D. Thesis, California Institute of Technology, 1994.
b) Uhlmann, E.; Engels, J. *Tet. Lett.* **1986**, *27*, 1023-1026.
7. a) Cohen-Adad, C.; Baret, P.; Chautemps, P.; Pierre, J. L. *Acta Crystallogr. Sect. C* **1983**, 1346.
b) Kang, H. C.; Hanson, A. W.; Eaton, B.; Boekelheide, B. *J. Am. Chem. Soc.* **1985**, *107*, 1979.
8. Schmidbauer, H.; Hager, R.; Huber, B.; Muller, G. *Angew. Chem.* **1987**, *99*, 354.
9. Sunner, J.; Nishizawa, K.; Kebarle, P. *J. Phys. Chem.* **1981**, *85*, 1814-1820.
10. Heginbotham, L.; Abramson, T.; MacKinnon, R. *Science* **1992**, *258*, 1152-1155.
11. Kumpf, R. A.; Dougherty, D. A. *Science* **1993**, *261*, 1708-1710.
12. Barrans, R. E. Ph. D. Thesis, California Institute of Technology, 1992.
13. Burley, S. K.; Petsko, G. A. *FEBS Lett.* **1986**, *203*, 138-143.
14. Stauffer, D. A. Ph. D. Thesis, California Institute of Technology, 1989.
15. *Advances in Analytical Chemistry and Instrumentation*; Vol 1; Wiley Interscience: New York, 1960; pp 1-117.

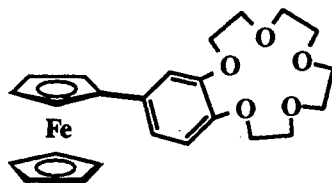
Chapter 3

Design of a Sensor for Organic Molecule Guests in Aqueous Media: A Photoactive Donor-Cyclophane-Acceptor Triad

I. INTRODUCTION

A. Sensors

The study of synthetic host molecules not only can provide insight into fundamental forces involved in molecular recognition, but also can lead to the development of molecular sensory devices. To create a sensor, a specific high-affinity receptor for organic molecules is incorporated into a structure in which a binding event is transduced into a measurable signal. Many successful sensing devices have relied on conducting polymers to generate an analyte-selective electronic signal.¹ Most of these systems rely on the influence of bound species to change the reversible redox chemistry of the conjugated backbone of the polymer as detected by cyclic voltammetry.² The specificity of the conducting polymer sensor may be imparted in several ways. The polymer may be manipulated by doping with different ions, modifying the monomers, or incorporating preformed binding sites into the polymer. The last approach has consisted mainly in the incorporation of crown ether groups into the polymers.³ The study of model compounds which contain redox centers coupled to crown ethers, such as **1** pictured below, demonstrated changes in reduction potential upon cation complexation.⁴ However, study of conducting polymers modified by crown ethers has not uniformly given promising results.



1

An alternative approach to the construction of sensors based on conducting polymers is to link molecular recognition to a change in polymer conductivity. The

observed macroscopic conductivity of bulk conducting polymer is believed to be limited by the interchain movement of charge carriers.⁵ Incorporation of a crosslinking macrocycle into the conducting polymer, as shown below in Figure 3.1, will create a conductivity switch based on the presence or absence of specific guest-binding interactions. A guest analyte tightly bound in the host cavity should facilitate interchain hopping of the charge carrier by providing an additional pathway for interchain charge movement. This hypothesis may be tested easily by studying the closely related phenomenon of electron transfer. Charge movement between chains in conducting polymers *is* electron transfer, and may be modelled by a photoinduced electron transfer (PET) donor-host-acceptor triad. If guest binding inside a macrocycle that bridges a PET donor and acceptor significantly alters electron transfer rates, Figure 3.1 represents a viable approach to creating a sensor.

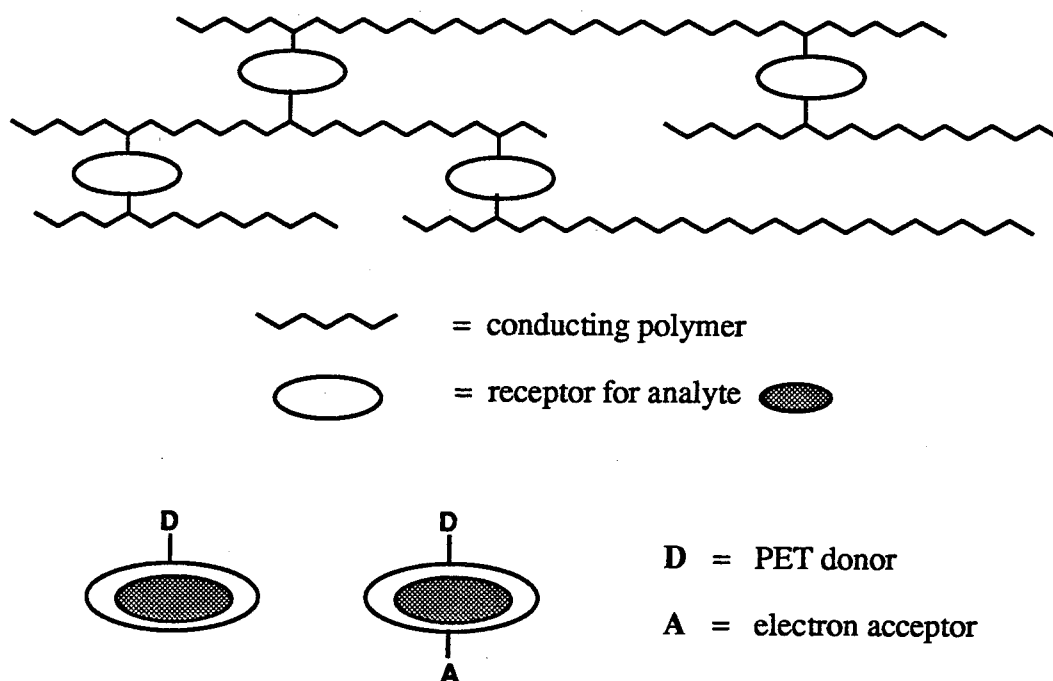


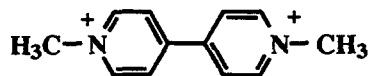
Figure 3.1. Representation of a conducting polymer crosslinked by a macrocyclic receptor (top) and of a photoactive donor-host-acceptor triad (bottom).

There are two ways a specific noncovalent binding interaction may enhance electron transfer rates between a donor and an acceptor.⁶ Equation (1) below describes the rate of electron transfer (k_{ET}) from a donor to an acceptor, where ΔG° is the driving force for electron transfer for that donor/acceptor pair:⁷

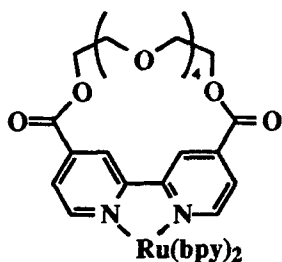
$$(1) \quad k_{ET} = \left(\frac{\pi}{\hbar^2 \lambda k_B T} \right)^{\frac{1}{2}} [H_{ab}]^2 \exp \left[-\frac{(\Delta G^\circ + \lambda)^2}{4 \lambda k_B T} \right]$$

The first term influencing electron transfer rates is H_{ab} , or the degree of coupling of reactant and product electronic states. The electron transfer rate is proportional to the square of the overlap of the donor and acceptor electronic wavefunctions. This coupling occurs by “through-space” or by “through-bond” (which involves the use of intervening covalent bonds to propagate the coupling in a superexchange type of interaction) mechanisms. A simplistic mathematical expression describing the donor/acceptor coupling is an exponential decay function. This reflects the decrease in coupling with an increase in distance between the donor and acceptor. The degree of attenuation of coupling also has a dependence on the nature of the intervening medium.⁸ Electron transfer studies of donor-bridge-acceptor triads show that unsaturated bridges covalently linking donor and acceptor moieties attenuate coupling less than saturated bridges do. The second term influencing k_{ET} is λ , or the reorganization energy. This quantity is the energy required to distort the nuclei from their reactant-state geometry to their product-state geometry without electron transfer. Any general perturbation of the surrounding solvent, especially solvent polarization, can influence the reorganization energy. Overall, a guest may alter electron transfer rates in a donor-host-acceptor triad either by altering the electronic coupling of donor and acceptor or by changing the reorganization energy.

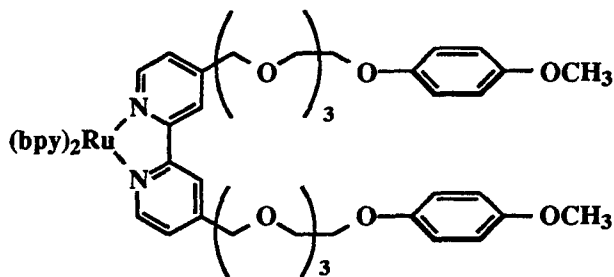
Other molecular recognition systems have been developed to study the effects of noncovalent interactions on photoinduced excited states.⁹ Sensors for protons¹⁰ and alkali metal ions¹¹ have been made by monitoring fluorescence quenching or enhancement, respectively, upon analyte binding. Two photochemical studies have described the intermolecular electron transfer from ruthenium bipyridine complexes to complexed N, N'-dimethyl-4,4'-bipyridinium (2). In one case, an appended crown ether (3) acted as the analyte binding site¹² and in the other a tethered dialkoxybenzene group (4) was the recognition element¹³ for the electron-deficient guest. These two systems are shown below. In these systems, electron transfer to the guest compound within the supramolecular assembly is very fast compared to transfer to uncomplexed guest. For example, photophysical studies of 4 show that luminescence decay is biexponential, with the time constants $\tau = 6$ ns and 160 ns. The slow decay is attributed to transfer to uncomplexed 2, while the faster decay is attributed to transfer within the complexed species of 4 and 2. These data support the idea that specific noncovalent binding interactions can substantially influence electron transfer processes.



2

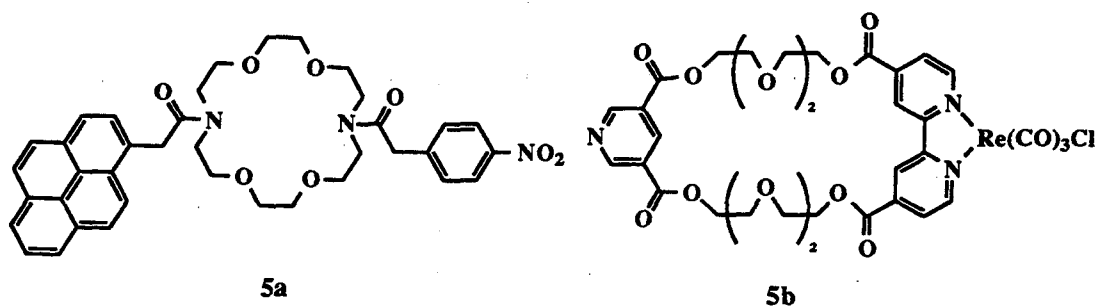


3



4

Only two donor-host-acceptor triads have been examined photophysically to date. In these triads, the intervening macrocycle is a crown ether.^{14a,14c} The triads (**5a**, **5b**) are pictured below. In this arrangement, unlike that for **3** and **4** above, the donor and acceptor are at a fixed distance from one another. When sodium is complexed to **5a**, or potassium to **5b**, electron transfer rates are increased three-fold. The authors invoke a through-bond superexchange mechanism for enhanced long-range electron transfer rates. Related donor-crown acceptor triads have been synthesized,^{14b} but no photophysical studies have been reported.

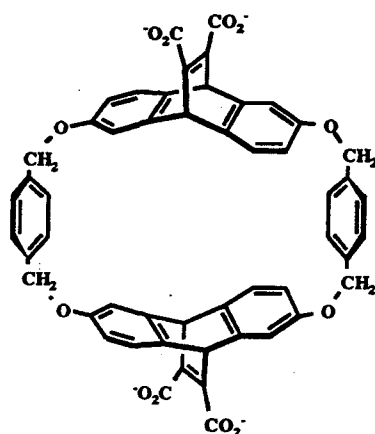


A photoactive donor-cyclophane-acceptor molecule has yet to be synthesized. A donor-cyclophane-acceptor triad may be used to explore the effects of hydrophobic and π -stacking interactions on H_{ab} and λ of equation (1). This chapter will describe the design and attempted synthesis of a photoactive donor-cyclophane-acceptor triad.

B. Design Constraints

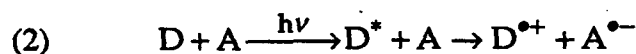
The host sensor model must satisfy several design criteria. First, in order to provide a well-characterized high-affinity receptor for small organic molecules in water, the binding cavity of host **P**, pictured below, should be incorporated in the sensor. Significant changes to the cavity would only complicate a system of subtle interactions that are generally understood.¹⁵ These interactions include hydrophobic effects, cation- π interactions, and polarizability effects. If the hydrophobic binding cavity of host **P** is the

basis for molecular recognition, the donor and/or the acceptor group must provide water solubility for the molecule. A water-soluble metal complex is the simplest group that would fulfill that requirement. Another consideration is the manner in which the metal complex is to be linked to the host. The linkage must be such that the donor cannot directly interact with the guest bound inside the cavity. This constraint implies that a relatively rigid monodentate linkage, or a chelating linkage, would be desirable.



P

Another restriction involves choosing a donor and an acceptor with appropriate redox properties. A photoinduced electron transfer reaction is shown below, in equation (2) where D is the donor, A is the acceptor, and * denotes an excited state. Clearly, no electron transfer should occur in the absence of excitation by light, and the reduction potentials of the ground-state acceptor and the excited-state donor must provide a relatively large driving force for electron transfer. Since $\Delta G^\circ = -(nF\Delta\epsilon^\circ)$, the sum of the standard reduction potentials for the desired redox reaction must be greater than zero for it to be thermodynamically favorable. Therefore, the reduction potentials of the ground and excited states of the species involved must satisfy the conditions $\epsilon^\circ(D^+/D) > \epsilon^\circ(A/A^-) > \epsilon^\circ(D^+/D^*)$.



The photophysical, electrochemical, and solubility demands of the project could be best met by using a ruthenium(II) complex as the photoinduced electron donor and a quinone as the electron acceptor. The ruthenium complexes have desirable photophysical properties and have been thoroughly characterized.¹⁶ Although many organic groups have appropriate redox properties as electron acceptors for ruthenium(II) excited state donors, 1,4-benzoquinone has the best solubility and size properties because it is small. Although methyl viologen (2) would be a good water-soluble electron acceptor, one concern is that the acceptor group may act as a good guest for the host cavity. The viologen compounds are well-suited for binding in the cavity of host **P** because they are electron deficient and the cation- π interaction is strong. Using this kind of group may result in aggregation.

The desired macrocycle should incorporate the considerations detailed above and also be synthetically accessible. The synthesis of host **P** was used as a model for the triad synthesis, and it is presented in Figure 3.2. Briefly, a protected 2,6-dihydroxyanthracene is prepared and subjected to a Diels-Alder cycloaddition with a conjugated diester. Keeping the donor and acceptor groups away from the cavity and preserving the binding cavity of host **P** require that the donor and acceptor groups be attached to the convex part of an anthracene Diels-Alder adduct. Generally speaking, the groups may be incorporated into the host as dienophiles themselves, or they may be incorporated after the Diels-Alder reaction as modifications to the adduct. The incorporation of groups as dienophiles is more desirable, because it not only reduces the overall number of steps in the synthesis, but it is also a more convergent synthesis. Quinone is a good dienophile¹⁷ and may most easily be introduced into the host macrocycle in that capacity. However, no single approach to incorporating the mono, di-, or tetradentate ligands for ruthenium into the host structure stands out as best. As a result, many kinds of ligands and linkages were tried.

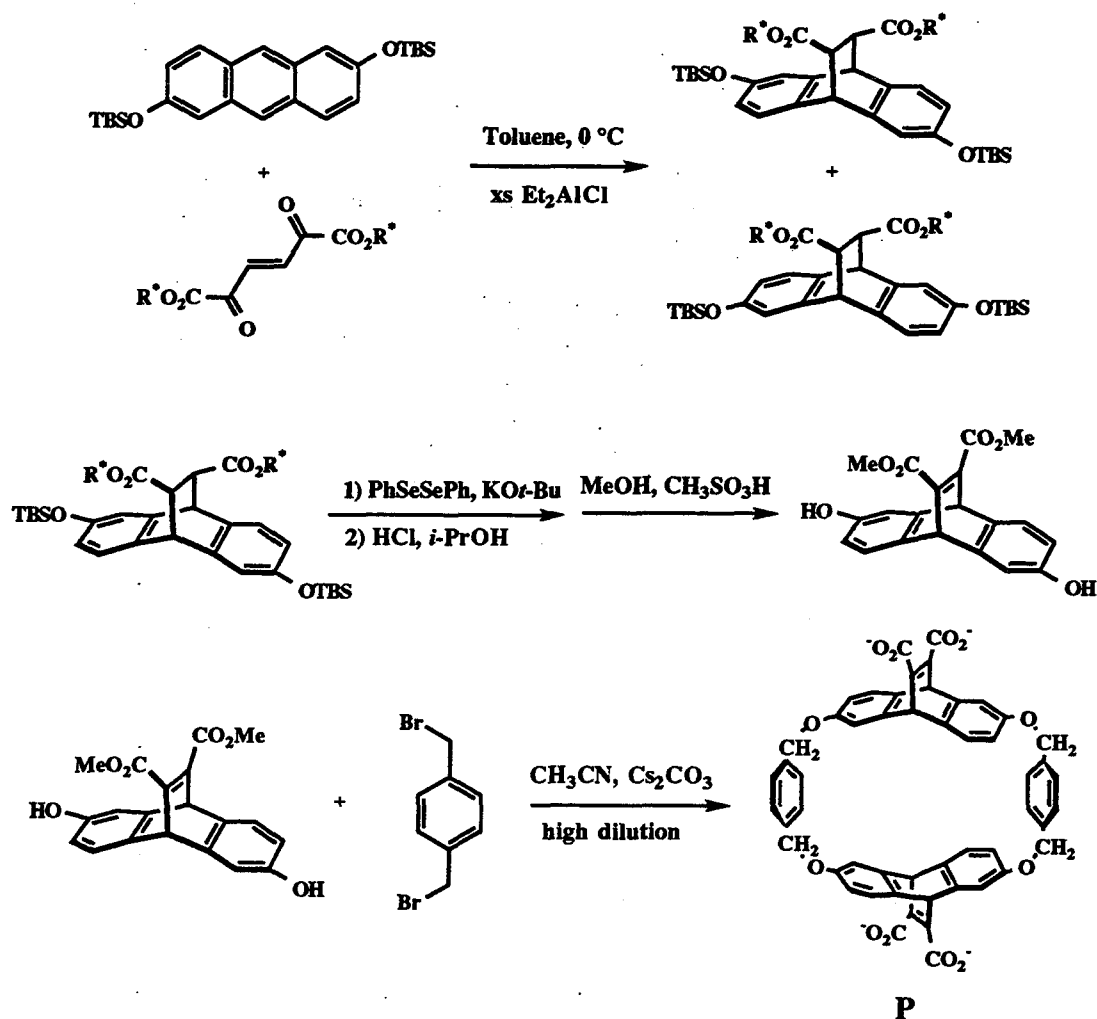
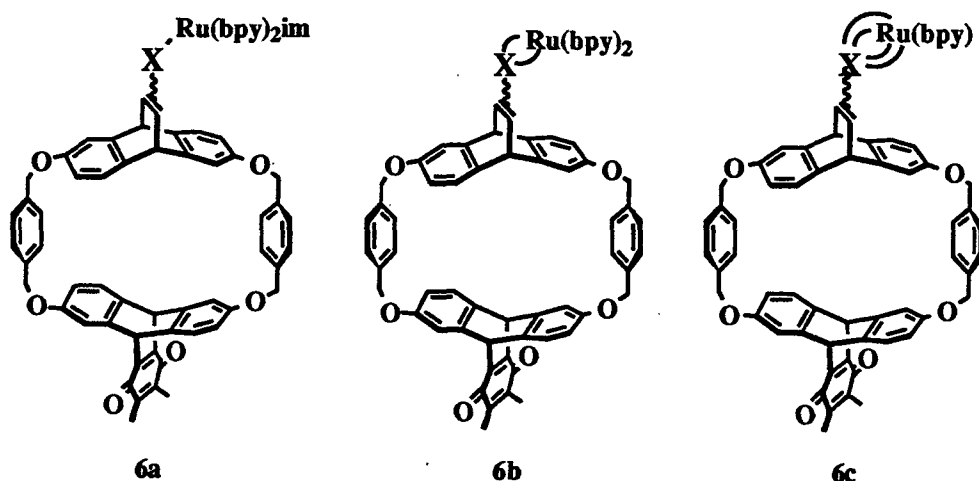


Figure 3.2. Synthesis of cyclophane host P.

A series of target host macrocycles (6) is drawn below. The picture includes a generalized X to represent the mono- (6a), di- (6b), and tetradentate (6c) ligands which can bind ruthenium. This chapter will describe the progress made towards the synthesis of a donor-cyclophane-acceptor triad.



II. RESULTS AND DISCUSSION

A. Electron Acceptor Portion of the Cyclophane

As shown in Figure 3.3 below, this part of the macrocycle synthesis was straightforward. The protected anthracene (7) and 2,3-dimethyl-1,4-benzoquinone (8) were condensed to form a Diels-Alder adduct (9). A methyl-substituted quinone was chosen in order to help prevent nucleophilic attack on the α,β -unsaturated ketone by steric hindrance.¹⁸ The initial Diels-Alder adduct was aromatized to a hydroquinone structure (10) under strongly acidic conditions. These conditions also deprotected the phenol groups. This substituted hydroquinone was then oxidized by 1,4-benzoquinone. The model compound (12) pictured below in Figure 3.4 was synthesized to test the reactivity of the substituted quinone group under various reaction conditions. For example, to test whether the quinone would survive macrocyclization conditions, the model compound, α,α' -dibromoxylene, and phenol were stirred in dry acetonitrile with cesium carbonate at room temperature for two weeks. No reaction occurred at the quinone, indicating its stability under the macrocyclization conditions.

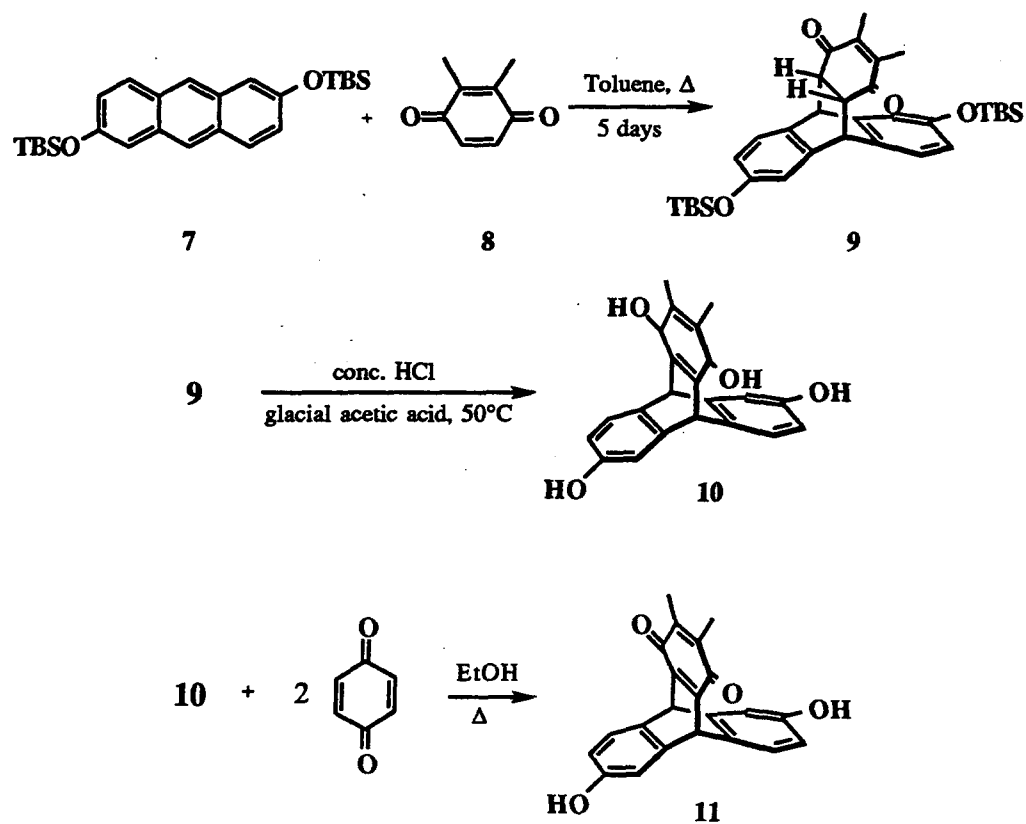


Figure 3.3. Synthesis of the acceptor (quinone) portion of the donor-cyclophane-acceptor triad.

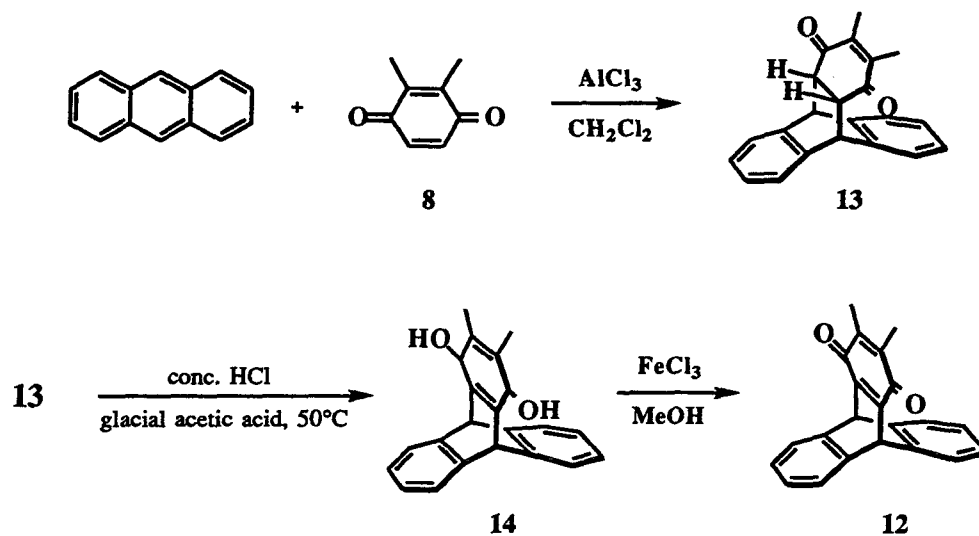


Figure 3.4. Synthesis of model acceptor quinone **12**.

The resulting quinone adduct (**11**) could then be used in the step-wise macrocyclization reaction illustrated in Figure 3.5.

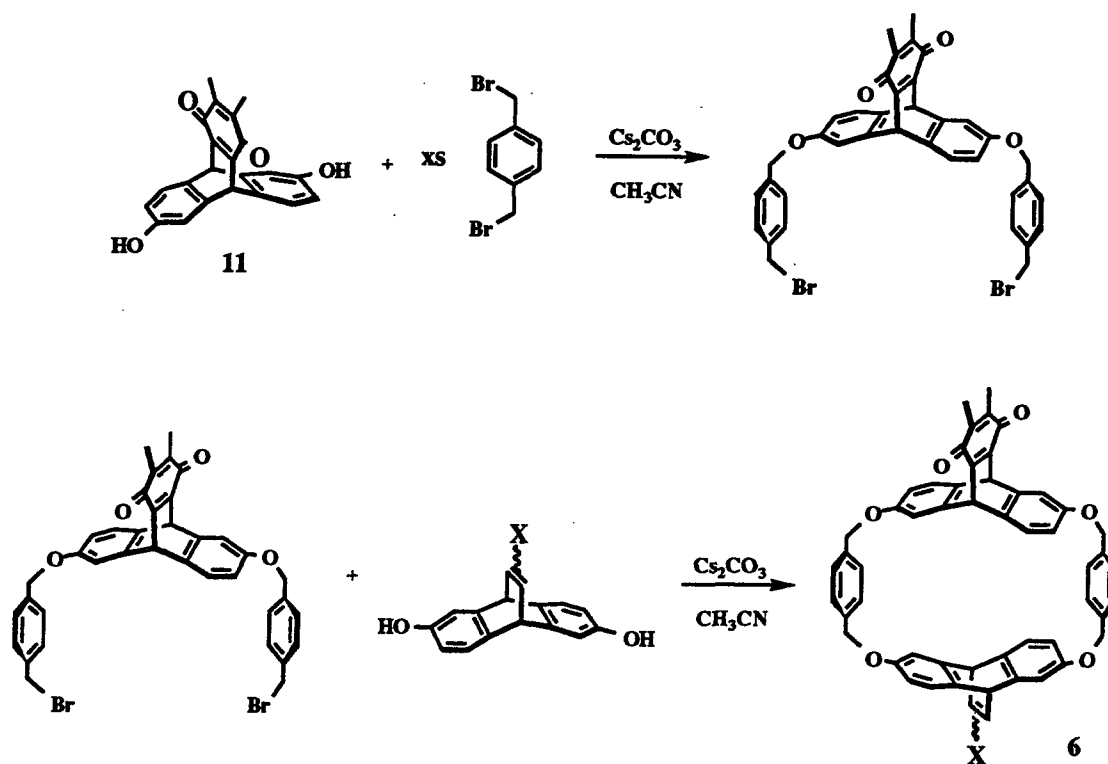
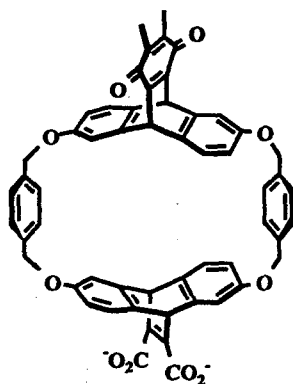


Figure 3.5. Proposed convergent synthesis of the target host by stepwise macrocyclization of donor (X) and acceptor portions of the triad.

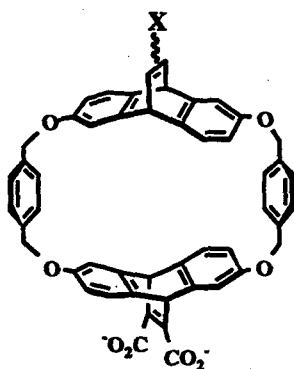
The synthesis of the compound **15** below would allow some intermolecular electron transfer studies similar to those described in the introduction for compounds **3** and **4**. The electron transfer would occur between a bound guest with appropriate ground state redox potential and the photoinduced electron acceptor quinone. The influence of noncovalent forces on electron transfer rates may be determined in this way. If the rate enhancement is large, a sensor based on this specific intermolecular binding interaction has a good chance for success. However, in the case of **15** the host methyl esters cannot be

hydrolyzed in the presence of the quinone. The only effective chemical hydrolysis conditions for methyl esters which should not react with the quinone¹⁹ are potassium *t*-butoxide in anhydrous dimethyl sulfoxide. However, the model quinone compound **12** decomposed under these conditions. Although studies involving the bis(methyl ester) of **15** could be performed in organic media, the binding affinities of guest compounds would be dramatically reduced.²⁰

**15**

B. Photoinduced Electron Donor Portion of the Cyclophane

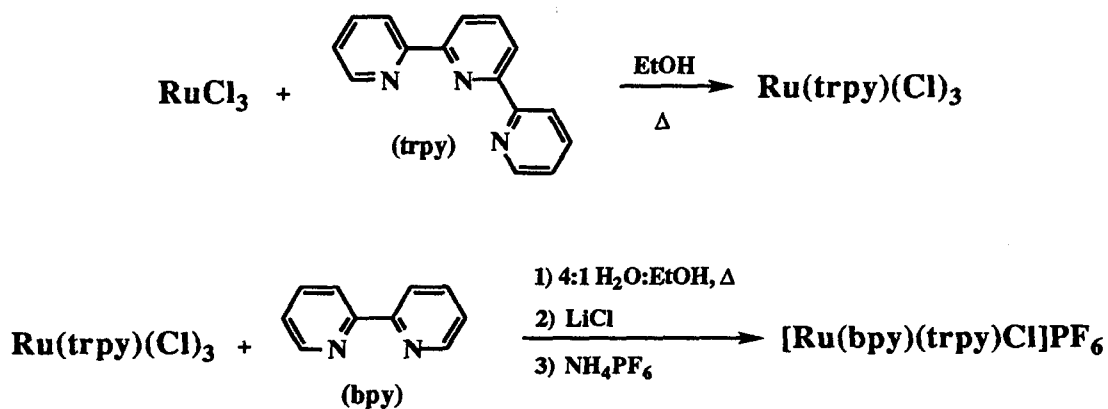
Many nitrogen-containing ligands can be envisioned for ruthenium. The following discussion of synthetic targets is organized by ligand type, including monodentate, bidentate, and tetradentate classes. Once a suitable ligand is chosen, the synthetic route for putting the pieces of the macrocycle together will be decided upon. As above, intermolecular electron transfer studies can be performed with **16**, the partially modified host **P** below.



16

1. Monodentate Ligands

All monodentate ligands were designed to be relatively rigid in order to prevent the ruthenium complex from nearing the opening of the host cavity. For a monodentate ligand, the coordination sphere of ruthenium would be filled by the additional ligands bipyridine and terpyridine. The complex $[\text{Ru}(\text{bpy})(\text{trpy})\text{Cl}]\text{PF}_6$ was easily synthesized as shown below, and would be coupled in a standard way to the host ligand.²¹ The main drawback to using a monodentate ligand is that the association with ruthenium can be weak.



The first monodentate ligand target was isoquinoline, which was to be attached to the molecule *via* direct Diels-Alder of 5,8-isoquinolinedione (**17**) and anthracene.

Heterocyclic quinones are substrates for Diels-Alder reactions,²² and this reaction, shown below in Figure 3.6, proceeded smoothly to form **18**.

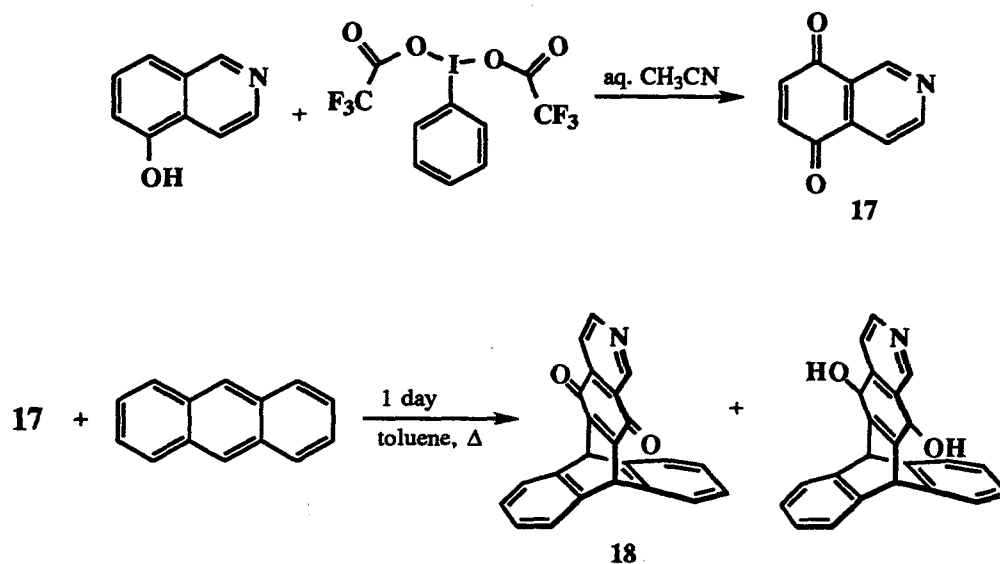
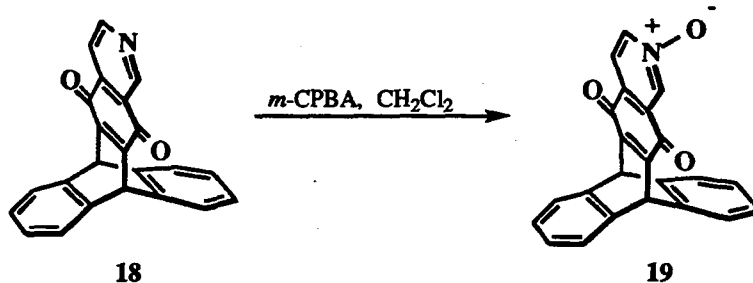


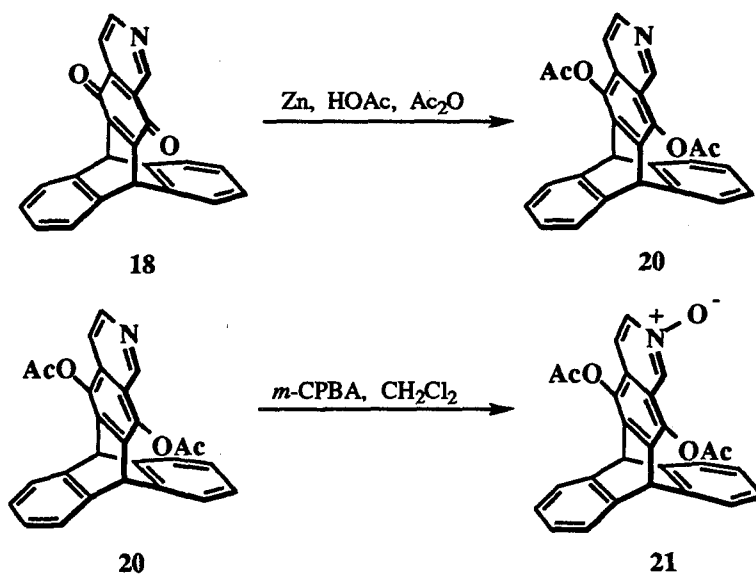
Figure 3.6. Synthesis of the cycloadduct **18** through the reaction of 5,8-isoquinolinedione and anthracene.

To prevent the isoquinoline quinone ligand from quenching the excited state of the ruthenium complex itself, the quinone functionality had to be removed. Reduction conditions which would deoxygenate the ring system are harsh, and they reduce isoquinoline itself.²³ However, reducing quinones with aluminum powder in hot sulfuric acid does not reduce isoquinoline. Unfortunately, when these conditions were applied to the model Diels-Alder adduct (**18**), it underwent a retro-Diels-Alder reaction and many other products formed. Reductive methylation²⁴ of the quinone is a milder way to transform the quinone group, but the isoquinoline nitrogen is quaternized in these reactions. Demethylation of pyridinium compounds is very difficult, and the best procedure is refluxing 1.1 equivalents of triphenylphosphine in dimethylformamide overnight.²⁵ This resulted in a 17% yield for N-methyl quinolinium iodide. This was not considered to be a satisfactory approach. The only reversible way to protect pyridine

nitrogen from methylation is by oxidizing it to the N-oxide as shown below. However, this protecting group does not stand up to reductive methylation conditions.



A simpler way to transform the quinone was to reductively acetylate the molecule. This produced the molecule 20 below. However, the acetate groups would not survive ester hydrolysis conditions. Aryl acetates may be converted to methyl ethers,²⁶ but using N-oxide protected 21 still resulted in nitrogen alkylation. Since a monodentate ligand is a weak ligand, the acetyl group may decrease binding affinity for the ligand even more. This monodentate acetylated ligand is synthetically and electrochemically viable, but perhaps it is not a strong ligand.



The second possible monodentate ligand for ruthenium was a pyridine group. For efficient synthesis, the direct attachment of pyridine to the host through a Diels-Alder reaction was the preferred route. Although some hetarynes can undergo the Diels-Alder reaction with some dienes, 3,4-dehydropyridine cannot.²⁷ Since substituted acetylene

compounds act as Diels-Alder dienophiles, a modified acetylene provided a conceptually simple route to the target molecule. The cycloaddition of methyl pyridin-4-ylpropiolate (22) to substituted anthracene (7) would give rise to a monodentate ligand for ruthenium that fixes the metal complex away from the binding cavity as shown in Figure 3.7. The model compound (23) is shown below. The methyl pyridin-4-ylpropiolate was made in 50% yield overall. However, the Diels-Alder reaction resulted in a very poor yield of less than 5%. The reaction was performed under many sets of conditions taken from a review of Diels-Alder reaction catalysis.²⁸ For example, the reaction was run under four atmospheres of pressure, using solvents such as methanol and ethylene glycol, with the addition of hydroquinone, diethylaluminum chloride, or ferrocenium hexafluorophosphate. The reaction was also run using the N-protonated 23, since electron deficient dienophiles are more reactive. None of these attempts resulted in improved yields.

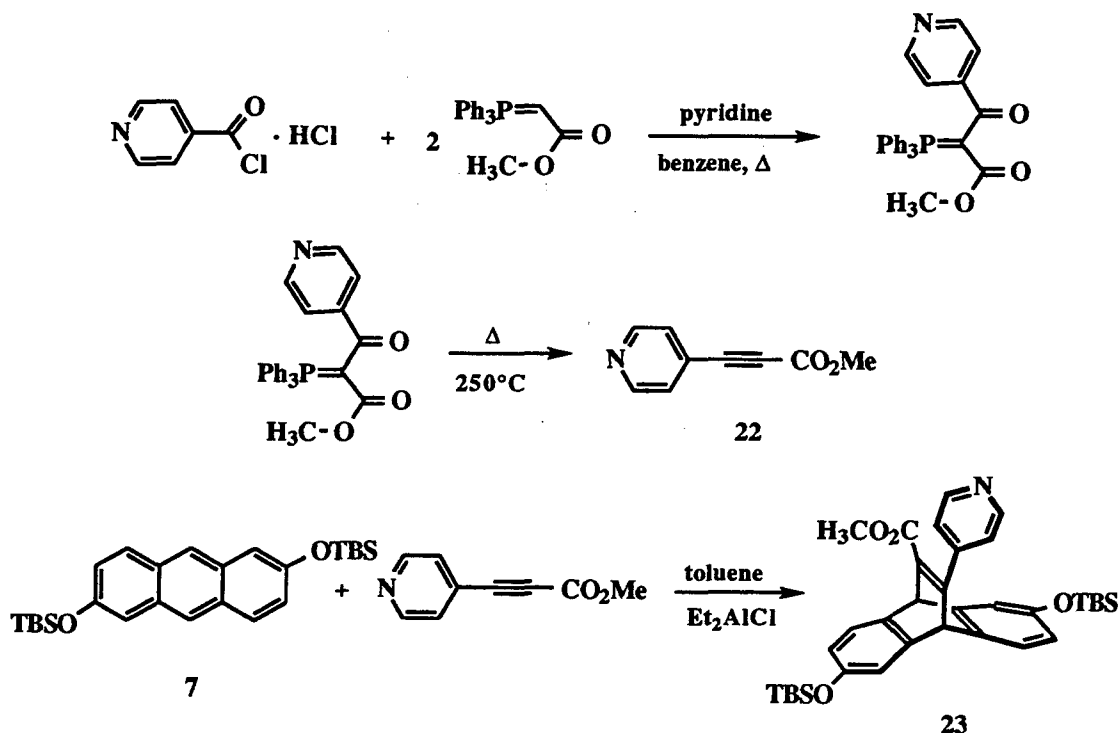


Figure 3.7. Synthesis of pyridyl compound 23 *via* the cycloaddition of pyridin-4-yl propiolate (22) and substituted anthracene 7.

An alternative route to the same pyridyl compound **23** involves the modification of a Diels-Alder adduct of methyl 3-bromopropiolate (**24**) and anthracene **7** by aryl-vinyl coupling with a 4-boropyridine. These reactions are given in Figure 3.8. This Diels-Alder reaction proceeded better than the methyl pyridin-4-ylpropiolate cycloaddition, but the yield was still low (5%). Although this yield was poor, palladium-catalyzed boronic acid and organoborane coupling to vinyl bromides is generally a very efficient reaction. In this case, however, only coupling with the boronic acid (**26a**) succeeded, yielding 15% product.

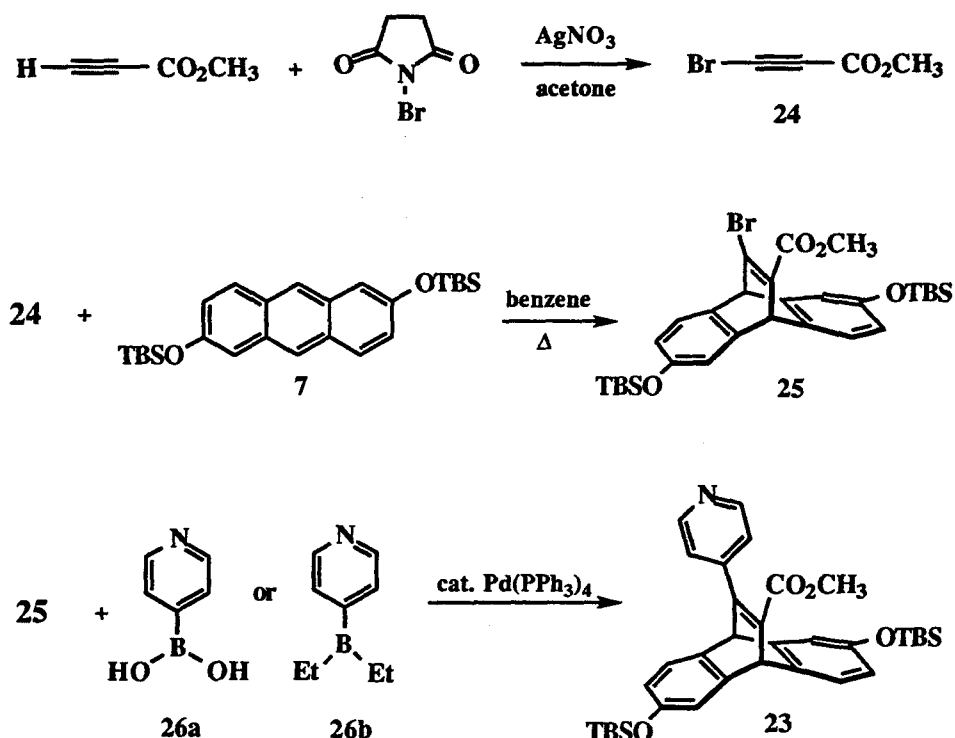


Figure 3.8. Synthesis of pyridyl compound **23** via the Diels-Alder reaction of methyl 3-bromopropiolate and anthracene **7** followed by palladium-catalyzed aryl-vinyl coupling.

One final attempt at producing a pyridine-type ligand for ruthenium required the modification of a Diels-Alder adduct of bromobenzynes and anthracene **7** by aryl-aryl coupling with a 4-pyridyl borane or boronic acid. This reaction sequence is shown in

Figure 3.9. The bromobenzene Diels-Alder proceeds smoothly to form **27**, but the coupling reaction did not work.

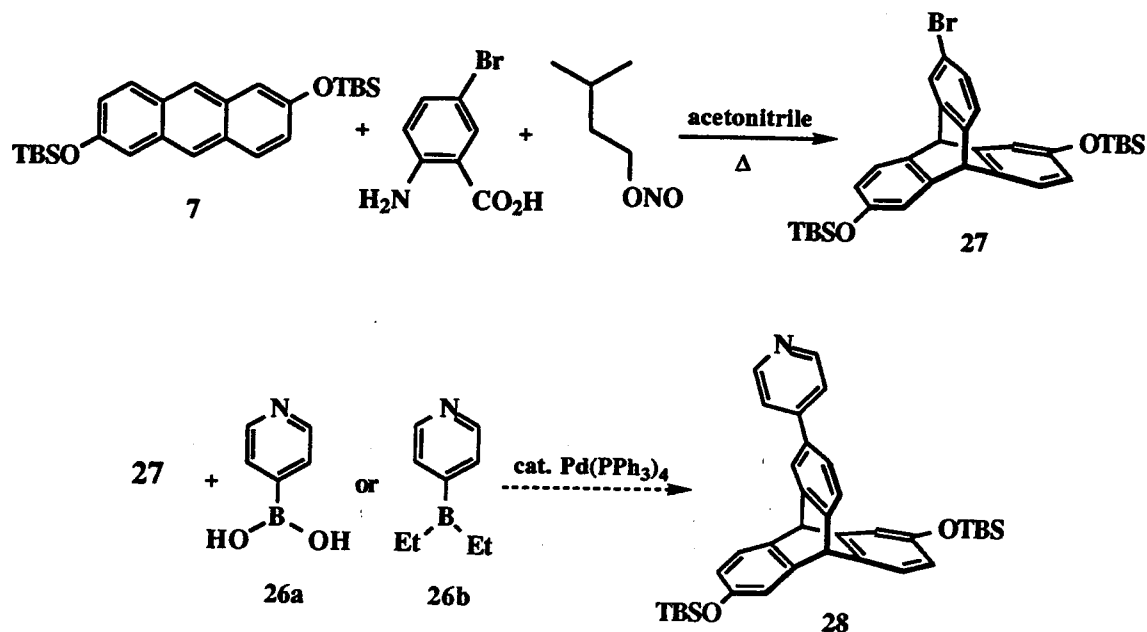


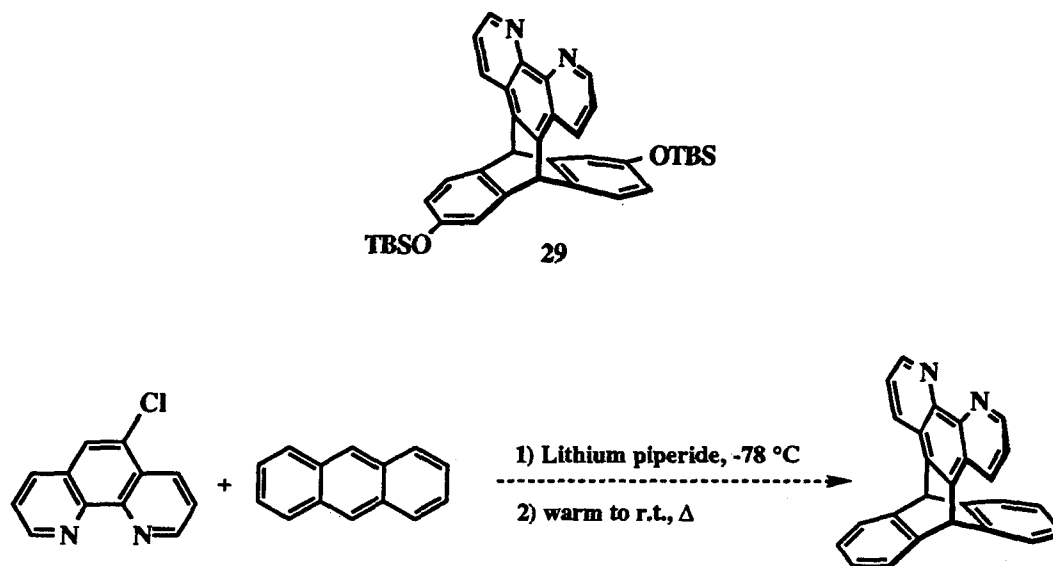
Figure 3.9. Attempted synthesis of ligand **28** via a bromobenzene Diels-Alder adduct with anthracene **7** and subsequent palladium-catalyzed aryl-aryl coupling.

2. Bidentate Ligands

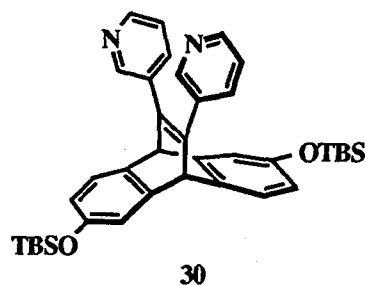
A chelating bidentate ligand was designed to hold the ruthenium complex tightly, and away from the binding cavity of the macrocycle. Unlike the monodentate ligand, the bidentate ligand does not require rigid attachment to the host. A pair of flexible attachments will still restrict the movement of the complex. For these bidentate ligands, the other ligands of the ruthenium complex would consist of two bipyridine molecules. The *cis* isomer of $\text{Ru}(\text{bpy})_2(\text{Cl})_2$ is commercially available and would be attached to the host ligand in a standard way.¹²

The direct incorporation of phenanthroline in a Diels-Alder reaction would create the simplest strong ligand for the ruthenium complex. This adduct (**29**) is pictured below.

According to the literature, the yield for the cycloaddition of hetaryne with anthracene drawn below is 1-3%.²⁹ I was unable to detect any product after several attempts.

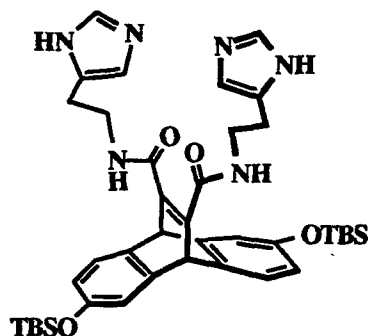


Another option for incorporating a bidentate ligand as a dienophile in a Diels-Alder reaction would be to make the dipyriddy ligand (30) pictured below. The dipyriddy acetylene undergoes cycloaddition with cyclopentadiene in good yield.³⁰ However, the cyclopentadiene adduct was reported not to bind copper or iron ions in solution.



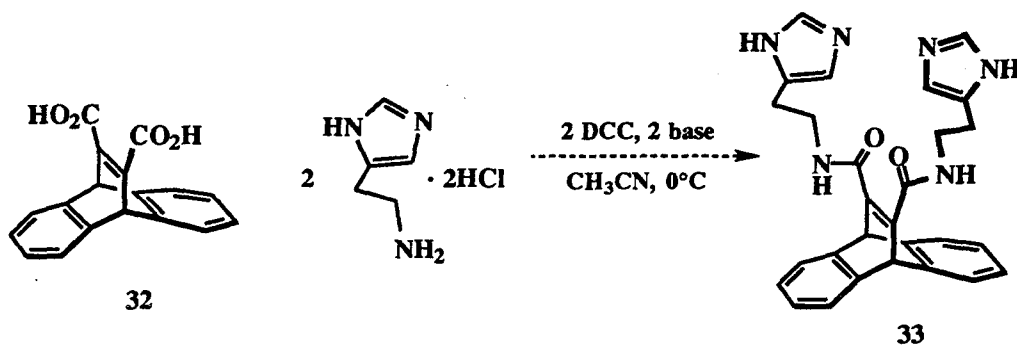
The bis-imidazole bidentate ligand (31) shown below also seemed promising. This ligand would be made by the modification of a Diels-Alder adduct that is produced during the host **P** synthesis. The formation of amide links between a diacid and two histamine

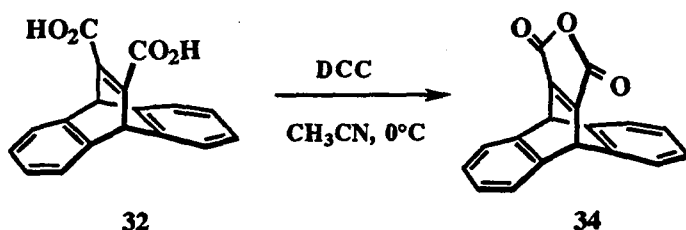
molecules (commercially available) presented an opportunity to take advantage of highly optimized peptide chemistry.³¹



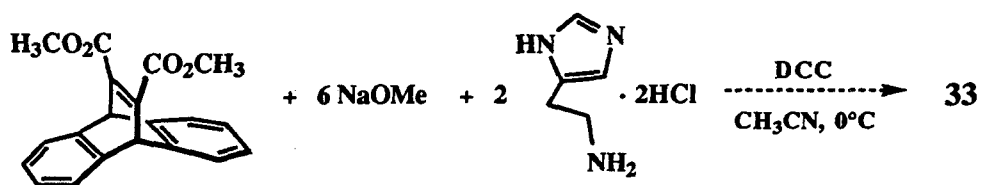
31

Unprotected histamine was used in the first attempts to make this compound. Direct coupling of the dicarboxylate model compound (32) below with histamine was attempted using 1,3-dicyclohexylcarbodiimide (DCC) to activate the carboxylic acids. Both triethylamine and pyridine were used as the base. When only one equivalent of diimide is used in the reaction, the model anhydride (34) is formed. This activated compound only reacts once with histamine. Attempts to resubmit the monoamide to another equivalent of histamine and diimide failed. A cyanomethyl group was added to the acid to activate it, but the reaction was not very efficient and no product was detected.





The last effort to use unprotected histamine was also unsuccessful. The reaction drawn below is selective for primary amines,³² and it was tried on this system using methanol and diethyl ether or benzene as solvents. No desired product was formed.



After realizing that the imidazole side chain of histidine can interfere in peptide bond forming reactions,³³ further attempts at amide formation required imidazole protecting groups. The imidazole nitrogen of histamine was protected with a tosyl group as shown in the reaction sequence below in Figure 3.10. The N(α)-*tert*-butoxycarbonyl (Boc) group was removed with acid and the resulting molecule was reacted with the dicarboxylic acid using dicyclohexylcarbodiimide and base as shown in Figure 3.11. However, the isolated products that were symmetrical by NMR did not have the correct mass spectrum for the desired product or for reasonable decomposition products.

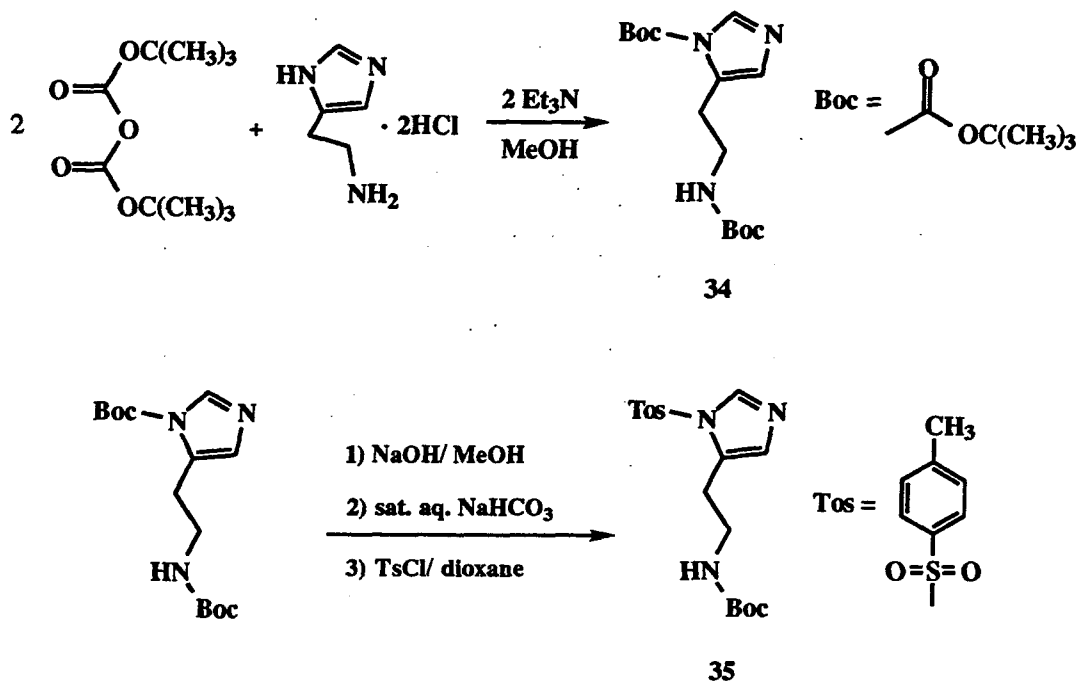


Figure 3.10. Synthesis of N(α)-*t*-butoxycarbonyl,N(im)-tosylhistamine (35).

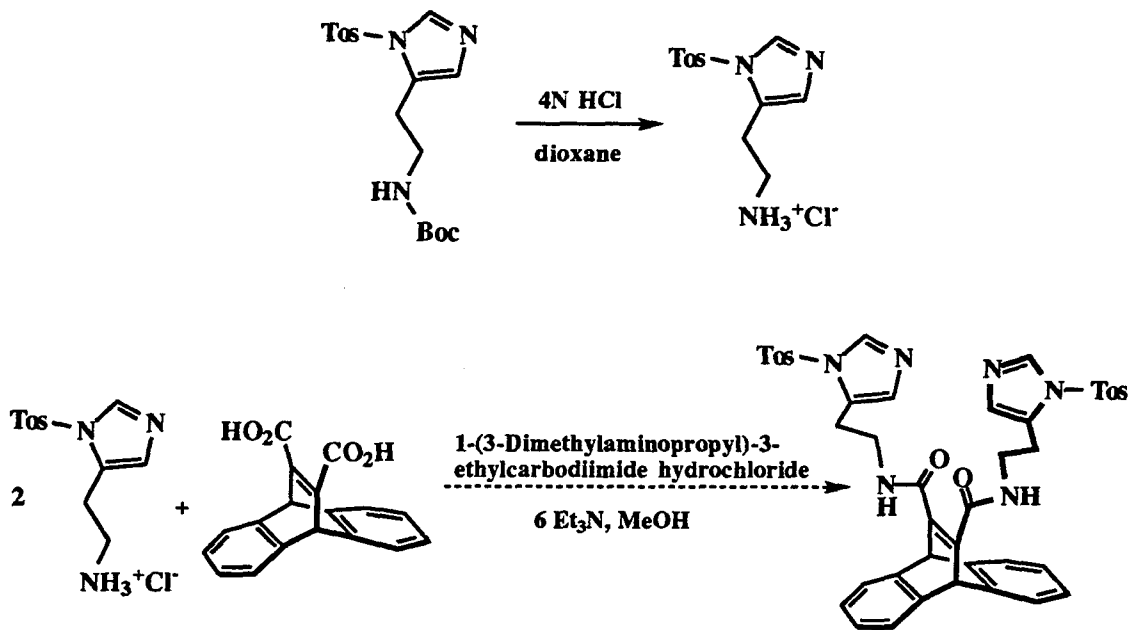


Figure 3.11. Attempted synthesis of tosyl-protected bidentate ligand **33** *via* carbodiimide coupling of diacid model compound **32** and N(im)-tosylhistamine.

Another bis-pyridyl bidentate ligand target molecule (38), pictured below, seemed like a good candidate for ruthenium complexation. While the first dipyridyl ligand (30) above cannot complex metals, in 38 the linkage between pyridine and the host structure is more flexible. This flexibility might allow a conformation that is favorable to metal binding. Although the pyridines are not attached directly to the cavity as a dienophile for a Diels-Alder reaction, all the synthetic steps shown below in Figure 3.12 proceed in good yield. The scheme relies on a reaction developed for the synthesis of a different host macrocycle that is described in Chapter 2 of this thesis.

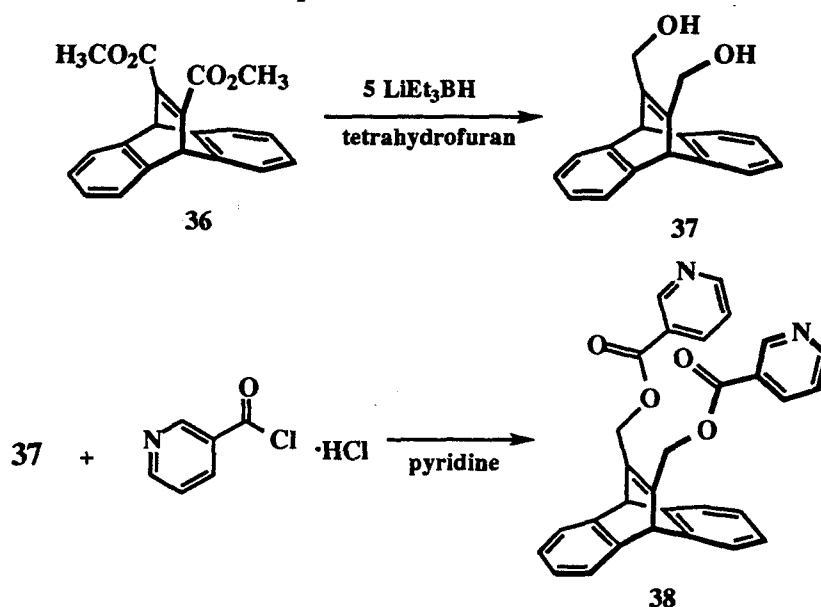
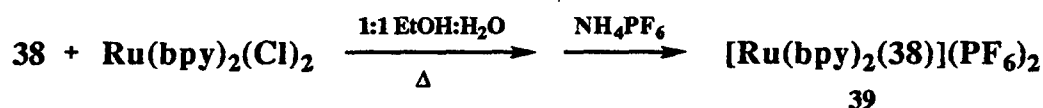


Figure 3.12. Synthesis of bis(pyridyl ester) model host 38.

Since this ligand seemed the best candidate synthetically, the ruthenium metal complex was formed. The reactions are shown below. The product mixture was analyzed by analytical reverse phase HPLC using a mobile phase gradient of 100 mM aqueous sodium acetate and acetonitrile. This separation showed three ruthenium-containing species, as detected by their characteristic absorbance at 450nm. Beyond providing evidence for the formation of a ruthenium-pyridine complex, the proton NMR was not

informative about the exact species formed. However, NMR did demonstrate that acetonitrile readily displaced the chelating ligand **38**. This weakness of binding for the bidentate complex suggested that either the pyridines are poor ligands or that they are positioned poorly for chelation.



3. Tetradentate Ligand

A tetradentate ligand should display much stronger binding than a bidentate ligand. The model ligand (**43**) pictured below in Figure 3.13 was synthesized easily after the acyl chloride **42** was synthesized. An alternative synthesis using an aryl-aryl coupling reaction³⁴ is probably more reliable. It was hoped that **43** would bind ruthenium strongly.

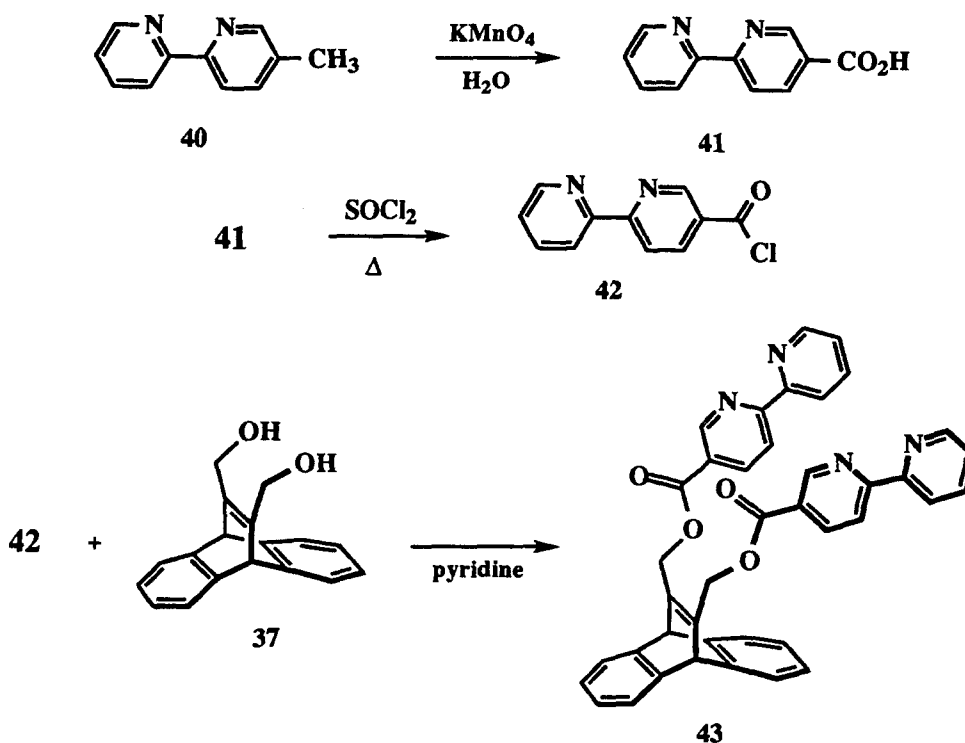
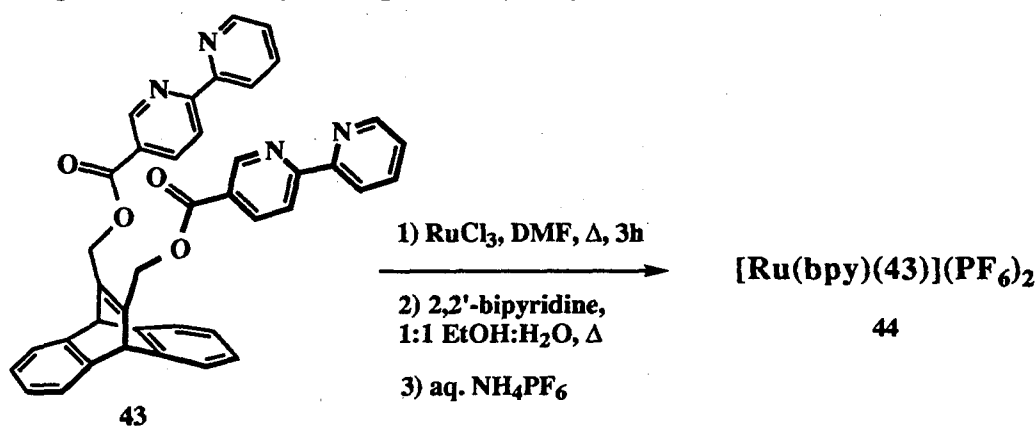


Figure 3.13. Synthesis of bis(bipyridyl ester) model host **43**.

The formation of the metal complex **44** by the reactions shown below proceeded smoothly according to UV and NMR spectroscopy. The solution of complex was purified by semi-preparative HPLC using a gradient mobile phase of 100 mM sodium acetate and methanol. Eight ruthenium-containing species were isolated. The proton NMR showed characteristic bipyridine resonances. The visible spectrum for each fraction revealed absorbances at 450 nm. Illumination with long-wave ultraviolet radiation resulted in red-orange fluorescence for five of the samples. These spectral characteristics are indicative of ruthenium complexes with bipyridine ligands. However, fast atom bombardment mass spectrometry did not reveal the desired product in any sample. The mass spectrum did show fragments which may correspond to hydrolyzed ester linkages.



III. FUTURE WORK

The possible reasons that the bidentate bis(pyridyl) model ligand **38** and the tetradentate bis(bipyridyl) model ligand **43** were not satisfactory include the reactivity and orientation of the ligands. The electron-deficient metal complex may activate the esters toward hydrolysis. If the connecting esters for both **38** and **43** are too active once the ruthenium complex is formed, this type of linkage to the macrocycle must be abandoned. The monodentate acetylated isoquinoline ligand **20** would then be a better choice if this

ligand proves strong enough to stably complex ruthenium. If, on the other hand, the problem with the bis(pyridyl) and bis(bipyridyl) ligands is a matter of ligand orientation, a different framework for linking the ligand to the macrocycle would be the solution. A related pair of ligands **46** and **47** may be synthesized easily using the saturated esters and alcohols as shown in Figure 3.14. The binding cavity is perturbed minimally, and so the molecular recognition elements of the macrocycle should be almost identical to those of host **P**. The resulting ligands would have a wider "bite" and perhaps would therefore be able to form more stable ruthenium complexes.

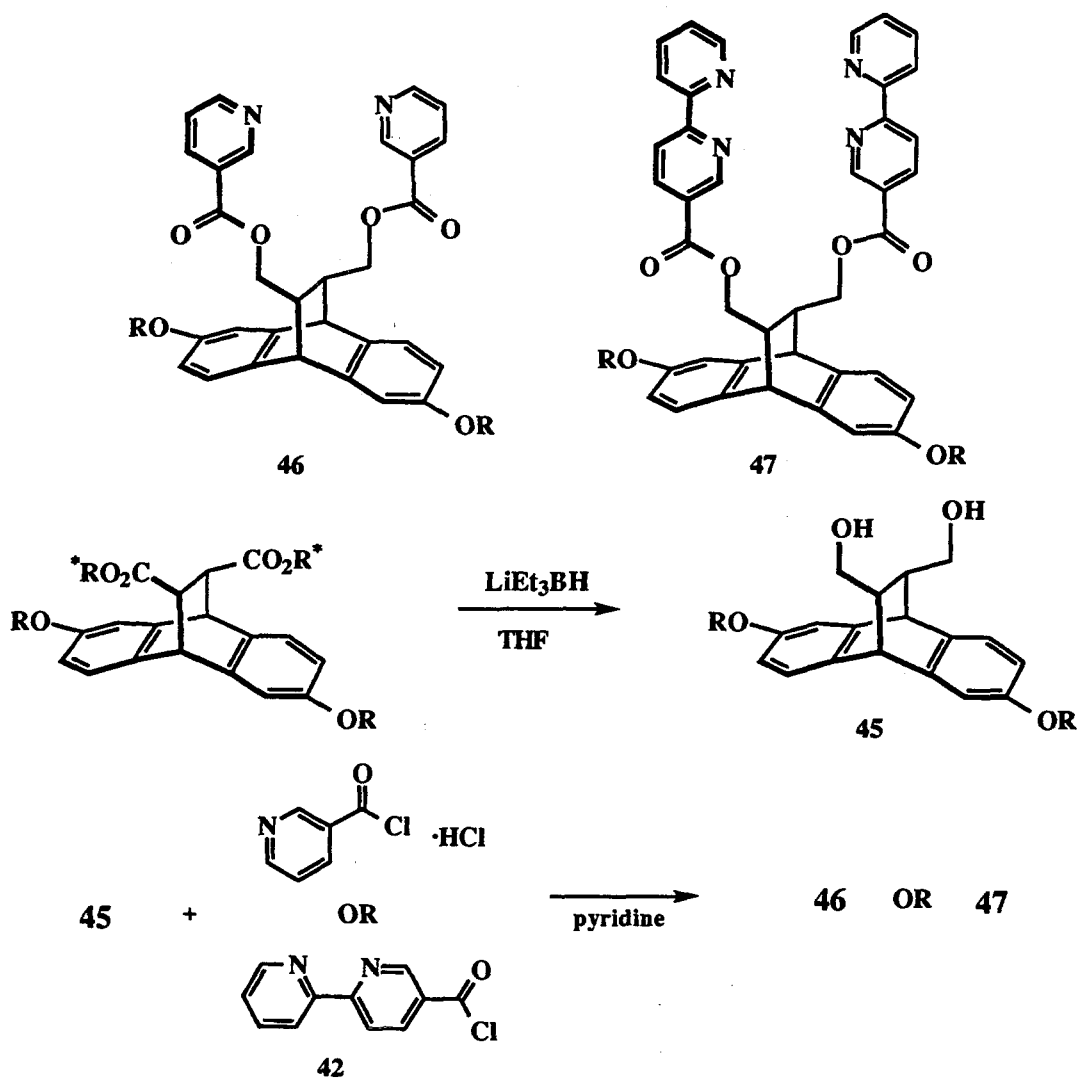


Figure 3.14. The proposed synthesis of ethanoanthracene ligands **46** and **47**.

An alternative to using a water-soluble metal complex would be to use standard organic donor and acceptor groups substituted with carboxylate or phosphate groups to provide water solubility to the macrocycle. Also, some studies could be performed in organic solvents using the macrocycle **15**. However, analytes would be limited to only a few very strong binders since the hydrophobic component to binding will be missing.

Once the donor-cyclophane-acceptor triad has been synthesized, photophysical studies will be performed. For example, a series of fluorescence lifetime studies at different ratios of guest to host will be performed to make a Stern-Vollmer plot to ascertain the binding constant and the electron transfer rates in the complex.³⁵ Non-macrocyclic control studies will also be performed. In addition, the driving force for electron transfer (ΔG° in equation 1) can be varied by using variously substituted bipyridine ligands for ruthenium. In this way, the nature of the electronic coupling and the solvent reorganization energy can be determined. The groups which link the anthracene Diels-Alder adduct donor and acceptor may be varied as well. The replacement of the xylyl groups of host **P** with cyclohexyl groups will change the intramolecular electron transfer pathway. If this intramolecular pathway is fast, the presence of a guest analyte is not likely to measurably change the electron transfer rate. If this pathway is disfavored by changing its molecular structure, then guest-mediated intermolecular electron transfer would be more likely to act as a conductivity switch.

Host **P** interacts strongly with guest molecules in solution, so one would predict that a donor-cyclophane-acceptor based on the binding cavity of host **P** will exhibit guest-mediated electron transfer. If guest binding enhances electron transfer rates, the mechanism of rate enhancement (changes to H_{ab} or λ) must be determined. The strong, specific, noncovalent binding interactions will then be exploited to create a sensor for organic compounds in water.

Experimental Section

^1H spectra were recorded on a JEOL JNM GX-400 spectrometer. Routine spectra were referenced to the residual proton and carbon signals of the solvents and are reported (ppm) downfield of 0.0 as δ values. The following packing material was used in column chromatography: E. Merck silica gel 60, 0.04-0.063 mm. 2,6-Bis(*tert*-butyldimethylsiloxy)anthracene (**7**),³⁶ $[\text{Ru}(\text{bpy})(\text{trpy})\text{Cl}]\text{PF}_6$,³⁷ Methyl 3-bromopropiolate (**24**),³⁸ Diethyl(4-pyridyl)borane (**26b**),³⁹ 4-pyridineboronic acid (**26a**),⁴⁰ model host diacid (**32**),⁴¹ 5-methyl-2, 2'-bipyridine (**40**),⁴² and 2,2'-bipyridine-5-carboxylic acid (**41**)⁴³ were made according to the literature.

2,3-Dimethyl-1,4-benzoquinone (8). 2,3-dimethylhydroquinone (7.32 mmol) was oxidized by 2 equivalents (7.32 mmol) of ceric ammonium nitrate in aqueous dioxane over a period of 3 hours. The mixture was extracted with chloroform several times. The organic solution was concentrated by rotary evaporation and the resulting solid was purified by sublimation. ^1H NMR (CDCl_3): δ 6.69 (s, 2H), 2.00 (s, 6H).

Quinone adduct of 2,3-Dimethyl-1,4-benzoquinone and 2,6-bis(*tert*-butyldimethylsiloxy)anthracene (11). 2,6-bis(*tert*-butyldimethylsiloxy)anthracene (**7**) and 2,3-dimethyl-1,4-benzoquinone (**8**) were heated to reflux in a minimum volume of toluene overnight. The initial cycloadduct (**9**) was purified by column chromatography using 10% diethyl ether in chloroform as eluant. ^1H NMR (CDCl_3): δ 7.17 (d, $J = 7.8$, 1H), 6.93 (d, $J = 7.8$, 1H), 6.84 (s, 1H), 6.60 (s, 1H), 6.59 (dd, $J = 2.0, 7.8$, 1H), 6.47 (dd, $J = 2.0, 7.8$, 1H), 4.60 (s, 1H), 3.04 (s, 1H), 1.69 (s, 3H), 1.67 (s, 3H), 0.95 (s, 9H), 0.91 (s, 9H), 0.16 (s, 6H), 0.08 (s, 6H). DEI/MS 574 (M^+); HRMS 574.2939, calc. for $\text{C}_{34}\text{H}_{46}\text{O}_4\text{Si}_2$ 574.2935. This adduct was dissolved in boiling glacial acetic acid and 1 ml of concentrated aqueous HCl was added.⁴⁴ This mixture was stirred overnight at

50 °C. The reaction was partitioned between water and ethyl acetate. After removing the ethyl acetate by rotary evaporation, the aromatized hydroquinone product (**10**) was purified by silica gel chromatography using 1:1 petroleum ether:ethyl acetate as eluant. EI/MS 346 (M⁺); HRMS 346.1196, calc. for C₂₂H₁₈O₄ 346.1205. A sample of pure hydroquinone would chromatograph on thin layer chromatography as two spots due to a small portion having oxidized to the quinone on the thin layer chromatography plate. The aromatized hydroquinone was converted to the product quinone (**11**) by refluxing the hydroquinone with two equivalents of unsubstituted 1,4-benzoquinone for two hours in ethanol.⁴⁵ ¹H NMR (CDCl₃): δ 7.19 (d, *J* = 8.1, 2H), 6.89 (d, *J* = 2.4, 2H), 6.41 (dd, *J* = 2.4, 8.0, 2H), 4.77 (s, 2H), 3.82 (s, 6H). ¹H NMR (acetone-*d*₆): δ 8.25 (s, 2H), 7.21 (d, *J* = 8.1, 2H), 6.95 (d, *J* = 2.6, 2H), 6.42 (dd, *J* = 2.6, 8.1, 2H), 5.60 (s, 2H), 1.95 (s, 6H). 50eV EI/MS 344(M⁺); HRMS 344.1047, calc. for C₂₂H₁₆O₄ 344.1049.

Quinone adduct of 2,3-Dimethyl-1,4-benzoquinone and anthracene (12**).**

Anthracene and 2,3-dimethyl-1,4-benzoquinone (**8**) were dissolved in dry methylene chloride. Excess aluminum trichloride powder was added in several batches.⁴⁶ The reaction was stirred four hours. The reaction mixture was poured into a slurry of ice and 1 mL of concentrated aqueous HCl. This mixture was partitioned between water and chloroform. The organic layer was dried with sodium sulfate and the solvent was removed by rotary evaporation. The product adduct (**13**) was purified by silica gel chromatography. The sample was dry-loaded and the column was eluted with methylene chloride. This adduct was then recrystallized from ethyl acetate. ¹H NMR (CDCl₃): δ 7.37 (m, 2H), 7.14 (m, 4H), 7.03 (m, 2H), 4.76 (s, 2H), 3.10 (s, 2H), 1.65 (s, 6H). To aromatize the adduct, it was dissolved in boiling glacial acetic acid and 1 mL concentrated aqueous HCl and heated at 50 °C overnight as above for **10**. Water was added to the cooled reaction mixture and filtered. The solid hydroquinone was then oxidized by ferric chloride in methanol at 80 °C.⁴⁷ A yellow solid (**12**) precipitated immediately. Water was added, and

the solid product was filtered off and then washed with water. ^1H NMR (CDCl_3): δ 7.39 (m, 4H), 6.94 (m, 4H), 5.79 (s, 2H), 1.94 (s, 6H).

Cycloadduct of 5,8-isoquinolinedione and anthracene (18). The 5,8-isoquinolinedione (17) (1.49 mmol) was freshly prepared as in the literature,⁴⁸ but the reaction workup was modified. The reaction was extracted into three 50 mL portions of toluene. The toluene layer was dried with sodium sulfate and then acetonitrile was removed from the reaction by rotary evaporation. Five equivalents of anthracene (7.45 mmol) were added and the reaction was heated to reflux for one day. The reaction mixture was passed over a short plug of silica and eluted with more toluene to remove the excess anthracene. The product was eluted from the silica with ethyl acetate. The ethyl acetate was removed by rotary evaporation and the product quinone was purified by column chromatography using 20% ethyl acetate in petroleum ether as eluant. ^1H NMR (CDCl_3): δ 9.29 (s, 1H), 8.99 (d, $J = 5.1$, 1H), 7.85 (d, $J = 4.6$, 1H), 7.46 (m, 4H), 7.04 (m, 4H), 6.00 (s, 1H), 5.97 (s, 1H). The hydroquinone was isolated by eluting the silica plug with methanol after the product (18) eluted.

N-oxide protection of 18 to form 19. The isoquinolinedione adduct (18) (0.107 mmol) and 1.3 equivalents of the oxidant *m*-chloroperoxybenzoic acid (0.140 mmol) were dissolved in chloroform.⁴⁹ This reaction stirred at room temperature overnight. The reaction was then washed with 0.1N aqueous sodium hydroxide twice and saturated aqueous sodium chloride solution once. The organic layer was dried with sodium sulfate and the solvent was removed by rotary evaporation. No further purification was necessary. ^1H NMR (CDCl_3): δ 8.64 (d, $J = 1.8$, 1H), 8.31 (dd, $J = 1.1$, $\Delta\nu = 6.7$ Hz, 1H), 7.87 (d, $J = 6.7$, 1H), 7.46 (m, 4H), 7.05 (m, 4H), 5.96 (d, $J = 5.9$, 1H).

Reductive acetylation of 18 to form 20.⁵⁰ Into a 10 mL flask were added a stir bar, 1.0 equivalent of isoquinolinedione adduct (18) (0.116 mmol), 10 equivalents acetic acid (0.122 mmol), 1.6 equivalents of potassium acetate (0.193 mmol) and excess acetic anhydride (800 μ L). Next, four equivalents of zinc dust (0.490 mmol) were added. The flask was equipped with a reflux condenser and heated to reflux for 30 minutes. The product (20) was isolated by silica gel chromatography using 40% petroleum ether in ethyl acetate as eluant. ¹H NMR (CDCl₃): δ 9.13 (s, 1H), 8.49 (d, J = 5.9, 1H), 7.48 (d, J = 5.9, 1H), 7.39 (m, 4H), 7.04 (m, 4H), 5.50 (s, 1H), 5.49 (s, 1H). EI/MS 421 (M⁺); HRMS 421.1335 calc. for C₂₇H₁₉NO₄ 421.1314.

N-oxide protection of 20 to form 21. The same procedure was followed as for the isoquinolinedione adduct oxidation above. ¹H NMR (CDCl₃): δ 8.63 (d, J = .8, 1H), 8.04 (d, J = .3, $\Delta\nu$ = 1.6, 1H), 7.52 (d, J = 7.2, 1H), 7.40 (m, 4H), 7.06 (m, 4H), 5.43 (s, 2H), 2.60 (s, 3H), 2.64 (s, 3H). FAB/MS 438 (MH⁺); HRMS 438.1331, calc. for C₂₇H₂₀NO₅ 438.1341.

Methyl pyridin-4-ylpropiolate (22). The procedure was taken from the literature, with some modifications.⁵¹ Isonicotinoyl chloride hydrochloride (11.31 mmol) was placed in a 500 mL flask with a stir bar. Two equivalents of methyl (triphenylphosphorane-diyl)acetate were placed in a 250 mL flask and dissolved in dry benzene. Dry benzene and 1.0 equivalent of pyridine were added to the acyl chloride. The phosphorane was transferred by cannula to the 500 mL flask. The flask was equipped with a condenser, and then heated to reflux for 16 hours. The reaction mixture was washed with water, and the product was obtained by silica gel chromatography using 40% tetrahydrofuran in diethyl ether as eluant. ¹H NMR (CDCl₃): δ 8.58 (d, J = 4.4, 2H), 7.72 (m, 4H), 7.48 (m, 11H), 3.10 (s, 3H). The decomposition of this product into the desired acetylene⁵² was accomplished using a Kugelrohr apparatus. The solid was placed

in the kugelrohr under aspirator vacuum and heated from 180 °C to 250 °C over 20 minutes and maintained at 250 °C until just before a yellow contaminant distilled into the collection flask. ^1H NMR (CDCl_3): δ 8.64 (d, J = 5.8, 2H), 7.40 (d, J = 6.0, 2H), 3.84 (s, 3H).

Cycloadduct of methyl pyridin-4-ylpropiolate and 2,6-bis(*tert*-butyldimethylsiloxy)anthracene (23). The methyl pyridin-4-ylpropiolate (22) (1.44 mmol) and 2,6-bis(*tert*-butyldimethylsiloxy)anthracene (7) (1.44 mmol) were dissolved in dry toluene, and excess diethyl aluminum chloride was added to the flask after it was cooled to 0 °C. The reaction was left to warm and stirred at room temperature overnight. The product was purified by silica gel chromatography using 1:1 petroleum ether:diethyl ether as eluant. ^1H NMR (CDCl_3): δ 8.57 (d, J = 5.5, 2H), 7.21 (d, J = 7.8, 2H), 7.15 (d, J = 5.6, 2H), 7.12 (d, J = 7.8, 1H), 6.91 (d, J = 2.2, 1H), 6.82 (d, J = 2.2, 1H), 6.46 (dd, J = 2.2, 8.0, 1H), 6.42 (dd, J = 2.2, 7.8, 1H), 5.58 (s, 1H), 4.99 (s, 1H), 3.57 (s, 3H), 0.94 (s, 9H), 0.93 (s, 9H), 0.15 (s, 6H), 0.14 (s, 6H). FAB/MS 600 (MH^+); HRMS 600.2931, calc. for $\text{C}_{35}\text{H}_{46}\text{NO}_4\text{Si}_2$ 600.2965.

Cycloadduct of methyl 3-bromopropiolate and 2,6-bis(*tert*-butyldimethylsiloxy)anthracene (25). The methyl 3-bromopropiolate (24) (4.25 mmol) and 2,6-bis(*tert*-butyldimethylsiloxy)anthracene (7) (4.25 mmol) were refluxed together in benzene overnight.⁵³ The reaction mixture was cooled and passed over a short silica plug and washed with benzene to elute unreacted 2,6-bis(*tert*-butyldimethylsiloxy)anthracene. The adduct was eluted with diethyl ether. The diethyl ether was removed by rotary evaporation, and the product was purified by silica gel chromatography using 3% diethyl ether in petroleum ether. ^1H NMR (CDCl_3): δ 7.14 (d, J = 7.9, 1H), 7.13 (d, J = 7.9, 1H), 6.84 (d, J = 2.0, 1H), 6.83 (d, J = 2.0, 1H), 6.43 (dd, J = 2.3, 7.8, 1H), 6.40 (dd, J = 2.3, 7.8, 1H), 5.56 (s, 1H), 5.08 (s, 1H), 3.78 (s, 3H), 0.94 (s, 18H), 0.14 (s, 12H).

Vinyl bromide coupling with diethyl(4-pyridyl)borane and 4-pyridineboronic acid.⁵⁴

1. To a 10 mL flask was added a stir bar and 1.5 equivalents of the vinyl bromide (**25**) (6.65×10^{-5} mol), 1 equivalent of diethyl(4-pyridyl)borane (**26b**), 0.5 equivalents of tetra-*n*-butylammonium bromide, and 5 mol% of tetrakis [triphenylphosphine]palladium.⁵⁵ Dry tetrahydrofuran was added and the reaction was heated to reflux for 5 hours. The reaction was cooled and partitioned between chloroform and water. No product could be isolated.
2. To a 10 mL flask was added a stir bar, vinyl bromide (**25**) (.0931 mmol), pyridine boronic acid (**26a**) (.158 mmol), 95 mL 2M aqueous sodium carbonate, benzene, and tetrakis [triphenylphosphine]palladium.⁵⁶ The reaction was refluxed for 5 hours. The product (**23**) was purified by silica gel chromatography using 1:1 petroleum ether:ethyl acetate.

Cycloadduct of 4-bromobenzyne and 2,6-bis(*tert*-butyldimethylsiloxy)anthracene (27**).** This procedure was adapted from the literature.⁵⁷ 2,6-bis(*tert*-butyldimethylsiloxy)anthracene (**7**) (2.16 mmol), 20 mL dry acetonitrile, and a stir bar were placed in an oven-dried 50 mL 3-necked flask fitted with a condenser. 5-Bromoanthranilic acid (1.08 mmol) was dissolved in 10 mL of dry acetonitrile and taken up in a syringe. A 250 mL syringe was filled with isoamyl nitrite (1.08mmol). The reaction flask was heated to reflux and the two other reagents were added simultaneously over 20 minutes. The reaction was refluxed for 30 minutes and cooled to room temperature. The solvent was removed by rotary evaporation. The product co-eluted with unreacted anthracene, so the anthracene was removed by reaction with maleic anhydride. The product was then purified by passing the residue dissolved in 10% diethyl ether in petroleum ether through a silica plug. The silica plug was washed with the same solution until the desired product eluted.

Aryl bromide cycloadduct coupling with diethyl(4-pyridyl)borane and 4-pyridineboronic acid. The same procedures were followed as for the compound 23 above. No product was detected.

Attempted cycloaddition of 5,6-dehydro-1,10-phenanthroline and anthracene.⁵⁸ One equivalent each of anthracene and 5-chloro-1,10-phenanthroline were dissolved in 25 mL of dry diethyl ether (or tetrahydrofuran) in an oven-dried 100 mL round bottom flask containing a stir bar. This flask was cooled to -78 °C. Lithium piperidide was added to the mixture. The reaction was left to warm to room temperature, and then heated to reflux for 3 hours. No product was found.

Unprotected histamine coupling reactions:

1. This was a standard coupling procedure.⁶¹ Model host diacid (32) (0.29 mmol) and a stir bar were placed in an oven-dried flask. In another flask, the 2 equivalents of histamine hydrochloride (0.603 mmol) and 2 equivalents of pyridine were dissolved in 3 mL of dry methanol. Dry acetonitrile and the methanol solution were added by cannula transfer to the reaction flask which was then chilled to 0°C. The 2 equivalents of dicyclohexylcarbodiimide (DCC, 0.582 mmol) were dissolved in a 1:1 acetonitrile:chloroform solvent and added to the reaction mixture. The reaction stirred for 6 hours. The precipitate (dicyclohexylurea) was filtered off. The solvent was removed by rotary evaporation. The residue was partitioned between chloroform and dilute aqueous acid. The aqueous layer was lyophilized. Only mono-amide linkages formed as shown by ¹H NMR. This reaction was also repeated using triethylamine as base.
2. The methyl ester model host was dissolved in benzene. A methanol solution of histamine hydrochloride was added, and then the sodium methoxide solution in methanol was added.³² The reaction was refluxed for several days. The reaction was cooled and

partitioned between an aqueous layer (pH = 11) and methylene chloride. Although the ^1H NMR looked consistent with product, the mass spectrum did not.

Model host anhydride (34). The model host diacid (32) (7.18×10^{-5} mole) was placed in a 10 mL flask with a stir bar and dissolved in .5 mL of dry acetonitrile. The flask was chilled to 0 °C. One equivalent of DCC (7.26×10^{-5} mole) was added. A precipitate formed immediately. After 15 minutes, the reaction mixture was filtered. The filtrate containing the product was concentrated to dryness. ^1H NMR (CDCl_3): δ 7.42 (m, 4H), 7.06 (m, 4H), 5.52 (s, 1H).

N(α),N(τ)-bis-*t*-butoxycarbonylhistamine (34). This procedure was adapted from one used to similarly protect histidine hydrochloride.⁵⁹ Histamine hydrochloride (1.18 mmol), di-*t*-butyldicarbonate (2.37 mmol), and triethylamine (2.37mmol) were stirred in methanol overnight. The reaction was partitioned between chloroform and 10% aqueous citric acid. The product was recrystallized from chloroform. ^1H NMR (CDCl_3): δ 7.99 (s, 1H), 7.12 (s, 1H), 4.95 (s, br., 1H), 3.40 (q, $J = 5.3$, 2H), 2.71 (t, $J = 7.0$, 2H), 1.59 (s, 9H), 1.41 (s, 9H). FAB/MS m/e 312 (MH⁺); HRMS 312.1912, calc. for $\text{C}_{15}\text{H}_{26}\text{N}_3\text{O}_4$ 312.1923.

N(α)-*t*-butoxycarbonyl,N(im)-tosylhistamine (35). This procedure was adapted from one used to similarly protect histidine hydrochloride.⁶⁰ N(α),N(τ)-bis-*t*-butoxycarbonylhistamine (34) (1.11 mmol) was dissolved in methanol and chilled to 0 °C. One equivalent of aqueous 0.1 N NaOH was added, and the reaction stirred at 0 °C for 1 hour. To the chilled reaction was then added 10 mL of saturated aqueous bicarbonate. One equivalent of tosyl chloride dissolved in dioxane was added. The reaction stirred for 3 hours. The white product was filtered from the reaction mixture. ^1H NMR (CDCl_3): δ 7.91 (d, $J = 1.0$, 1H), 7.79 (d, $J = 8.3$, 2H), 7.34 (d, $J = 8.3$, 2H), 7.02 (s, 1H) 4.89

(s, br., 1H), 3.35 (q, $J = 6.3$, 2H), 2.67 (t, $J = 6.3$, 2H), 2.42 (s, 3H), 1.40 (s, 9H).

FAB/MS m/e 366 (MH⁺); HRMS 366.1497, calc. for C₁₇H₂₆N₃O₄ 366.1487.

Protected histamine couplings. First, the primary amine (0.150 mmol) of N(α)-*t*-butoxycarbonyl,N(im)-tosylhistamine (**35**) was deprotected by stirring it for 5 minutes at room temperature in a solution of 4N HCl in dioxane (3 mL of concentrated aqueous HCl in 6 mL of dioxane). This mixture was lyophilized. Next, the model diacid (**32**) (0.0753 mmol) was added to the flask and they were dissolved in dry methanol. Triethylamine (0.359 mmol) was added, and then 1,3-dimethylaminopropyl-3-ethyl carbodiimide. After one day of stirring at room temperature, the solvent was removed by rotary evaporation and the residue was eluted with ethyl acetate through a silica plug. The mass spectrum did not reveal product.

Model host diol (32). The ester was added to an oven-dried flask with a stir bar. Dry tetrahydrofuran was added to create a 0.05 to 0.1 M solution. The lithium triethylborohydride (commercially available in 1M solution in tetrahydrofuran) was added dropwise, using 2.2 equivalents per ester to be reduced. After stirring overnight, at room temperature, ethyl acetate was added to quench excess reductant and the solvent was removed by rotary evaporation. The residue was partitioned between water and ethyl acetate. The organic layer was dried and concentrated. The product was purified by silica gel chromatography, using 40% petroleum ether in ethyl acetate as an eluant.

Bis(pyridyl ester) model host (38). Isonicotinoyl chloride hydrochloride was placed in an oven-dried 10 mL flask with a stir bar and dry pyridine (0.5 mL). The model diol (**32**) (0.272 mmol) in a solution of dry pyridine was added to the suspension in the reaction flask. The reaction was left to stir for two days at room temperature. The reaction mixture was partitioned between saturated aqueous bicarbonate and methylene chloride.

The organic layer was dried with sodium sulfate. This solution was passed through a silica plug and eluted with ethyl acetate. ^1H NMR (CDCl_3): δ 9.17 (d, $J = 1.6$, 2H), 8.77 (dd, $J = 1.6$, 4.8, 2H), 8.23 (dt, $J = 1.9$, 8.0, 2H), 7.38 (m, 2H), 7.29 (m, 4H), 6.97 (m, 4H), 5.23 (s, 2H), 5.14 (s, 4H); DCI/MS m/e 475 (MH^+); HRMS 475.1369, calc. for $\text{C}_{30}\text{H}_{24}\text{N}_2\text{O}_4$ 475.1658.

[Ru(38)(bpy) $_2$](PF $_6$) $_2$ (39). A solution of 1:1 ethanol:water was degassed and added to a 25 mL flask containing the ligand (4.21×10^{-5} mole) and cis-Ru(bpy) $_2$ Cl $_2$ \cdot nH $_2$ O (4.23×10^{-5} mol). The model ligand (38) was sparingly soluble in this solvent. The flask was then fitted with a reflux condenser. The reaction was heated to reflux for 3 hours and then cooled. A saturated aqueous solution of ammonium hexafluorophosphate was added to precipitate the dark red metal complex. The reaction mixture was filtered. The solid product was passed over an alumina column. The UV spectrum of the three major fractions showed absorbances at 431 or 436nm. The reaction mixture was analyzed by reverse-phase analytical HPLC using a solvent system of 100mM aqueous sodium acetate and acetonitrile. Several ruthenium-containing species were detected at 450nm. ^1H NMR (CD_3CN) revealed that acetonitrile displaced the ruthenium from the model host ligand.

Bis(bipyridyl ester) model host (43). 2,2'-bipyridine-5-carboxylic acid (41) (4.69 mmol), thionyl chloride (20 mL), and a stir bar were placed in a 250 mL flask. The flask was fitted with a condenser and heated to reflux overnight. The thionyl chloride was removed by rotary evaporation under high vacuum. To this flask were added model diol (32) (0.783 mmol), 40 mL dry pyridine, and a stir bar. The reaction was left to stir for two days. The pyridine was removed by rotary evaporation and the residue was partitioned between methylene chloride and saturated aqueous bicarbonate. The organic layer was dried with sodium sulfate and then passed through an alumina plug. The product was purified by dissolving in chloroform and triturating with diethyl ether. ^1H NMR (CDCl_3):

δ 9.24 (d, $J = 1.5$, 2H), 8.67 (d, $J = 3.9$, 2H), 8.47 (m, 2H), 8.32 (dd, $J = 2.2$, 8.3, 2H), 7.78 (dt, $J = 1.7$, 7.6, 2H), 7.34 (m, 4H), 7.29 (m, 4H), 6.98 (m, 4H), 5.29 (s, 2H) 5.19 (s, 4H).

[Ru(43)(bpy)](PF₆)₂ (44). The bis(bipyridyl ester) model ligand (43) (0.203 mmol) was placed in a 250 mL flask with a stir bar and 75 mL of dimethylformamide. One equivalent of ruthenium trichloride hydrate was dissolved in 65 mL of dimethylformamide and added to the flask. The flask was fitted with a reflux condenser and heated to reflux for three hours. The blue reaction solution was cooled. The solvent was removed by rotary evaporation under high vacuum. The flask was carefully maintained under argon during the next step. One equivalent of 2,2'-bipyridine was added to this flask and then 80 mL of degassed 1:1 ethanol:water solution was added by cannula transfer to this flask. The flask was equipped with a condenser and the reaction was heated to reflux for 3 hours. The dark red solution was cooled. Saturated aqueous ammonium hexafluorophosphate was added to precipitate the metal complex. The ethanol was removed by rotary evaporation. The suspension was filtered. ¹H NMR (methanol-*d*-4) was consistent with the product metal complex. Semi-preparative HPLC was used to isolate 8 samples which absorb at 450 nm. Five of these eight samples fluoresced red-orange under longwave ultraviolet light. All samples showed UV absorbance maxima at 452 nm. Mass spectrum (FAB) revealed a peak 2 mass units off of the desired product, plus a peak 3 mass units off of a species [Ru{bpy}(bpy-5-CO₂H)₂]PF₆.

References

1. Teasdale, P. R.; Wallace, G. G. *Analyst* **1993**, *118*, 329-334.
2. Wallace, G. G. *Chem. Brit.* **1993**, 967-970.
3. a) Bauerle, P.; Scheib, S. *Adv. Mater.* **1993**, *5*, 848-853.
 b) Bartlett, P. N.; Benniston, A. C.; Chung, L.-Y.; Dawson, D. H.; Moore, P. *Electrochim. Acta* **1991**, *36*, 1377-1379.
 c) Roncali, J.; Garreau, R.; Lemaire, M. *J. Electroanal. Chem.* **1990**, *278*, 373-378.
 d) Dickert, F. L.; Zeltner, D. *Angew. Chem. Int. Ed. Engl. Adv. Mater.* **1989**, *28*, 813-814.
 e) Gasiorowski, R.; Jorgensen, T.; Moller, J.; Hansen, T. K.; Pietraszkiewicz, M.; Becher, J. *Adv. Mater.* **1992**, *4*, 568-570.
4. Beer, P. D. *Endeavor* **1992**, *16*, 182-189.
5. Bredas, J. L.; Street, G. B. *Acc. Chem. Res.* **1985**, *18*, 309-315.
6. a) Winkler, J. R.; Gray, H. B. *Chem. Rev.* **1992**, *92*, 369-490.
 b) Closs, G. L.; Miller, J. R. *Science*, **1988**, *240*, 440-446.
 c) Moser, C. C.; Keske, J. M.; Warncke, K.; Farid, R. S.; Dutton, P. L. *Nature* **1992**, *355*, 796-802.
7. a) Marcus, R. A. *Ann. Rev. Phys. Chem.* **1964**, *15*, 155-196.
 b) Marcus, R. A. *J. Phys. Chem.* **1956**, *24*, 966-978.
 c) Marcus, R. A.; Sutin, N. *Biochim. Biophys. Acta* **1985**, *811*, 265-327.
8. Bowler, B. E.; Raphael, A. L.; Gray, H. B. *Prog. Inorg. Chem.* **1990**, *38*, 259-322.
9. a) Balzani, V. *Tetrahedron*, **1992**, *48*, 10443-10514.
 b) Ueno, A.; Osa, T. In *Photochemistry in Organized and Constrained Media*; Ramammurthy, V. Ed; Wiley: New York, 1991; Chapter 16.
10. de Silva, A. P.; Gunaratne, H. Q. N.; Lynch, P. L.; Patty, A. J.; Spence, G. L. *J. Chem. Soc. Perkin. Trans. 2* **1993**, 1611-1616.
11. Masilamani, D.; Lucas, M. E. *ACS Symp. S.* **1993**, *538*, 162-182.
12. Durr, H.; Kilburg, H.; Bossmann S. *Synthesis*, **1990**, 773-778.
13. Seiler, M.; Durr, H.; Willner, I.; Joselevich, E.; Doron, A.; Stoddart, J. F. *J. Am. Chem. Soc.* **1994**, *116*, 3399-3404.
14. a) Iyoda, T.; Morimoto, M.; Kawasaki, N.; Shimidzu, T. *J. Chem. Soc. Chem. Commun.* **1991**, 1480-1481.
 b) Morimoto, M.; Fukui, K.; Kawasaki, N.; Iyoda, T.; Shimidzu, T. *Tetrahedron Lett.* **1993**, *34*, 95-98.

- c) Yoon, D. I.; Berg-Brennan, C. A.; Lu, H.; Hupp, J. T. *Inorg. Chem.* **1992**, *31*, 3192-3194.
15. Kearney, P. C.; Mizoue, L. S.; Kumpf, R. A.; Forman, J. E.; McCurdy, A.; Dougherty, D. A. *J. Am. Chem. Soc.* **1993**, *115*, 9907-9919.
16. a) Juris, A.; Barigeletti, F.; Compagna, F.; Balzani, V.; Zelewsky, A. *Coord. Chem. Rev.* **1988**, *84*, 85.
b) Balzani, V.; Juris, A.; Barigeletti, F.; Belser, P.; Zelewsky, A. V. *Sci. Pap.* **1984**, 78-85.
17. Butz, L. W.; Rytina, A. W. In *Organic Reactions*, John Wiley: New York, 1949; Vol. 5, pp 136-192.
18. Kuttyrev, A. A. *Tetrahedron* **1991**, *47*, 8043-8065.
19. Chang, F. C.; Wood, N. G. *Tet. Lett.* **1983**, *24*, 3365.
20. Stauffer, D. A.; Dougherty, D. A. *Tet. Lett.* **1988**, *29*, 6039-6042.
21. Altabet, A. B.; de Gallo, S. B. R.; Folquer, M. E.; Katz, N. E. *Inorg. Chim. Acta* **1991**, *188*, 67-70.
22. Middleton, R. W.; Parrick, J. In *The Chemistry of the Quinonoid Compounds*; Patai, S., Rappoport, Z., Eds.; John Wiley: New York, 1988; Vol. 2, Chapter 17.
23. *Heterocyclic Compounds* Grethe, G., Ed. Wiley: New York, 1981; Vol. 38, pt. 1, pp 44-51.
24. a) Gripenberg, J.; Hase, T. *Acta Chem. Scand.* **1963**, *17*, 2250-2252.
b) Kraus, G. A.; Man, T. O. *Synth. Comm.* **1986**, *16*, 1037-1042.
25. Kutney, J. P.; Greenhouse, R. *Syn. Commun.* **1975**, *5*, 119.
26. Banerjee, S. K.; Gupta, B. D.; Singh, K. *J. Chem. Soc. Chem. Comm.* **1982**, 815.
27. Hoffman, R. W. *Dehydrobenzene and Cycloalkynes*; Academic Press: New York, 1966; Chapter 6.
28. Pindur, U.; Lutz, G.; Otto, C. *Chem. Rev.* **1993**, *93*, 741-761.
29. Kauffmann, T. *Angew. Chem. Int. Ed. Engl.* **1965**, *4*, 543-618.
30. Yamashita, Y.; Hanaoka, T.; Takeda, Y.; Mukai, T.; Miyashi, T. *Bull. Chem. Soc. Jpn.* **1988**, *61*, 2451-2458.
31. Jones, J.; *The Chemical Synthesis of Peptides*; Clarendon Press: 1991.
32. De Feoand, R. J.; Strickler, P. D. *J. Org. Chem.* **1963**, *28*, 2915-2917.
33. Badanszky, M.; Martinez, J. *Synthesis*, **1981**, 333-356.
34. Ghadiri, M. R.; Soares, C.; Choi, C. *J. Am. Chem. Soc.* **1992**, *114*, 825-831.
35. Bossmann, S.; Seiler, M.; Durr, H. *J. Phys. Org. Chem.* **1992**, *5*, 63-73.
36. Petti, M.A.; Shepodd, T. J.; Barrans, B.E., Jr.; Dougherty, D. A. *J. Am. Chem. Soc.* **1988**, *110*, 6825-6840.

37. a) Sullivan, B. P.; Calvert, J. M.; Meyer, T. J. *Inorg. Chem.* **1980**, *19*, 1404-1407.
b) Calvert, J. M.; Schmehl, R. H.; Sullivan, B. P.; Facci, J. S.; Meyer, T. J.; Murray, R. W. *Inorg. Chem.* **1983**, *22*, 2151-2162.
38. Leroy, J. *Synth. Commun.* **1992**, *22*, 567-572.
39. Ishikura, M.; Ohta, T.; Terashima, M. *Chem. Pharm. Bull.* **1985**, *33*, 4755-4763.
40. Fischer, F. C.; Havinga, E. *Rec. Trav. Chim.* **1965**, *84*, 439-440.
41. Barrans, R. E. Ph.D. Thesis, California Institute of Technology, 1992.
42. a) Krohnke, F. *Angew. Chem. Int. Ed. Engl.* **1963**, *2*, 225-276.
b) Krohnke, F. *Synthesis* **1976**, 1-24.
c) Huang, T. L. J.; Brewer, D. G. *Can. J. Chem.* **1981**, *59*, 1689.
43. Black, G.; Depp, E.; Corson, B. B. *J. Org. Chem.* **1949**, *14*, 14.
44. Ansell, M. F.; Nash, B. W.; Wilson, D. A. *J. Chem. Soc.* **1963**, 3012-3028.
45. Cason, J. In *Organic Reactions* John Wiley: New York, 1948; Vol. 4, Chapter 6.
46. Patney, H. K. *Synthesis* **1991**, 694-696.
47. Bergmann, E.; Bergmann, F. *J. Org. Chem.* **1938**, *3*, 125-136.
48. Barret, R.; Daudon, M. *Tet. Lett.* **1990**, *31*, 4871-4872.
49. Chemistry of the Heterocyclic N-oxides, Katritzky, *Acta. Chem. Scand.* **1967**, *21*, 1841.
50. Fukumi, H.; Kurihara, H.; Mishima, H. *Chem. Pharm. Bull.* **1978**, *26*, 2175-2180.
51. a) Babin, P.; Dunogues, J.; Duboudin, F. *J. Heterocycl. Chem.* **1981**, *18*, 519-523.
b) Lok, W. N.; Ward, A. D. *Aust. J. Chem.* **1978**, *31*, 617-625.
52. Cadby, P. A.; Hearn, M. T. W.; Ward, A. D. *Aust. J. Chem.* **1973**, *26*, 557-570.
53. Leroy, J. *Tet. Lett.* **1992**, *33*, 2969-2972.
54. a) Kalinin, V. N. *Synthesis* **1991**, 413-432.
b) Suzuki, A. *Acc. Chem. Res.* **1982**, 178-184.
55. Ishikura, M.; Kamada, M.; Ohta, T.; Terashima, M. *Heterocycles* **1984**, *22*, 2475-2478.
56. Miyaura, N.; Yanagi, T.; Suzuki, A. *Synth. Commun.* **1981**, *11*, 513-519.
57. Friedman, L.; Logullo, F. M. *J. Org. Chem.* **1969**, *34*, 3089-3092.
58. Benkeser, R. A.; DeBoer, C. E. *J. Org. Chem.* **1956**, *21*, 281-284.
59. Brown, T.; Jones, J. H.; Richards, J. D. *J. Chem. Soc. Perkin I* **1982**, 1553-1561.
60. Fuji, T.; Sakakibara, S. *Bull. Chem. Soc. Jap.* **1974**, *47*, 3146-3151.
61. Klausner, Y. S.; Bodansky, M. *Synthesis* **1972** 453-463.